Charles University in Prague
Third Faculty of medicine

Energy metabolism of skeletal muscle

A thesis submitted for the degree of
Doctor of Philosophy

Moustafa Elkalaf

2015

I would like to dedicate this thesis to my family

This thesis has been written in the classical form according to the specifications recommended by the Board of Doctoral Study Programmes in Biomedicine.

Identification record

Title: Energy metabolism of skeletal muscle

Author: MUDr. Moustafa Elkalaf

Study program: Human Physiology and Pathophysiology

Supervisor: Prof. MUDr. Michal Anděl, CSc.

Consultant: MUDr. Jan Trnka, PhD, MPhil.

Institute: Third Faculty of Medicine, Charles University in Prague

Keywords:
[Oxidative phosphorylation, mitochondria, galactose, substrate metabolism, triphenylphosphonium]

Declaration

I declare that I carried out this doctoral thesis independently, and only with the cited sources, literature and other professional sources.

I understand that my work relates to the rights and obligations under the Act No. 121/2000 Coll., the Copyright Act, as amended, in particular the fact that the Charles University in Prague has the right to conclude a license agreement on the use of this work as a school work pursuant to Section 60 paragraph 1 of the Copyright Act.

Prague November 11, 2015 Signature

.....

Acknowledgements

I would like to sincerely acknowledge my supervisor Prof. Anděl for his persistent patience, guidance, and support that made this doctoral study possible.

A usual thank you will never be enough to thank my adviser and director Jan Trnka. I am fully indebted to him for teaching me a lot about bioenergetics, and the confidence he inspired to conduct mitochondrial research. I deeply appreciate the priceless encouragement that pushed me further than I thought I could achieve.

My gratitude goes out to all members of the Third Faculty of Medicine for helping and teaching me from their rich experience. I thank Lenka Rossmeislová for her advices and help with the confocal microscopy and immunofluorescence staining. I also thank Lucia Mališová for her help with the staining. I thank Jana Kračmerová for her help with the flow cytometry and reviewing the thesis summary report. I thank Vlasta Němcová for her help with Western blotting. I thank Petr Tůma for his consultations in chemistry. I thank Jan Polak for dealing with lab animals and for proofreading my work, also together with Martin Weiszenstein for the fruitful discussions and the friendly lab meetings. I thank Jana Matějčková and Martin Jaček for the help with spectrophotometry. I thank Adéla Krajčová and František Duška for the collaboration and being such a nice team. I thank Veronika Šrámková for the help with Czech translation of the thesis summary and together with Kateřina Westlake for proofreading this thesis.

My special thanks go to my lab colleagues for having a wonderful time with them. I thank Jana Tůmová for introducing me to the lab life and her countless aids with Czech translations, also for her valuable

comments on the thesis. I am also thankful for our ex-colleague Adela Prokopcová for creating a pleasant atmosphere inside the lab and the clinic, and of course for her admirable concerts.

I am thankful for the government of the Czech republic represented by the Ministry of Education, Youth and Sports for the scholarship that opened the doors to experience the Czech culture and to study Czech language in Mariánské Lázně and later to make my postgraduate study in Charles University in Prague.

I wish to share my upmost gratitude with my family. I acknowledge the continuous moral support afforded to me by all of you and the financial commitments that enabled my dreams to gain my qualifications so far from home.

Abstract

Skeletal muscle is the largest tissue in the body and plays a marked role in the homeostasis of the body metabolic state. Mitochondria have been proven to contribute to the pathophysiology of various metabolic diseases, either due to defects in their bioenergetic properties or the production of reactive oxygen species. In this work murine myoblasts C2C12 were used as a model of skeletal muscle *in vitro*, and rat muscle was used to prepare homogenate enriched in the mitochondrial fraction.

This work investigates the changes in respiratory parameters in models where mitochondrial oxidative phosphorylation is induced by changing the available consumable substrates in the culture media, such as replacing glucose by galactose, and the effect of treating the cells with high glucose concentration during the process of differentiation on mitochondrial performance. It also investigates the changes in bioenergetic profiles in samples treated with inactive derivatives of the widely used triphenylphosphonium (TPP^+) salts to target mitochondria by various probes and antioxidants.

The methods used in this study included evaluating mitochondrial parameters in intact and permeabilized cells by real time measurement of the oxygen consumption rate using the extracellular flux analyzer, measuring the enzymatic activity of Krebs cycle and the electron transport chain complexes spectrophotometrically, and measuring changes in mitochondrial membrane potential ($\Delta\psi_m$) fluorometrically.

The results confirmed that low glucose concentration is the main inducer of mitochondrial respiration and changes observed with galactose-treated models are due to glucose deprivation. The presence of glucose in the culture media is essential to induce differentiation and increasing the glucose level during the myogenic process decreases in the respiratory capacity due to the decrease in the enzymatic activity of complex I and III. More hydrophobic long alkyl side chain of the TPP^+ derivatives induces mitochondrial uncoupling and proton leak respiration, while the least hydrophobic methytriphenylphosphonium (TPMP) causes a gradual decrease of mitochondrial respiration by interruption of the Krebs cycle and inhibition of oxoglutarate dehydrogenase complex.

Souhrn*

Kosterní svalovina, jakožto nejobjemnější tkáň v těle, má nezastupitelnou úlohu při udržování metabolické homeostázy. Bylo dokázáno, že mitochondrie přispívají k patofyziologii nejrůznějších metabolických onemocnění, ať již kvůli poškození bioenergetických vlastností nebo produkcí reaktivních forem kyslíku. V této práci byly jako *in vitro* model kosterního svalu použity myší myoblasty C2C12 a sval krysy, ze kterého byl připraven homogenát obohacený o mitochondriální frakci.

Cílem práce bylo stanovit změny v mitochondriálních respiračních parametrech daných dostupností využitelných substrátů v kultivačním mediu, např. nahrazením glukózy galaktózou, a také zjistit vliv vysokých koncentrací glukózy na mitochondriální aktivitu během diferenciace. Dalším cílem bylo objasnit efekt inaktivních derivátů trifenyl fosfoniových (TPP^+) solí, hojně využívaných pro doručení různých prób a antioxidantů do mitochondrií, na bioenergetický profil buněk.

Data byla získána pomocí metod umožňující měření spotřeby kyslíku v reálném čase na extracelulárním flux analyzátoru a to jak v buňkách s neporušenou membránou, tak v permeabilizovaných buňkách, dále pomocí spektrofotometrického měření enzymatické aktivity Krebsova cyklu a elektronového transportního řetězce, a nakonec pomocí fluorometrické detekce změn membránového potenciálu mitochondrií ($\Delta\psi_m$).

Výsledky potvrzují, že nízká koncentrace glukózy je hlavním spouštěčem mitochondriálního dýchání a že změny pozorované u modelů kultivovaných s galaktózou jsou způsobeny nedostatkem glukózy. Přítomnost glukózy v kultivačním media je tedy nezbytná pro indukci diferenciace a zvyšování hladiny glukózy během myogenního procesu vede k poklesu respirační kapacity následkem snížení enzymatické aktivity komplexu I a III. Dlouhý alkylový postranní řetězec TPP^+ derivátů, který se vyznačuje silnějšími hydrofobními vlastnostmi, indukuje mitochondriální odpřažení a únik protonů, zatímco nejméně hydrofobní metyltrifenylfosfoniová sůl (TPMP) způsobuje postupný pokles aktivity mitochondriální respirace přerušením Krebsova cyklu a inhibicí komplexu oxoglutarát dehydrogenázy.

*Translation to Czech language was a kind offer of Veronika Šrámková

Contents

List of Figures

List of Abbreviations

$\Delta\rho$	proton-motive force
$\Delta\psi_m$	electrical membrane potential difference between mitochondrial matrix and cytoplasm
ADP	adenosine-5′-diphosphate
ANOVA	analysis of variance
ATP	adenosine-5′-triphosphate
BCA	bicinchoninic acid
BSA	bovine serum albumin
DCIP	2,6-dichloroindophenol
DMEM	Dulbecco's-modified Eagle's medium
DMSO	dimethyl sulfoxide
DTNB	5,5′-dithiobis-2-nitrobenzoic acid
DTT	DL-dithiothreitol
ECAR	extracellular acidification rate
EDTA	ethylenediaminetetraacetic acid
EGTA	ethylene glycol-bis(2-aminoethylether)-N,N,N′,N′-tetraacetic acid
ETC	electron transport chain
$FADH_2$	flavin adenine dinucleotide (reduced)
FAD	flavin adenine dinucleotide

FCCP	carbonylcyanide-*p*-trifluoromethoxyphenylhydrazone
$FMNH_2$	flavin mononucleotide (reduced)
FMN	flavin mononucleotide
GDP	guanosine-5′-diphosphate
GTP	guanosine-5′-triphosphate
HEPES	4-(2-hydroxyethyl)-1-piperazineethanesulfonic acid
KHB	Krebs-Henseleit buffer
MAS	mitochondrial assay solution
MHC	myosin heavy chain
NAD^+	nicotinamide adenine dinucleotide
NADH	nicotinamide adenine dinucleotide (reduced)
$NADP^+$	nicotinamide adenine dinucleotide phosphate
NADPH	nicotinamide adenine dinucleotide phosphate (reduced)
OCR	oxygen consumption rate
PBS	phosphate-buffered saline
PPR	proton production rate
ROS	reactive oxygen species
TMRM	tetramethylrhodamine methyl ester
TNB	2-nitro-5-thiobenzoate
TPMP	methyltriphenylphosphonium
TPP^+	triphenylphosphonium moiety
TRIS	tris(hydroxymethyl)aminomethane
UDP	uridine diphosphate
UTP	uridine triphosphate

Chapter 1

Introduction

The study of mitochondrial functions and pathways has gained increasing interest due to the involvement of mitochondria in the development of many pathological disorders through defects in oxidative phosphorylation, reactive oxygen species (ROS) production, or mitochondrial DNA mutations. The links between mitochondrial dysfunction and specific diseases were illustrated in many recent reviews, including cardiovascular diseases (Chrissobolis et al., 2011; Ichiki and Sunagawa, 2014; Yang et al., 2014; Wohlgemuth et al., 2014), cerebrovascular (Orsucci et al., 2013), neurodegenerative (Kang et al., 2013; Morava and Kozicz, 2013; Morris et al., 2014; Scarffe et al., 2014; Winklhofer, 2014; Stroh et al., 2014; Mohanty and McBride, 2013), psychological disorders (Anglin et al., 2012a,b; Marazziti et al., 2012), ophthalmic diseases (Jarrett et al., 2010; Sadun et al., 2013), and diabetes (Phielix and Mensink, 2008; Rieusset, 2011; Martins et al., 2012; Newsholme et al., 2012; Szendroedi et al., 2012; Li and Yu, 2013; Dela and Helge, 2013; Jelenik and Roden, 2013; Martin and McGee, 2014; Blake and Trounce, 2014). As a consequence of this expansion in mitochondrial contribution in diverse diseases, targeting mitochondria represented a plausible therapeutic approach for various conditions (Sheu et al., 2006; Sorriento et al., 2014).

The present work is concerned with the study of energy metabolism in skeletal muscle, particularly the mitochondrial respiratory function and the changes in respiratory parameters corresponding to changes in the available consumable substrates. In studies examining *in vitro* models, the composition of growth media is usually considered as a background condition, which has no significant effect

on observed phenomena. Proper controls are usually considered to elucidate the response to novel treatments or concentrations, disregarding the contribution of media in reforming the bioenergetic characterization of the tested model, which complicates viewing of final conclusions with objective detachment. In the following pages I will describe what seems to be the most reliable changes in growth media composition for a more suitable analysis of mitochondrial respiratory function, considering that a comprehensive investigation of mitochondrial 'function' and 'dysfunction' is difficult to include within one study, due to the broad range of mitochondrial metabolic roles. Therefore, the major goal of this study is addressed to testing the predominant physiological function of mitochondria, which is the generation of energy by oxidative phosphorylation.

One of the major complications facing *in vitro* studies is the decrease in the reliance on mitochondria oxidative phosphorylation to provide energy. Cells cultured in media with standard concentrations of glucose tend to acquire highly glycolytic phenotypes ("Crabtree effect", (Ibsen, 1961)), despite the presence of satisfactory levels of oxygen, which makes them less suitable as models for metabolic studies aiming to test mitochondrial respiration. Attempts have been made to overcome this phenomenon, by substituting glucose for galactose, which does not support anaerobic glycolysis. This is usually explained by the fact that galactose cannot be oxidized to pyruvate without prior conversion to glucose, which consumes two molecules of ATP, thus making anaerobic glycolysis insufficient to produce energy. Galactose-fed cells then should rely on mitochondrial oxidative phosphorylation to produce ATP, hence providing researchers with a metabolically improved model for studying mitochondrial respiratory function. Several studies performed on various tissues and cell lines have shown substantial changes in energy metabolism under such conditions where galactose-based media are often recommended to circumvent the Crabtree effect (Rossignol et al., 2004; Marroquin et al., 2007; Palmfeldt et al., 2009; Aguer et al., 2011).

The use of galactose supplemented cell culture media instead of glucose, although being simple, is exposing the cultured cells to glucose deprivation, which is another metabolic factor that participates in the observed results of the previous studies. Hence it was a necessity to differentiate the changes caused by using galactose from that resulted from glucose fasting. Moreover, the use of galactose

with tissues such as skeletal muscle is questionable, due to the lack of decisive amount of information about galactose metabolism in skeletal muscle cells. On the other hand, it is necessary to provide a suitable model of laboratory cultured skeletal muscle where the cultured cells possess more tendency to produce energy by mitochondrial oxidative phosphorylation pathway for a relevant investigation of mitochondrial performance, and describe an optimal substrate concentration to support cellular growth and differentiation, inclusive of testing the response of cultured muscle cells to different concentrations of the available substrates.

In this work I tried to perform a detailed study on using different substrates that can drive the cells towards a less glycolytic behavior, and analyze the mitochondrial membrane properties in response to changes of media substrate concentration, and I provide evidence arguing against the use of galactose instead of glucose to enhance mitochondrial respiration and increase the reliance on oxidative ATP production. I compare the bioenergetic profiles of different metabolic phenotypes as well as the cellular behavior and ability to differentiate in the presence or absence of glucose, to demonstrate the cause of previous studies published observations that used galactose and documented alterations in mitochondrial respiration in skeletal muscle were substantially due to glucose deprivation but not because of galactose metabolism.

I devoted a part of the study to present a comparison between hyperglycemic and normoglycemic environmental changes in mitochondrial respiratory parameters of *in vitro* muscle cells grown and differentiated in either case, and I will provide data supporting that high glucose levels may eventually result in a mitochondrial respiratory dysfunction and the possible causes of the lower respiratory capacity associated with the constant presence of high glucose level.

The final part of this work includes a detailed study about the adverse effects of the lipophilic triphenylphosphonium (TPP^+) compounds, the most used mitochondrial targeting moieties. I used moieties conjugated to inactive alkyl side chains to focus the comparison on the degree of the lipophilic character, mediated by the length of the alkyl side chain. I will provide data confirming interaction of the highly lipophilic alkylTPP^+ compounds with mitochondrial inner membrane enzymatic function, and draw the attention to the adverse inhibition of Krebs cycle by the least hydrophobic moiety methyltriphenylphosphonium (TPMP).

1.1 Mitochondrial respiration

The unique mitochondrial function is to extract energy from nutrients, and the released energy is used to form the high-energy compound ATP. Mitochondria possess the required enzymes for the production of reduced coenzymes as a final degradation of carbohydrates, fatty acids and amino acids, which eventually donate electrons to the oxidative metabolic pathway. The process of energy transfer is performed by a series of redox (reduction-oxidation) reactions, during which the enzymatic complexes of the electron transport chain (ETC) located in the inner mitochondrial membrane re-oxidize the reduced coenzymes produced from the citric acid cycle, using molecular oxygen as a final electron acceptor. The released energy is translated in the form of an electrochemical potential gradient across the inner mitochondrial membrane. This difference in potential is used to phosphorylate ADP producing ATP by the enzyme ATP synthase. In the coupled state, the electron transfer is indirectly connected to ATP synthesis via the electrochemical gradient, and ATP production relies on the efficiency of the ETC to keep a sufficient rate of proton translocation to maintain this gradient. Alteration in the activity of one or more of the enzymatic complexes of ETC can lead to a defect in energy production, either in basal conditions or during stress.

An electron microscope scanning of a mitochondrion will reveal a membrane

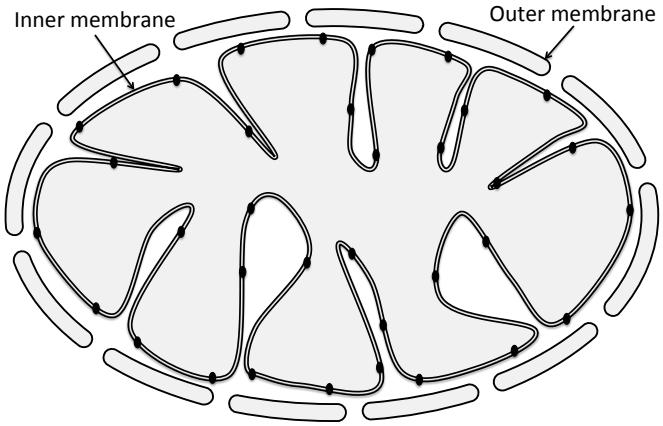

Figure 1.1: Classical mitochondrion as seen under electron microscope

bound organelle with a continuous change in the shape of cristae. According to the examined tissue, the number and shape of cristae and the total number of active mitochondria can dramatically change. In tissues with a high energy requirement, such as the cardiac muscle, the mitochondrial mass and the surface area of cristae is several times higher than in liver tissue, due to the high respiratory activity. Figure 1.1 illustrates a scheme of a classical mitochondrion viewed by electron microscope.

1.1.1 The citric acid cycle

The citric acid cycle is a series of enzymatic reactions taking place in the mitochondrial matrix. The main input to the cycle is acetate in the form of acetyl-CoA, produced from the breakdown of carbohydrates, lipids or proteins. The energy extraction from the cycle intermediates occurs in the form of electron transfer to the available oxidized NAD^+ to be reduced to NADH. Electrons are also transferred by the enzyme succinate dehydrogenase directly to the quinone pool reducing ubiquinone to ubiquinol. Other energy transfer occurs in the form of production of a molecule of guanosine-5′-triphosphate (GTP) from GDP and inorganic phosphate (P_i). The net energy production of each acetate molecule entering the cycle is equal to 3 NADH molecules, one GTP molecule and reduction of one molecule of ubiquinone to ubiquinol. The enzymatic reactions of the citric acid cycle are schematically summarized in figure 1.2.

1.1.2 Components of the electron transport chain

The first enzyme complex in the electron transport chain is NADH dehydrogenase or complex I. It binds to NADH liberated from Krebs cycle and catalyses its oxidation to NAD^+ and uses the removed 2 electrons from each NADH molecule to reduce ubiquinone CoQ to ubiquinol $CoQH_2$ in the quinone pool. The path of electrons through the complex includes binding to flavin mononucleotide FMN prosthetic group which becomes reduced to $FMNH_2$ then through a series of [Fe-S] clusters. The flow of each pair of electrons through the complex causes translocation of 4 protons from mitochondrial matrix to the intermembrane space, creating a proton gradient across the membrane.

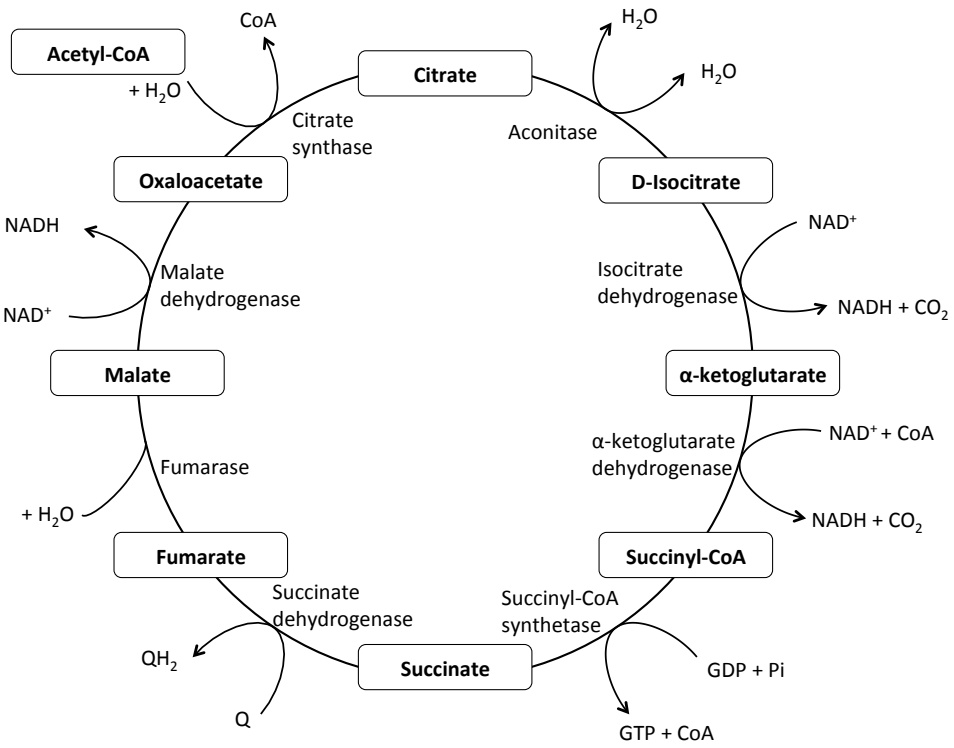

Figure 1.2: Scheme of the citric acid cycle

Complex II or succinate dehydrogenase is also an enzyme of the citric acid cycle that catalyses the oxidation of succinate to fumarate coupled with the reduction of ubiquinone to ubiquinol by delivering additional electrons to the quinone pool. The redox centers of complex II include FAD in the succinate binding site attached to a series of Fe-S clusters, however, the tunnelling of electrons through the complex is not associated with proton translocation. The electron transfer flavoprotein-ubiquinone oxidoreductase and the glycerol-3-phosphate dehydrogenase are other FAD containing enzymes beside complex II, that catalyze the transfer of electrons from substrate directly to the quinone pool without any proton translocation, by pairing the oxidation of $FADH_2$ produced during the oxidation of fatty acids or amino acids to the reduction of ubiquinone.

Both complex I and II converge electrons to the quinone pool formed of coenzyme Q, which is a fat soluble electron carrier floating in the phospholipid bilayer of the mitochondrial membrane. It is freely mobile and found as a functional

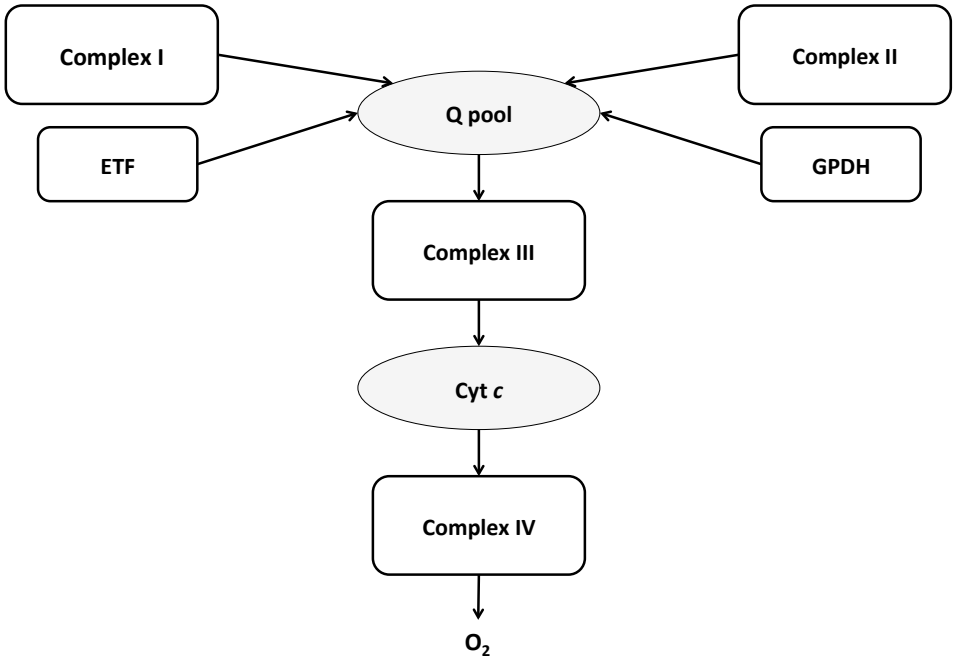

Figure 1.3: Scheme of electron transport chain

element in all cellular membranes, with the highest concentration in mitochondrial membrane. Thanks to its unique chemical structure it can be found in three redox states, fully oxidized (ubiquinone), ubisemiquinone, and fully reduced (ubiquinol). The three forms contribute in the quinone pool which maintains the cyclic electron transfer to complex III.

Complex III or ubiquinol-cytochrome c oxidoreductase catalyses the transfer of electrons from the quinone pool to the cyt c associated with the translocation of more protons from the mitochondrial matrix. The pathway of electron transfer through complex III passes through the redox centers of the complex -Rieske Fe-S center, cyt b and cyt c_1- in cyclic three stages with the net oxidation of one molecule of ubiquinol to ubiquinone per cycle.

Cyt c is a highly water soluble protein found related to complex III in the inner mitochondrial membrane, and can be easily solubilized from the intact mitochondria. Cyt c is reduced by the electron transfer from complex III and re-oxidized by the action of complex IV.

Complex IV or cytochrome c oxidase performs the final step of the electron

transfer in the respiratory chain by catalyzing reduced cytochrome c oxidation by molecular oxygen, which becomes reduced to two molecules of water. The mechanism of electron transfer takes place in a five stages cycle, with the last two stages requiring proton translocation in order to release the water molecules.

The main reactions of the mitochondrial electron transport chain can be summarized in the following equations

$$\mathrm{NADH} + \mathrm{Q} + 5\mathrm{H^+}_{in} \xrightarrow{\text{Complex I}} \mathrm{NAD^+} + \mathrm{QH_2} + 4\mathrm{H^+}_{out} \tag{1.1}$$

$$\text{succinate} + \mathrm{Q} \xrightarrow{\text{Complex II}} \text{fumarate} + \mathrm{QH_2} \tag{1.2}$$

$$\mathrm{QH_2} + 2\ \text{cyt}\ c(\mathrm{Fe^{+3}}) + 2\mathrm{H^+}_{in} \xrightarrow{\text{Complex III}} \mathrm{Q} + 2\ \text{cyt}\ c(\mathrm{Fe^{+2}}) + 4\mathrm{H^+}_{out} \tag{1.3}$$

$$4\ \text{cyt}\ c(\mathrm{Fe^{+2}}) + 8\mathrm{H^+}_{in} + \mathrm{O_2} \xrightarrow{\text{Complex IV}} 4\ \text{cyt}\ c(\mathrm{Fe^{+3}}) + 4\mathrm{H^+}_{out} + 2\mathrm{H_2O} \tag{1.4}$$

Three of the four complexes of the ETC act as oxidation-reduction-driven proton pumps, and since all the reactions catalyzed by the ETC enzymes are reversible, it is essential to impose the presence of both the oxidized and reduced forms of each enzyme substrate at appropriate concentrations. As the complexes of the mitochondrial ETC move protons from the matrix into the intermembrane space an electrochemical potential difference (proton-motive force $\Delta\rho$) builds up across the highly impermeable mitochondrial inner membrane. This potential is used to produce ATP by ATP synthase to perform the phosphorylation division of the oxidative phosphorylation process.

1.1.3 Phosphorylation by ATP synthase

ATP synthase uses the established membrane gradient to produce ATP from ADP and inorganic phosphate. This reaction is reversible and maintaining the mitochondrial membrane potential is essential to maintain ATP production. The

enzyme is formed of two fractions, F_1 and F_O which couple the release of energy from protons returning from the intermembrane space down the electrochemical gradient to the mitochondrial matrix to the phosphorylation of ADP to ATP in a binding-change mechanism.

1.1.4 The bioenergetic profile

A cellular bioenergetic profile provides an analytical picture of mitochondrial respiration in the examined example. The profile consists of various respiratory parameters concluded from measuring the cell respiratory control in intact cells. Remarkable variations in one or more of these parameters can be a sign, or lead eventually to mitochondrial dysfunction. So far, the cell respiratory control allows a reliable, sensitive and specific estimate of the bioenergetics in intact cells, assuming that the measured cells have sufficient glycolytic activity to support cellular metabolism (Nicholls et al., 2010; Brand and Nicholls, 2011), since mitochondrial respiration is interrupted during the test. The main advantage of this measure is obtaining results with more physiological relevance, since it depends on measuring the oxygen consumption rate of intact cells in the external environment, thus avoiding the artifacts due to cellular permeabilization and mitochondrial isolation.

However, intact cells lack their *in vivo* environment and the results are more vulnerable to extreme changes depending on the available substrates provided during the experiment. The cell respiratory control (mitochondrial stress test) uses specific enzymatic inhibitors to perturb the function of electron transport chain complexes. The method is discussed in detail in the experimental procedures chapter (2.7.1). After measuring cellular respiration in state with a given concentration of respiratory substrates, successive addition of mitochondrial inhibitors is used to show differences in other respiratory parameters, such as basal mitochondrial respiration, ATP turnover-driven respiration, maximal and spare respiratory capacity, proton leak and non-mitochondrial respiration, provided that proper normalization is performed to avoid the variations in respiratory rate due to cell size and phenotype. In this section I review briefly the major respiratory parameters concluded from a mitochondrial stress test.

1.1.4.1 Basal respiration

Basal respiration represents the least cellular oxygen consumption rate during resting condition. Factors controlling basal respiratory rate include ATP turnover-driven respiration and proton leak (Brown et al., 1990; Ainscow and Brand, 1999) after exclusion of non-mitochondrial respiration, so it varies according to the demand to mitochondrial ATP. External factors such as the available substrates, hormones or drugs can change the basal respiration accordingly. A change in the basal respiration indicates a metabolic change, however, the nature of this change can be elucidated by completing the bioenergetic profile. Data in chapter 5 and chapter 6 show an example of changes in basal respiration induced by treatment with mitochondrial targeting molecules with different mechanisms.

1.1.4.2 Non-mitochondrial respiration

Non-mitochondrial respiration of residual oxygen consumption is the oxygen consumption after application of ETC inhibitors, namely complex I and III as the last step of a respiratory control experiment. The dependence on extra mitochondrial NADPH oxidases may dominate the cellular uptake, hence the accurate estimation of non-mitochondrial oxygen consumption is essential to provide a more reliable description of mitochondrial respiration. The non-mitochondrial respiration can account for up to 10% of the total cellular respiration (Nobes et al., 1990; Porter and Brand, 1995; Jekabsons and Nicholls, 2004; Affourtit and Brand, 2008; Amo et al., 2008). This is due to various desaturases and other cytosolic enzymes. The value of the non-mitochondrial respiration is assumed to be constant during the whole assay, and is subtracted from other values to distinguish the actual mitochondrial consumption.

1.1.4.3 ATP turnover-driven respiration

ATP turnover-driven respiration represents the rate of mitochondrial ATP synthesis in a certain basal condition. This estimate can be obtained by inhibiting the ATP synthase by oligomycin, which is followed by a shift of the entire ATP production glycolytic pathway and the rapid production of lactate, provided that sufficient glucose is available. A change in the ATP turnover-driven respiration is

due to a change in ATP demand, which is reflected on the basal respiratory rate. However, a decrease in its rate in response to increasing ATP demand indicates a dysfunction in the mitochondrial ATP synthesis machinery (Brand and Nicholls, 2011). The estimation of this parameter is not absolutely accurate, due to induction of mitochondrial hyperpolarization following the addition of oligomycin. This state may lead to underestimation of ATP synthesis by less than 10% (Affourtit and Brand, 2009) and an increase in proton leak rate by 15-20% (Brand and Nicholls, 2011).

1.1.4.4 Maximal respiratory rate

It is a state simulating a condition with a sudden increased demand on mitochondrial ATP. It is therefore strictly related to the available substrates and the efficiency of the respiratory machinery to accelerate ATP production to near maximum activity of the ETC. It is induced artificially by the application of protonophores (uncouplers) leading to a collapse of the mitochondrial membrane potential and uncoupling respiration from phosphorylation process. The concentration of the available substrates must be considered, since the increase in demand may not match with the available substrates in intact cells.

There is a large difference when protonophores are used with isolated mitochondria, because consumable substrates are used with high non-physiological concentrations in such a design. Also using protonophores has a different effect when used with isolated mitochondria and it may give higher results for maximum respiratory rates than when used with intact cells, due to the non-selective mode of action of the protonophore (Brand and Nicholls, 2011). The significance of maximum respiratory rate parameters is to reveal established or potential mitochondrial dysfunction that is not apparent in the basal state. A decrease in this parameter reflects a defect in ETC or insufficient respiratory substrates.

1.1.4.5 Spare respiratory capacity

This is another important parameter that is concluded after the artificial induction of respiration. It is a diagnostic parameter that can indicate mitochondrial dysfunction, that is not apparent under basal condition. Similar to maximum

respiratory rate, it reflects the ability to supply substrates and transport electrons in response to a sudden increase in energy demand (Yadava and Nicholls, 2007; Choi et al., 2009). it can be concluded quantitatively by subtracting the respiratory rate in basal conditions from maximal respiratory rate.

1.1.4.6 Proton leak

Proton leak occurs physiologically in normally functioning electron transport system, in parallel to proton re-entry through ATP synthase (Nicholls, 1977). Therefore, it is found in mitochondria *in situ* in intact cells, and it doesn't represent an artifact of mitochondrial isolation (Nobes et al., 1990; Brand, 1990; Brand et al., 1994; Rolfe et al., 1999). Experimentally, it is the mitochondrial respiratory rate while inhibiting the ATP synthase by oligomycin. After correction by removing non-mitochondrial respiration, it represents the proton leak across the mitochondrial membrane *in situ* in the preceding basal condition.

To achieve this state, the flow of electrons to the electron transport chain is interrupted by inhibiting the main providers at complex I and complex III sites. The proton leak rate is then obtained by subtracting this value from the respiratory rate after addition of oligomycin. Due to uncoupling, the respiration in this state is relatively insensitive to changes in substrate oxidation and completely insensitive to ATP demand. Changes in the proton leak rate indicate mitochondrial uncoupling, which can be moderate due to certain substrate, or large due to severe mitochondrial damage, which is shown in chapter 5.

1.2 Metabolic importance of skeletal muscles

Skeletal muscle is the most abundant tissue in the body representing 40%-45% of total body mass. Each skeletal muscle represents a distinct organ, composed of varying number of muscle fibers. Beside its function in the locomotor system, skeletal muscle tissue has an important metabolic function (Sinacore and Gulve, 1993; Petersen et al., 2007; Phielix and Mensink, 2008; Kus et al., 2008) being a regulator of the whole body metabolism and energy expenditure. Skeletal muscle tissue help achieve glucose homeostasis, due to the necessity to control glucose

uptake during muscle activity in order to produce sufficient energy and in the same time to replenish the depleted glycogen stores. Therefore, an impairment in any of the mechanisms mediating glucose transport into skeletal muscles can eventually result in an alteration in the whole body glucose metabolism.

Glucose transport to skeletal muscle is induced by muscle contraction or by insulin as most peripheral tissue. Contraction induce glucose transport even in absence of insulin from the environment (Ploug et al., 1984; Nesher et al., 1985; Wallberg-Henriksson and Holloszy, 1985). It has been observed that an increase in glucose transport can be induced by exercise (Garetto et al., 1984), (Wallberg-Henriksson et al., 1988), by muscle stimulation *in situ* (Richter et al., 1984), and by stimulation of isolated muscles *in vitro* (Nesher et al., 1985; Constable et al., 1988).

While ≈90% of insulin mediated glucose transport occurs in the peripheral tissues (DeFronzo, 1988), skeletal muscle tissue represents the major site of insulin-dependent glucose uptake (DeFronzo, 1988; Kraegen et al., 1985; Baron et al., 1988). Insulin induces storage of transported glucose to skeletal muscle in the form of glycogen (Bogardus et al., 1983; Lillioja et al., 1986) in a process highly dependent on muscle sensitivity to insulin level (Bogardus et al., 1983).

Skeletal muscles not only represent a store for excess glucose in the form of glycogen, maintaining the blood glucose level, but also the protein of the skeletal muscles acts as a major store from which amino acids can be drawn when circumstances lead to a fall in the levels of blood glucose and of amino acids in the circulation (Spargo et al., 1979). In addition, skeletal muscle contributes by 20%-30% to the basal metabolic rate (Guyton and Hall, 2006).

1.3 Changes in metabolic profile during skeletal muscle differentiation

The process of myogenesis describes the differentiation of undifferentiated myoblasts into multinucleated myotubes, and the expression of contractile proteins. This process also induces mitochondrial proliferation since undifferentiated myoblasts posses from 5%–20% of the mitochondrial content of the differenti-

ated cells (Moyes et al., 1997). Increasing the mitochondrial mass switches the metabolic phenotype from glycolytic to oxidative ATP production (Leary et al., 1998), associated with an increase in the reliance on oxidative phosphorylation and decrease in reactive oxygen species (ROS) production (Fiaschi et al., 2001) which is not correlated to changes in the content of the ETC (Lyons et al., 2004).

The importance of changing the metabolic phenotype during muscle differentiation is related to alteration in cellular structure and enzymatic activity. This simulates pathological conditions in which defects in the mitochondrial ATP production modify the bioenergetic profile and ROS production (Beal, 2000).

1.4 Using galactose in muscle research

Researchers have studied the use of galactose with skeletal muscle *in vivo* and muscle cell lines *in vitro*. Galactose was used to test the effect of polyol pathway activation due to the similarity in manifestations with diabetic myopathy. Recently, it was suggested to use galactose, although not being a consumable substrate for skeletal muscle, to induce mitochondrial respiration in the highly glycolytic tissue culture models.

1.4.1 Muscle dysfunction in experimental galactosemia

Using experimental hypergalactosemia in the study of diabetes was suggested because both hypergalactosemia and diabetes are known to activate the polyol pathway in most tissues, including skeletal muscle, leading to the accumulation of polyols. Defects of muscle metabolism that are common to galactosemia and diabetes are closely associated with the development of myopathy and might play a role in the pathogenesis of the muscle disease in the two models (diabetes and galactosemia).

In 1992, a study tested the effect of high galactose supplemented diet on muscle and nerve function in rats (Cameron et al., 1992). The study concluded that the over activity of the polyol pathway might contribute to the etiology of diabetic myopathy and neuropathy, because galactitol accumulates in muscle and nerve tissues leading to changes similar to these observed in diabetes, in the form

of fiber damage, changes in contraction speed, tension production and resistance to fatigue. These changes could be delayed by using an aldose reductase inhibitor, which guarantees blocking of the polyol pathway.

Cameron et al. recommended this example of experimental hypergalactosemia as a suitable model to investigate other effects of the polyol pathway, due to the complex metabolic and hormonal changes in diabetes. The study also demonstrated the similarities and differences between diabetic and galactosemic effects on both slow and fast twitch muscles.

1.4.2 Using galactose to enhance mitochondrial respiration

Previous studies on murine myoblasts showed that despite the availability of oxidizable fuel in the incubation medium, myoblasts in the early stage of differentiation derive approximately 60% of their energy demands by lactate production from glucose (Leary et al., 1998). For that reason attempts to develop a more oxidative model were made either by lowering the glucose level (Mailloux and Harper, 2010) or by substituting galactose for glucose where Aguer et al. presented data showing that the differentiation of human primary myoblasts in a galactose-containing medium revealed mitochondrial dysfunction in samples derived from formerly diabetic patients, who lost weight and became normoglycemic (Aguer et al., 2011).

Galactose has been already used in many studies in attempts to abolish the Crabtree effect, and to increase the reliance on mitochondrial oxidative respiration in models used to study mitochondrial function/dysfunction *in vitro* (Rossignol et al., 2004; Marroquin et al., 2007; Palmfeldt et al., 2009) in tissue cultures not including skeletal muscle.

Since skeletal muscle lacks the ability to metabolize galactose (Resnick and Hechter, 1957; Dvornik, 1987; Heidenreich et al., 1993), the study of Mailloux et al. in 2010 suggested decreasing glucose concentration in growth media and investigated the effect of two glucose concentrations, 5 mM and 25 mM, on the basal and maximal respiration of differentiated C2C12 myotubes (Mailloux and Harper, 2010). They stated that cells grown and differentiated in high glucose

environment possessed lower maximal respiratory capacity than those grown and differentiated in lower glucose level.

The later study of Aguer et al. found significant effects of galactose medium on the metabolic function of human primary myoblasts (Aguer et al., 2011), however, the authors in this study compared cellular respiration in media with different compositions thus making it difficult to distinguish acute effects of substrate availability from longer-term phenotypic changes in cells grown in galactose-containing medium. A detailed study of effect of galactose on mitochondrial bioenergetic profile of C2C12 cells is discussed in chapter 3, and in this chapter I review briefly galactose general metabolism.

1.5 Galactose metabolism

Galactose is a hexose monosaccharide that is different from glucose in the position of the hydroxyl group on the 4th carbon atom forming a C–4 epimer of glucose. It exists in nature in both open chain and ring forms. There are two anomers of galactose in human body, α-D-galactose, and β-D-galactose. Galactose binds with glucose to form lactose, a disaccharide, which is found mainly in milk and dairy products. Galactose is found as well in some vegetables and fruits (Acosta and Gross, 1995; Berry et al., 1993).

In humans, galactose can be absorbed in the proximal jejunum and renal epithelium driven by Na^+/glucose co-transporters SGLT1 and SGLT2 (Wright et al., 1992; Martín et al., 1996). The adult 70 kg male can produce up to 2 grams of galactose per day by endogenous production and turnover of glycolipids and glycoproteins (Berry et al., 1995, 1997, 2004), as galactose is used with other monosaccharides, especially fructose, to form complex oligosaccharide side chain in the process of glycation, relying on its higher glycation activity comparing to glucose (McPherson et al., 1988).

1.5.1 Leloir pathway

Most organisms can utilize galactose through the Leloir pathway (Figure 1.4) and congenital defects in one of its enzymes or the increase of galactose level can cause

hypergalactosemia. Once present inside the cells, β-D-galactose is epimerized to α-D-galactose through the action of the enzyme galactose mutarotase (Thoden et al., 2004). Galactose is mainly metabolized in the liver by the Leloir pathway, which needs three enzymes: galactokinase (GALK) consuming one ATP converts galactose to galactose-1-phosphate. Then galactose-1-phosphate uridylyltransferase (GALT) catalyzes the transfer of UDP from UDP-glucose to form UDP-galactose and glucose-1-phosphate. Lastly, UDP-galactose-4-epimerase (GALE) converts UDP-galactose back to UDP-glucose (Holden et al., 2003), or UDP-galactose can be a galactosyl donor in glycoproteins and glycolipids biosynthesis (Salo et al., 1968).

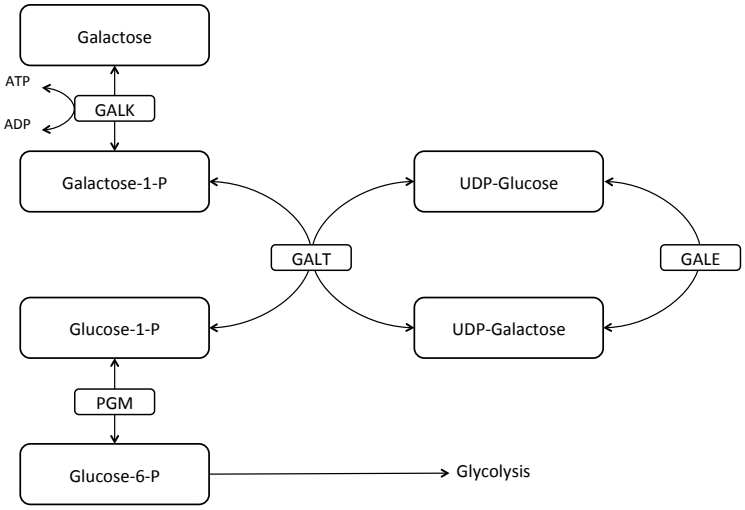

Figure 1.4: Leloir Pathway. GALK, galactokinase; GALT, galactose-1-phosphate uridylyltransferase; GALE, UDP-galactose-4-epimerase; PGM, Phosphoglucomutase.

The other product of the second step, glucose-1-phosphate, can enter glycolysis or reacts with UTP to form another molecule of UDP-glucose (Duggleby et al., 1996); or it can be dephosphorylated by inositol monophosphatase to form galactose (Parthasarathy et al., 1997). Genetic mutations in one or more of these enzymes (GALK, GALT and GALE) can lead to a build up of D-galactose and its metabolites to toxic levels, galactosemia, which can be presented by variable clinical symptoms according to the affected gene (Reichardt, 1992).

1.5.2 The polyol pathway

While Leloir pathway is responsible for metabolizing galactose in liver, galactose undergoes an alternative pathway in skeletal muscle and other tissues. The polyol pathway (Figure 1.5) is responsible for galactose metabolism due to absence of the Leloir pathway (Dvornik, 1987). The polyol pathway, also known as sorbitol-aldose reductase pathway, converts the unused glucose to fructose on two steps by two enzymes: the aldose reductase reduces glucose to sorbitol by oxidizing NADPH to $NADP^+$, and then the sorbitol dehydrogenase oxidizes sorbitol to fructose (Cogan et al., 1984).

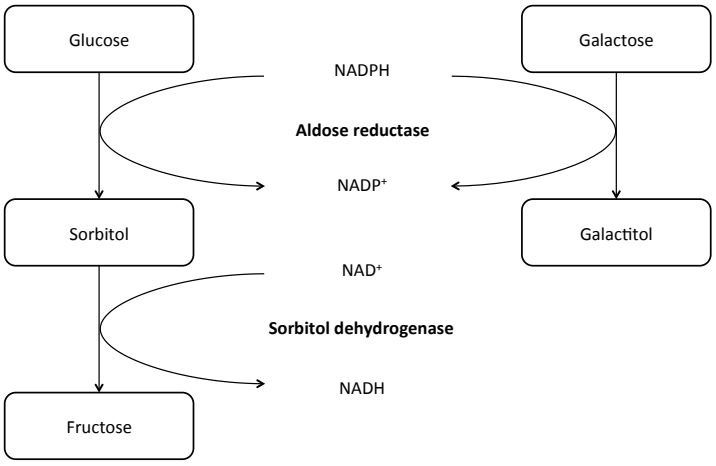

Figure 1.5: The polyol pathway (sorbitol-aldose reductase pathway). Both glucose and galactose are substrates for the enzyme aldose reductase. Accumulation of sugar alcohols in muscle fibers leads eventually to myopathy.

Galactose is another substrate for the aldose reductase enzyme, which reduces galactose to its alcohol galactitol. The second polyol pathway enzyme, sorbitol dehydrogenase, does not further metabolize galactitol, leading to the accumulation of galactitol inside the muscle cell (Berry, 1995) and the myopathic manifestations observed in experimental hypergalactosemia (Cameron et al., 1992). In tissues other than skeletal muscle, higher activity of the polyol pathway causes a build up of $NADP^+$, and more reliance on the hexose monophosphate shunt to reduce excess $NADP^+$ for metabolic regulation (Davidson and Murphy, 1985).

1.6 Targeting mitochondria

The critical role of mitochondria in cellular metabolism led to the introduction of mitochondriotropic species which can influence mitochondrial biochemical pathways. An agent with high affinity to mitochondria must be membrane permeable to freely cross the cytoplasmic and mitochondrial membranes. Synthesizing these agents provided a wide variety of probes to study mitochondria, as well as new therapeutic approaches. Mitochondrial targeting agents include lipophilic cations that use the unique nature of mitochondrial membrane in maintaining a constant potential across mitochondrial inner membrane to selectively accumulate within mitochondria. Hydrophobicity plays a greater role in penetrating mitochondrial membrane, and accounts for faster negatively charged anions across lipid membranes (Flewelling and Hubbell, 1986).

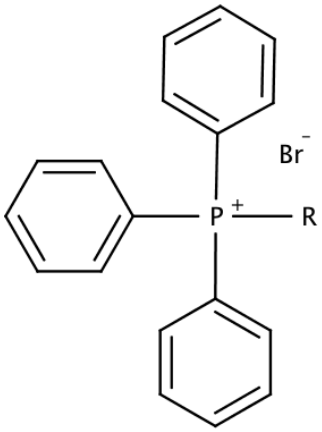

Figure 1.6: Triphenylphosphonium bromide (TPP^+) moiety

Triphenylphosphonium cations (TPP^+) are considered the most widely used cations to conjugate various mitochondrial targeting probes due to their unique design (Figure 1.6). Mitochondrial uptake and binding to the phospholipid bilayers of alkylTPP^+ is directly proportional to the degree of hydrophobicity of the compound, which is mediated by the length of the alkyl side chain in alkylTPP^+ (Ross et al., 2005, 2008). To enter mitochondria, alkylTPP^+ compounds bind to the outer surface of the inner membrane, then permeate the hydrophobic potential energy barrier of the phospholipid bilayer, before binding to the inner surface

of the membrane from where they desorb into the mitochondrial matrix (Ross et al., 2008). In the presence of a membrane potential there is ≈100 to 1000-fold accumulation of the cation into the matrix, the extent of which is determined by Nernst equation (1.5), where $\Delta\psi$ represents mitochondrial inner membrane potential, R is the universal gas constant, T is the absolute temperature, n is the valence of the used ion and F is Faraday's constant.

$$\Delta\psi = \frac{RT}{nF} ln \left(\frac{[cation_{in}]}{[cation_{out}]} \right) \tag{1.5}$$

Lipophilic cations based on the triphenylphosphonium moiety have been widely used to target various biologically active substances such as antioxidants (Smith et al., 1999; Kelso et al., 2001; Filipovska et al., 2005; Brown et al., 2007; Trnka et al., 2008; Kelso et al., 2012), spin traps (Murphy et al., 2003; Hardy et al., 2007; Xu and Kalyanaraman, 2007; Quin et al., 2009) or various other chemical probes into mitochondria (Robinson et al., 2006; Cochemé et al., 2011). The accumulation of TPP^+ derivatives in mitochondria was first described in 1970 (Grinius et al., 1970; Bakeeva et al., 1970) where it was suggested to be used to measure mitochondrial membrane potential using mainly methyltriphenylphosphonium salts, TPMP.

Assuming a perfectly Nernstian behavior, a membrane-permeable cation will accumulate in a negatively charged compartment approximately ten-fold for each 60 mV of potential difference. In the case of TPP^+ derivatives, this ideal behavior is complicated by the fact that the hydrophobicity of the derivative affects both the extent and the rate of accumulation, which means that more lipophilic derivatives accumulate faster and with higher concentrations than the more hydrophilic ones (Ross et al., 2005, 2008).

The TPP^+ moiety itself is often assumed not to exhibit any significant biological activity, however, its high affinity for phospholipid membranes (Trnka, 2008; Trnka et al., 2009; James et al., 2005) makes it likely to disrupt membrane integrity (Leo et al., 2008; Cunniff et al., 2013; Trendeleva et al., 2012) especially in mitochondria where such compounds accumulate and due to non-specific binding to membranes, which could also alter the function of mitochondrial membrane proteins such as complexes of the respiratory chain (O'Malley et al., 2006).

It has been previously observed that some TPP^+ compounds negatively affect mitochondrial and cellular respiration (Wingrove and Gunter, 1986; Brand, 1995; Patkova et al., 2014) and may increase proton leak across the inner mitochondrial membrane, for example by enhancing the uncoupling effect of free fatty acids such as palmitate (Severin et al., 2010) or the anionic protonophores (Antonenko et al., 2013).

Most published studies used TPP^+ derivatives with chemically active moieties (Plecitá-Hlavatá et al., 2009) making it difficult to separate the effect of the TPP^+ moiety itself. One notable exception is a recent paper by Reily et al., who studied not only the impact on mitochondrial function of biologically active TPP^+ compounds MitoQ, MitoTEMPOL and MitoE but also 'inactive' alkyl derivatives methyl-, butyl- and decylTPP^+ (Reily et al., 2013). Their results from Seahorse measurements on MES-13 cells show a general inhibitory effect of all TPP^+ derivatives on basal respiration accompanied by signs of mitochondrial uncoupling for decylTPP^+.

The study of Reily et al., while useful in highlighting the significant effects of alkylTPP^+ on cellular respiration, relied on only one source of data, namely the measurements of oxygen consumption rate (OCR) and extracellular acidification rate (ECAR). These parameters make it difficult to separate the effects on membrane potential and the respiratory chain activity. Another interesting point was the inhibitory effect of methyltriphenylphosphonium (TPMP), which was not explained. TPMP has the shortest alkyl side chain, and compared to other alkylTPP^+ salts is the least lipophilic. This excludes the role of hydrophobic nature of this molecule from the general more lipophilic inhibitors of the same family.

The field of mitochondrial targeting expands progressively, and different antioxidants and probes are being introduced continuously. We tried to obtain more understanding of the mechanism of action of mitochondrial targeting molecules and their adverse reactions, and I devoted a part of this work to study the 'inactive' TPP^+ derivatives on cellular respiration. We employed additional assays to study the mechanism of their toxic effects on mitochondrial respiration, in the presence of various mitochondrial substrates in order to pinpoint, if possible, the specific sites of their action.

1.7 Aims of the project

The project was designed to investigate the energy metabolism of skeletal muscle in various metabolic conditions, which provided freedom in selecting research subjects. Mitochondria, as the main energy producing organelles, and changes in mitochondrial activity due to tissue culture conditions provided an opportunity to study skeletal muscle metabolism *in vitro*.

As our understanding of the effects of low glucose and galactose on cultured skeletal muscle cells is still far from satisfactory, the first intention was to investigate the changes of growth patterns and several parameters of mitochondrial metabolism in C2C12 myoblasts and myotubes in response to differing availability of glucose or galactose while considering some of the shortcomings of previously published studies in an attempt to avoid them. The goal was to provide experimental data demonstrating all aspects of the relationship between cell culture conditions and the metabolic activity of the cultured cells.

Another aim was to analyze the changes and if possible the deterioration in mitochondrial respiratory parameters of cultured cells in a high glucose concentration imitating uncontrolled hyperglycemia, and to compare the mitochondrial performance to cells cultured in moderate glucose concentration.

While the main target was to study metabolism, using different probes to study mitochondrial function opened an additional area of mitochondrial research, and the subject of adverse reactions of mitochondrial targeting molecules attracted increasing attention. This allowed to investigate the effect of the length of the alkyl side chain of the hydrophobic TPP^+ moieties on mitochondrial respiration, and try to answer the questionable TPMP inhibitory effect.

Chapter 2

Experimental procedures

2.1 Materials

Unless otherwise stated in the text, all materials, chemicals and substrates were purchased from Sigma-Aldrich, Prague, Czech republic.

2.1.1 Solvents, buffers and stock solutions

Deionized water (18.2 $M\Omega.cm^{-1}$) was used throughout, other solvents were of analytical grade. Water insoluble reagents were dissolved in ethanol or DMSO according to solubility recommendations.

2.1.1.1 Composition of frequently used buffers

Krebs-Henseleit Buffer Modified (KHB) 111 mM NaCl, 4.7 mM KCl, 12 mM $MgSO_4$, 1.2 mM Na_2HPO_4, 2.5 mM glucose, 0.5 mM l-carnitine, pH 7.4.

Mitochondrial assay solution (MAS) 70 mM sucrose, 220 mM D-mannitol, 10 mM KH_2PO_4, 5 mM $MgCl_2$, 2 mM HEPES, 1 mM EGTA, 0.2% BSA, and 4 mM ADP. The pH was adjusted with 10 M KOH to 7.4 at 37°C.

Phosphate-buffered saline (PBS) 137 mM NaCl, 2.7 mM KCl, 10.2 mM $NaHPO_4$, 1.8 mM KH_2PO_4, pH 7.4.

Mitochondrial recommended buffers Buffers were used for mitochondrial isolation and homogenates during the preparation of enriched mitochondrial fractions for spectrophotometric analysis of mitochondrial electron transport chain enzymatic activities.

CHM (cell homogenization medium)
10 mM Tris, 10 mM KCl and 150 μM $MgCl_2$, pH 6.7.

CHM + sucrose
10 mM Tris, 10 mM KCl, 150 μM $MgCl_2$ and 1 M sucrose, pH 6.7.

Sucrose/Mg^{2+}
10 mM Tris, 150 μM $MgCl_2$ and 250 mM sucrose, pH 6.7.

MSM (mitochondrial separation medium)
10 mM Tris and 250 mM sucrose, pH 7.0.

STEB (sucrose-Tris-EGTA-BSA)
250 mM sucrose, 5 mM Tris, 1 mM EGTA and 0.1% fatty-acid free BSA, pH 7.4.

MHM (muscle homogenization medium)
20 mM Tris, 40 mM KCl, 250 mM sucrose and 2 mM EGTA, pH 7.4.

2.1.1.2 Stock solutions

Inhibitors and uncouplers Oligomycin (5 mM), rotenone (5 mM), antimycin A (5 mM), carbonylcyanide-*p*-trifluoromethoxyphenylhydrazone (FCCP) (5 mM) were dissolved in DMSO. Malonate (1 M) was dissolved in water and the pH was adjusted to 7.4 with KOH.

Respiratory substrates and coenzymes Succinate, glutamate, malate and pyruvate (1 M) were dissolved in water and the pH was adjusted to 7.4 with KOH. Oxaloacetate, citrate, isocitrate and oxoglutarate (10 mM) were dissolved in water and aliquots were stored at –20°C for a maximum period of two weeks. Coenzyme A, acetyl–CoA and succinyl–CoA were dissolved in water and aliquots

were stored at –20°C. ADP (10 mM) was prepared freshly before use by dissolving in 10 mM KOH, the pH was adjusted to 7.4 by KOH.

Cofactors NADH and NAD^+ (10 mM) were prepared fresh on the day of use. Thiamine pyrophosphate (10 mM) was dissolved in water and stored at –20°C.

Electron carriers An analogue to coenzyme Q_{10}, decylubiquinone, was used in assays of complexes I, II and III. For complex I and II, a stock of 50 mM was prepared by dissolving in DMSO. For complex III assay and before reduction to decylubuquinol, another stock with the same concentration was prepared in acidified ethanol (10 ml, ethanol 95% and 10 μl of 1 M HCl to give a pH $\leq$4). Stocks of 1 mM ferricytochrome *c* and 10 mM 2,6-dichloroindophenol (DCIP) were prepared by dissolving in water. Aliquots of each compound were stored at –20°C.

Other stocks L-carnitine (50 mM) was dissolved in KHB and aliquots were stored at –20°C for a maximum period of one month. L-cysteine (10 mM) and DL-dithiothreitol (10 mM) were prepared fresh by dissolving in water. Stock of 10 mM 5,5′-dithiobis-2-nitrobenzoic acid (DTNB) was dissolved in ethanol and stored at –20°C. EDTA (100mM) was dissolved in water and pH was adjusted to 7.2 by NaOH.

BSA stock BSA (50 mg/ml) was dissolved in warm water at 37°C, then filtered sterile in the laminar flow hood. Aliquots were stored at –80°C. Immediately before use, it was thawed at 37°C.

Fluorescent probes The mitochondrial probe tetramethylrhodamine methyl ester (TMRM) was purchased from Molecular Probes®- Life Technologies, Prague, Czech republic, and a stock of 0.5 mM was prepared by dissolving in ethanol. Aliquots were stored at –20°C.

Triphenylphosphonium moieties Dry salts of various alkyl triphenylphosphonium bromide (alkylTPP^+) were dissolved in DMSO at a concentration of

100 mM and stored at –20°C. TPP^+ derivatives dissolved in DMSO included propyl-, hepty-, decyl-, and dodecylTPP^+, while TPMP was dissolved in water at the same concentration. To ensure equimolar concentrations, standard curves of different stocks were created with concentrations ranging from 0-200 μM. In UV spectral scan, TPP^+ conjugated compounds show 3 distinctive peaks at 261, 267, and 275 nm. The extinction coefficient for alkylTPP^+ compounds in DMSO at 278 nm is ε_{278} = 2500 $M^{-1}cm^{-1}$ (Trnka, 2008).

2.1.2 Collection of rat tissues

Rat skeletal muscle tissue was used to provide samples with high yield of mammalian mitochondria. Wistar rats 13-15 weeks old weighing 200-300 gm were obtained from AnLab Ltd., Prague, Czech Republic. The rat was sacrificed by anaesthetic overdose prior to tissue isolation. Both gastrocnemii muscles were collected to prepare a homogenate enriched in mitochondrial fraction. Animal use and sacrifice was approved in accordance with Charles University in Prague, Third Faculty of Medicine animal use protocols.

2.1.3 Preparations

2.1.3.1 Isolation of mitochondria from cultured cells

C2C12 myoblasts were harvested by trypsin and suspended in growth medium supplemented with 10% FBS, then the suspension was centrifuged in a swinging-bucket rotor at 1000× g at room temperature for 15 minutes. Differentiated myotubes were scraped by a sterile tissue scraper in ice-cold PBS, followed by centrifugation at equal speed and temperature used with myoblasts. Supernatant was removed and the pellets were suspended in 750 μl ice-cold cell homogenization medium (CHM). The cells were disrupted mechanically with a 2 ml glass tight-fitting Dounce homogenizer (Wheaton type B) on ice. After homogenization, 250 μl of ice-cold CHM + sucrose were added. The homogenate was centrifuged (5 min at 1000× g and 4°C) in a fixed-angle rotor. The 1 ml supernatant was removed and centrifuged again (10 min at 5000× g and 4°C), and the resulting supernatant was carefully removed. The mitochondrial pellet was resuspended in

0.5 ml of sucrose/Mg^{2+} medium and centrifuged (10 min at 5000× g and 4°C). The pellet was resuspended finally in mitochondrial separation medium then flash frozen in liquid nitrogen and stored at –80°C.

2.1.3.2 Preparation of muscle homogenate enriched in the mitochondrial fraction

A skeletal muscle homogenate was prepared by modifying a previously described protocol (Spinazzi et al., 2012). A freshly removed rat gastrocnemius was washed three times by ice-cold buffer STEB buffer then flash frozen in liquid nitrogen, and stored at –80°C. On the preparation day, the visible fat and connected tissue were removed by a scalpel blade, then the muscle was finely dissected into small fragments (≈ 5×5 mm) in a glass dish on ice. The muscle pieces were diluted 1:10 in ice-cold MHM then the suspension was transferred to a glass tube and chopped with an UltraTurrax blender followed by homogenization in a Dounce homogenizer with a motor-driven Teflon plunger at 500 r.p.m (≈ 10 passes). The homogenate was then centrifuged for 15 min at 600 × g at 4°C. The supernatant was transferred into ice-cold tubes then flash frozen in liquid nitrogen and stored at –80°C.

2.1.3.3 Preparation of BSA conjugated palmitate

The protocol of preparation was obtained from *www.seahorsebio.com*, and it is designed for studying the free fatty acid oxidation using the XF-24 analyzer. Palmitate was prepared with a minimum concentration of BSA due to interference of BSA with the measuring process. The final concentration was aimed to be 1 mM sodium palmitate /0.17 mM BSA (6:1 FA:BSA).

Dissolving BSA Prior to the preparation of palmitate, a solution of 0.34 mM ultra-fatty acid free BSA was prepared in a glass beaker by dissolving in a freshly prepared solution of 150 mM NaCl in a pre-warmed water bath at 37°C on a heated stir plate. Temperature was not allowed to exceed 40°C and the mixture was continuously stirred till complete dissolving, while the beaker was covered with a parafilm. The BSA solution was transferred to the laminar flow hood

and was filtered sterile. One half of the solution volume was taken for palmitate conjugation and returned to the warm water bath and the other half was diluted with 150 mM NaCl to reach a final concentration of 0.17 mM. Aliquots were stored frozen in glass tubes at –20°C.

Dissolving palmitate Sodium palmitate was dissolved into a solution of 150 mM NaCl in a covered glass tube by continuous stirring on a heated stir plate at 70°C water bath. Once the solution became colorless indicating complete dissolving of sodium palmitate, the parafilm cover was removed and dissolved sodium palmitate was drop wise transferred to the warm BSA solution with maintained stirring to start the conjugation process.

Conjugation of free palmitate to BSA For conjugation of palmitate to BSA the mixture was left with continuous stirring at 37°C for 1 hour, while monitoring the temperature of the water bath not to exceed 40°C. The final volume was adjusted in a glass graduated cylinder by 150 mM NaCl and the pH was adjusted to 7.4 by NaOH. Aliquots were frozen in sealed glass tubes at –20°C under argon for a maximum period of 2 weeks. Before use, palmitate and BSA were warmed to 37°C for 30 min.

2.1.3.4 Reduction of decylubiquinone to decylubiquinol

Reduced decylubiquinone (decylubiquinol) was prepared by modifying a previously published protocol (Trounce et al., 1996). Decylubiquinone (50 mM) dissolved in acidified ethanol was reduced by adding few grains of $NaBH_4$ on a 10 μl pipet tip. The mixture was then vigorously vortexed till the solution became colorless. The mixture was immediately centrifuged at 5000 $\times g$ then the supernatant was stored at –20°C under argon.

2.1.3.5 Reduction of ferricytochrome *c*

Ferrocytochrome *c* was prepared by modifying a previously published protocol (Spinazzi et al., 2012), and it was freshly prepared by adding few grains of sodium

dithionite to 1 mM stock of ferricytochrome *c* and vortexing till the dark brown color of ferricytochrome *c* slightly changed to pink brownish color.

2.1.3.6 DodecylTPP$^+$ re-purification*

Approximately 500 mg of dodecylTPP$^+$ salt were dissolved in minimal volume of dichloromethane, then added drop wise to ether producing a white suspension, that was left to precipitate at 4°C. The ether was decanted and the precipitate was washed 2 times in ether. These steps were repeated three times to ensure the highest possible purification. The last precipitation step took place in a glass Petri dish. After washing with ether, the white solid precipitate was scratched gently and left to dry.

2.2 Cell culture

C2C12 cells were obtained from Sigma-Aldrich, and the first subcultures were frozen in liquid nitrogen until needed for experiments. The cell culture conditions were similar through the time of the study. All cultures were incubated at 37°C in an atmosphere of 95% humidity and 5% CO_2. The medium was changed every 48 hours.

2.2.1 Cell proliferation protocol

Prior to experiments of comparison between different metabolic phenotypes, cells were grown for seven days in the various culture media (low glucose, LG; high glucose, HG; galactose, GAL or carbohydrate-free, CF) to allow cellular adaptation. All variants of growth media consisted of Dulbecco's-modified Eagle's medium (DMEM, Life Technologies) containing no glucose and supplemented with 10% fetal bovine serum, 100 unit/ml penicillin- 100 μg/ml streptomycin, and 1 mM sodium pyruvate. LG and HG medium further contained 1 g/l or 5 g/l of D-glucose respectively. GAL medium was supplemented with 1 g/l D-galactose, and CF medium was left without any carbohydrate addition.

*Re-purification of dodecylTPP$^+$ was a kind advise of prof. Robin A.J. Smith to get rid of impurities that might induce a misleading redox activity, such as triphenylphosphine.

2.2.2 Differentiation protocol

To induce differentiation, cells were seeded in culture plates or Seahorse XF-24 cell plates and were allowed to grow to approximately 80-90% confluence in the growth medium. The growth medium was then replaced with a differentiation medium (DMEM supplemented with 2% FBS, 100 unit/ml penicillin and 100 μg/ml streptomycin, 1 mM sodium pyruvate) to induce myogenic differentiation and changed every 48 hours (Mailloux and Harper, 2010; Miyake et al., 2011) for seven days prior to any assay. The LG phenotype was treated with growth and differentiation media containing 1 g/l glucose, while the HG phenotype was treated with media supplemented with 5 g/l glucose.

2.3 Spectrophotometric assays

The spectrophotometric measurements of both endpoint and kinetic assays were performed using the single wavelength microplate reader Infinite M200Pro from TECAN. Commercial kits were purchased for the endpoint measurements, while all the reaction mixtures for the kinetic assays were prepared by modifying previously published protocols*.

2.3.1 Endpoint assays

2.3.1.1 Galactose assay

Galactose concentration in tissue culture media was measured using Amplex® Red galactose/galactose oxidase kit (Life Technologies). Samples were collected from growth medium with controls of medium incubated without seeded cells during 24 hours with a time interval of 3 hours between each collection. Collected samples were stored at –20°C till the time of the assay. Before the assay, samples were left to reach room temperature. Galactose oxidation in the samples is catalyzed by the enzyme galactose oxidase, generating hydrogen peroxide which then reacts with Amplex® Red reagent in the presence of horseradish peroxidase enzyme producing the red fluorescent resourfin. A standard curve of 0-40 μM

*The used protocols were modified mainly to fit in the microplate reader.

galactose was prepared and measured simultaneously with other samples. The plate was incubated at 37°C for 30 min and the endpoint absorbance at 560 nm was measured in the microplate reader.

2.3.1.2 Bicinchoninic acid (BCA) assay

Samples and BSA standards (0-1000 μg/ml) were diluted in deionized water and 25 μl aliquots were added in triplicate to a 96-well microtitration plate. The assay buffer was prepared by mixing 50 parts of reagent A (1% BCA, 2% Na_2CO_3, 0.16% Na_2-tartrate, 0.4% NaOH, 0.95% $NaHCO_3$ (all w/v), pH 11.25) with 1 part of reagent B (4% (w/v) $CuSO_4$.5 H_2O) and 200 μl was pipetted into each well. The plate was incubated at 37°C for 30 min and the endpoint absorbance at 562 nm was measured in the microplate reader.

2.3.2 Enzymatic assays

The enzymatic activities were assessed using samples that included enriched mitochondrial fraction of isolated mitochondria from cultured cells and homogenate prepared from rat skeletal muscle, except the pyruvate dehydrogenase complex which was obtained purified from porcine heart due to the high interference of the active lactate dehydrogenase in the prepared samples, even after trials to limit the activity of lactate dehydrogenase by including its inhibitor sodium oxamate in the assay reaction mixture (Schwab et al., 2005).

When the prepared samples were used and prior to the assays, samples were exposed to three cycles of rapid freeze-thawing. All the samples were always handled on ice. In assays where the extinction of NAD(H) was followed, a final concentration of 10 μM rotenone and 1 μM antimycin A were included to block the activity of the respiratory chain complexes.

2.3.2.1 Pyruvate dehydrogenase complex

Using the manufacturer protocol, in an assay mixture containing 100 mM Tris (pH 7.4), 0.2 mM $MgCl_2$, 10 μM $CaCl_2$, 2 mM NAD^+, 2.6 mM L-cysteine, 0.12 mM CoA, 2.5 mM L-carnitine, 0.3 mM thiamine pyrophosphate and 0.005

U/ml purified pyruvate dehydrogenase. The reaction was started with the addition of sodium pyruvate to reach a final concentration of 1 mM. The extinction was followed at 340 nm for 3 minutes with 20 seconds interval at 30°C. The activity was calculated using the linear increase in absorbance due to accumulation of NADH.

2.3.2.2 Citrate synthase assay

Using a previously published protocol (Spinazzi et al., 2012), in an assay mixture containing 100 mM Tris (pH 8), 0.1% Triton X-100, 0.1 mM 5,5′-dithiobis-2-nitrobenzoic acid DTNB, and 0.3 mM acetyl-CoA. The reaction was started with the addition of freshly prepared sodium oxaloacetate to reach a final concentration of 0.5 mM. The activity was calculated using the linear increase in absorbance at 412 nm due to formation of 2-nitro-5-thiobenzoate (TNB) over 3 minutes with 20 seconds interval at 37°C.

2.3.2.3 NAD^+ dependent isocitrate dehydrogenase*

Using a modified protocol (Chen and Plaut, 1963), in an assay mixture containing 70 mM Tris-acetate (pH 7.6), 0.1% Triton X-100, 0.1 mM EDTA, 10 μM rotenone, 1 μM antimycin A, 2.5 mM $MnCl_2$, 1 mM DL-dithiothreitol (DTT), 0.8 mM NAD^+, and 1 mM ADP. The reaction was started with the addition of trisodium isocitrate to reach a final concentration of 8 mM. The extinction was followed at 340 nm for 3 minutes with 20 seconds interval at 30°C. The activity was calculated using the linear increase in absorbance due to accumulation of NADH.

2.3.2.4 2-Oxoglutarate dehydrogenase complex

Using a modified protocol (Goncalves et al., 2010), in an assay mixture containing 100 mM Tris (pH 8), 0.1% Triton X-100, 0.1 mM EDTA, 10 μM rotenone, 1 μM antimycin A, 2 mM $MgCl_2$, 2 mM $CaCl_2$, 0.8 mM NAD^+, 2 mM DTT, 0.5 mM CoA, and 0.1 mM thiamine pyrophosphate. The reaction was started with the addition of sodium oxoglutarate to reach a final concentration of 2 mM. The

*The cytosolic isoforms of isocitrate dehydrogenase (IDH1 and IDH2) use $NADP^+$ as a cofactor, unlike the mitochondrial isoform (IDH3) which uses NAD^+.

extinction was followed at 340 nm for 3 minutes with 20 seconds interval at 30°C. The activity was calculated using the linear increase in absorbance due to accumulation of NADH.

2.3.2.5 Malate dehydrogenase*

Using a modified protocol (Goncalves et al., 2010), in an assay mixture containing 100 mM Tris (pH 8), 0.1% Triton X-100, 0.1 mM EDTA, 10 μM rotenone, 1 μM antimycin A, 2.5 mM $MgCl_2$, 0.8 mM NAD^+, 1 mM DTT, and 0.3 mM acetyl-CoA. Acetyl-CoA was added to accelerate the elimination of the formed oxaloacetate to obtain a linear reaction. The reaction was started with the addition of sodium malate to reach a final concentration of 10 mM, and the extinction was followed at 340 nm for 3 minutes with 20 seconds interval at 30°C. The activity was calculated using the linear increase in absorbance due to accumulation of NADH.

2.3.2.6 Complex I assay

Using a modified protocol (Janssen et al., 2007), in an assay mixture composed of 20 mM potassium phosphate (pH 7.8), 3.5 g/l BSA, 2 mM EDTA, 60 μM 2,6-dichloroindophenol (DCIP), 70 μM decylubiquinone, 1 μM antimycin A and 0.2 mM NADH. The reaction was induced by the addition of NADH. The activity was calculated using the linear decrease in absorbance at 600 nm over 5 minutes with 20 seconds interval at 37°C. Rotenone sensitive activity was then calculated by inhibiting the reaction in the control wells by a concentration of 10 μM of rotenone, and subtracting the average activity of the control wells from the average activity of the non inhibited wells.

2.3.2.7 Complex II assay

Using a modified protocol (Janssen et al., 2007), in an assay mixture composed of 80 mM potassium phosphate (pH 7.8), 1 g/l BSA, 2 mM EDTA, 10 mM succinate, 1 mM sodium azide, 80 μM DCIP, 50 μM decylubiquinone, 1 μM antimycin A

*The cytosolic isoform (MDH1) and the mitochondrial isoform (MDH2) of malate dehydrogenase use NAD^+ as a cofactor.

and 3 μM rotenone. The reaction was induced by the addition of succinate. The activity was calculated using the linear decrease in absorbance at 600 nm over 5 minutes with 20 seconds interval at 37°C. Malonate sensitive activity was then calculated by inhibiting the reaction in the control wells by a concentration of 20 mM of potassium malonate (pH 7.8), and subtracting the average activity of the control wells from the average activity of the non inhibited wells.

2.3.2.8 Complex III assay

Using a modified protocol (Luo et al., 2008), in an assay mixture composed of 25 mM potassium phosphate (pH 7.4), 50 μM ferricytochrome *c*, 4 mM sodium azide, 0.1 mM EDTA, 0.025% Tween®20 and 50 μM decylubiquinol (2.1.3.4). The reaction is induced by the addition of decylubiquinol. The activity was determined using the linear increase in absorbance at 550 nm due to gradual reduction of ferricytochrome *c* over 5 minutes with 20 seconds interval at 37°C. Antimycin A sensitive activity was then calculated by inhibiting the reaction in the control wells by a concentration of 10 μM of antimycin A, and subtracting the average activity of the control wells from the average activity of the non inhibited wells.

2.3.2.9 Complex IV assay

Using a modified protocol (Cooperstein and Lazarow, 1951), in an assay mixture composed of 30 mM potassium phosphate (pH 7.4) and 50 μM of freshly reduced ferrocytochrome *c* (2.1.3.5). The absorbance was measured at 550 nm over 5 minutes with 20 seconds interval at 37°C. The extinction of completely oxidized samples by few grains of potassium hexacyanoferrate(III) was first subtracted from that at any given time, then the natural logarithm of this difference was plotted against time.

2.3.2.10 Interaction of TPP^+ with DCIP

To test the effect of alkylTPP^+ on electron transport chain complexes, it was necessary to use TPP^+ concentrations equivalent to those in energized mitochondria exposed to micromolar extracellular concentrations, assuming an approximate

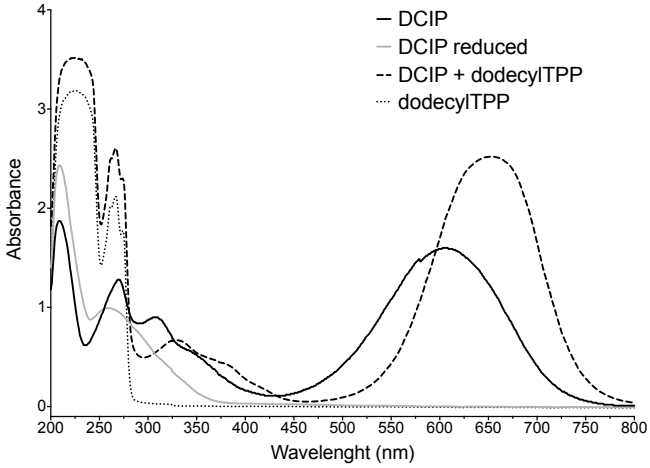

Figure 2.1: Interaction of 1 mM dodecylTPP$^+$ with 100 μM DCIP.

1000 $\times$ accumulation according to the Nernst equation and normal mitochondrial membrane potential. However, high concentrations of decyl- and dodecyl-TPP$^+$ ($\geq$ 300 μM) appear to interfere with complex I and II assays due to the formation of a complex with DCIP with a shifted absorbance maximum.

DCIP at the same concentrations also interferes with complex IV assay, as the addition of ferricyanide to the reaction mixture induces the formation of a precipitate complicating the reading of absorbance. Therefore, instead of running the assay in the presence of adding 1 mM concentration of the alkylTPP$^+$ derivatives, the muscle homogenate was preincubated with the compounds at this concentration and then the rest of the assay mixture was added. Thus the final concentration of the TPP$^+$ decreased in order to avoid this interference.

2.4 Immunofluorescence imaging

Immunofluorescence was carried out in tissue culture dishes and plates containing glass coverslips, where the cells had been seeded and left to adhere for 30 minutes. The cells were allowed to grow to ≈80-90% confluence then the differentiation* was induced by changing to differentiation induction medium (2.2.2). Cells were

*Immunofluorescence staining was used in this work to target myogenic differentiation markers also in cases where certain phenotypes failed to differentiate.

rinsed with warm PBS then fixed with 4% paraformaldehyde in PBS for 30 minutes at room temperature, then washed with PBS and permeabilized with 0.1% Saponin for another 30 minutes.

The proteins of interest were then targeted by the specific antibodies over night at at 4°C. On the following day, slides were carefully washed with PBS and secondary anti-mouse Alexa Fluor 488 conjugate antibody (Life Technologies), was applied at a dilution of 1:200 in PBS for one hour. Final rinsing with PBS and the coverslips were mounted on glass slides using Prolong Gold Antifade Reagent (Life Technologies). The pictures were taken using Leica TCS SP II Confocal microscope.

2.4.1 Myosin heavy chain MHC

After the permeabilization step, the coverslips were carefully washed with PBS then incubated with primary monoclonal anti-myosin (skeletal, slow) antibody (Sigma-Aldrich, catalogue number M8421) at a dilution 1:4000 in PBS at 4°C over night, then the staining protocol continued as previously mentioned on the next day.

2.4.2 MyoD transcriptional factor

After the permeabilization step, the coverslips were carefully washed with PBS then incubated with primary anti-MyoD (C-20) antibodies (Santa Cruz biotechnology) at a dilution 1:100 in PBS at 4°C over night, then the staining protocol continued on the next day.

2.5 Live imaging

The electrical potential difference $\Delta\psi_m$ together with the difference in pH between mitochondrial matrix and the cytoplasm form the two components of the the proton-motive forces $\Delta\rho$ which links the electron transport chain to the ATP synthase enzyme.

Since later experiments were planned to compare $\Delta\psi_m$ of different pretreated cells, setting the quench limit for tetramethylrhodamine methyl ester (TMRM)

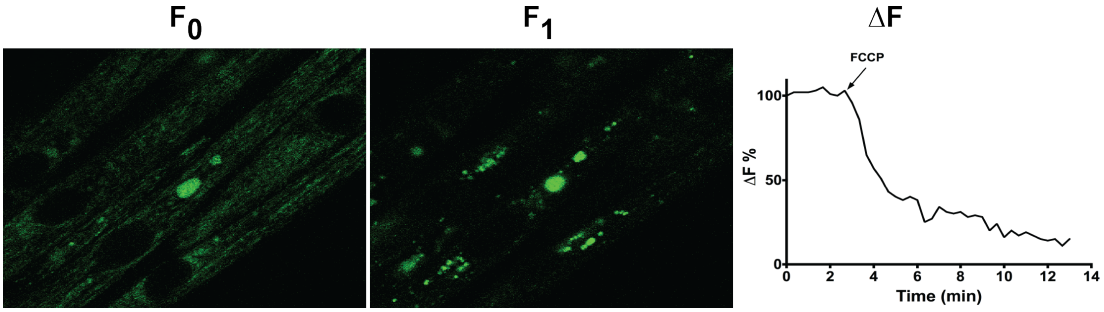

Figure 2.2: A confocal microscope scanning of C2C12 differentiated myotubes in KHB buffer and stained with 50 nM TMRM. F_0 presents the polarized state with an intact mitochondrial membrane potential. F_1 shows a diminished fluorescent signal after 2 μM FCCP treatment. Absence of an initial spike following FCCP addition confirms the run of experiment in non-quench mode. ΔF is used to determine the mitochondrial membrane potential $\Delta\psi_m$.

was necessary to ensure that all measurements are done in the non-quench mode (Nicholls, 2012). This was confirmed by the live imaging of TMRM (Life Technologies) stained cells with a time course, then 2 μM FCCP were added to induce a rapid collapse in membrane potential and a decrease in the fluorescence intensity, which was not preceded by an initial transient spike (Nicholls, 2012).

2.6 Flow cytometric analysis of $\Delta\psi_m$

Qualitative changes in $\Delta\psi_m$ were determined as the changes in TMRM fluorescence in C2C12 myoblasts (Scaduto and Grotyohann, 1999; Floryk and Houstěk, 1999). C2C12 myoblasts were allowed to grow and reach $\approx$ 80% confluence, then after washing with warm PBS, the cells were detached using trypsin for harvesting. A warm growth medium was added to deactivate trypsin and then the cell suspension was centrifuged at 500 $\times g$ at room temperature for 5 minutes. The pellet was resuspended in warm DMEM containing 50 nM TMRM for 20 minutes at 37°C with continuous gentle shaking. The cell suspension was then centrifuged and the pellet was resuspended in warm DMEM and exposed for 10 minutes to the tested compounds or the vehicle. A FACSCalibur flow cytometer (BD Bioscience) was used to read fluorescence with an excitation wavelength of 488 nm.

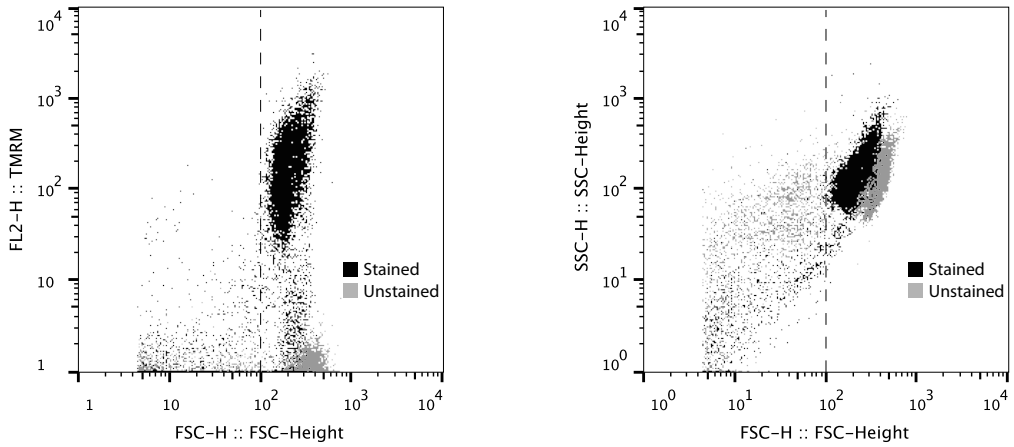

Figure 2.3: Analysis of unstained and stained C2C12 with 50 nM TMRM as a representative example of TMRM staining strategy detected by the flow cytometry. The selection of the events of interest was based on the forward and side scatter. Events with a low FSC were excluded.

2.7 Analysis of metabolism

Cellular respiration was measured using the extracellular flux analyzer XF-24 from Seahorse Bioscience. This technology allows a real time simultaneous detection of oxygen and free proton rates in the tested environment as indicators of cellular metabolism. The used protocols differed according to the general settings of each set of experiments. However, the seeding protocol was identical in all cases, except when different phenotypes were to be examined within the same plate.

When myoblasts were the subject of investigation, the cells were seeded according to the tested phenotype in the same culture conditions (2.2.1). Approximately 25,000 cells per well of LG and HG phenotypes, and 30,000 cells per well of GAL and CF phenotypes were seeded onto the analysis plates and left overnight to attach in the respective culture medium to obtain a monolayer of cells. The higher seeding number of GAL and CF cells was to compensate for slower growth rates. When myotubes were used for experiments, the cells were grown in the seeding plates to confluence and then differentiation was allowed for 7 days as previously mentioned (2.2.2).

2.7.1 Intact cells

In intact cells, mitochondrial bioenergetic assays were performed based on published protocols (Wu et al., 2007). The assay medium was composed of XF assay medium (HCO_3^- free modified DMEM, Seahorse Bioscience), which was supplemented with 4 mM L-glutamine and 1 mM pyruvate and with further additions relevant to the experiment. The pH was adjusted to 7.4 at 37°C by NaOH.

The culture medium was changed to the assay medium, followed by an hour incubation in a CO_2 free incubator. The mitochondrial respiration test was then performed by sequential additions of 1 μM oligomycin, 0.4 μM FCCP and 1 μM rotenone/antimycin A in the case of myoblasts and 1 μM oligomycin, 1.5 μM FCCP and 1 μM rotenone / antimycin A in the case of myotubes.

2.7.2 Free fatty acid oxidation in myotubes

The cells were seeded and allowed to differentiate using the same protocol (2.2.2). The culture medium was changed to KHB (2.1.1.1), followed by an hour incubation in a CO_2 free incubator. After measuring the respiration in the basal state, BSA-conjugated palmitate 100 μM was introduced twice to reach a final concentration of 200 μM. The control wells were treated with a vehicle containing BSA at a concentration of 17 μM, and 34 μM with the second injection of palmitate. This was followed by an injection of 1 μM oligomycin then 1 μM rotenone/antimycin A.

2.7.3 Permeabilized cells

The respiratory activity in permeabilized C2C12 myoblasts were assayed using a modification of a published protocol (Salabei et al., 2014). Cells were seeded and left to attach and proliferate overnight as previously mentioned. The assay was performed in mitochondrial assay solution (2.1.1.1). The used substrates included 5 mM pyruvate/ 2.5 mM malate, 5 mM glutamate/ 2.5 mM malate or 10 mM succinate and 10 μM rotenone. Cellular permeabilization was performed using the XF plasma membrane permeabilizer reagent (XF-PMPR, Seahorse Biosciences) at a final concentration of 1 nM just prior to the measurement. No further

incubation of the cells was required and the measurement started as recommended without the equilibration step. After measuring the OCR in basal state, 10 μM TPMP or vehicle were injected, followed by injection of 0.5 μM FCCP and 1 μM antimycin A. The term proton production rate (PPR) was preferably used as an analogue to ECAR in the permeabilized cells.

2.7.4 Normalization of data

The normalization was done using two methods. When more than one phenotype were examined, parallel experiments were conducted, in which the cells were seeded identically into the assay plates. At the time of measurement, the cells of the parallel plates were lysed to quantify the protein content using BCA assay for protein determination (2.3.1.2). The results of respiratory analysis (OCR) were expressed in pmol $(O_2).min^{-1}.(\mu g\ protein)^{-1}$ and the results of glycolytic activity (ECAR) were expressed in $mpH.min^{-1}.(\mu g\ protein)^{-1}$.

When the experiments were designed to investigate the effect of alkylTPP$^+$ compounds, the measured factor was normalized to its value in the basal state. The data therefore is expressed as the percentage of basal OCR (OCR%), ECAR (OCR%) or PPR (PPR%).

2.7.5 Calculation of respiratory and glycolytic parameters

The concluded mitochondrial respiratory parameters were represented as oxygen consumption rate (OCR). These parameters included basal respiration, basal mitochondrial respiration (*basal cellular OCR minus non-mitochondrial OCR*), ATP turnover-driven respiration (*basal OCR minus oligomycin-inhibited OCR*), maximal respiratory capacity (*maximal uncoupled OCR minus non-mitochondrial OCR*), spare respiratory capacity (*maximal uncoupled OCR minus basal OCR*), proton leak (*oligomycin-inhibited OCR minus non-mitochondrial OCR*) and non-mitochondrial respiration (*rotenone/antimycin A inhibited OCR*).

Glycolytic activity represented as extracellular acidification rate (ECAR) was measured simultaneously with respiration and the following parameters were established: basal ECAR, oligomycin-stimulated ECAR (maximal glycolytic capacity), and glycolytic reserve (*oligomycin-stimulated minus basal ECAR*).

2.8 Statistical analysis

The mentioned values in this work are presented as means or difference of means and 95% confidence interval (CI) between square brackets (Gardner and Altman, 1986; Cumming, 2012).

When more than 2 groups were to be compared, one-way ANOVA with Tukey post-hoc test for statistical significance of difference of means was performed. When the comparison included two groups, Student's t-test with Welch's correction with the alpha level set to 0.05 was performed. Differences passing these tests were considered statistically significant and are marked with an asterisk. Statistical analyses were performed using GraphPad Prism version 6.0d for Mac OS X, GraphPad Software, La Jolla California USA, www.graphpad.com. The number of independent experiments is denoted as n.

Results and Discussion

Chapter 3

Low glucose but not galactose enhances oxidative respiration

This chapter discusses the ability of the C2C12 myoblasts to grow and differentiate in galactose supplemented culture media, and the associated changes in mitochondrial respiratory function. Several studies demonstrated the inability of skeletal muscle to consume galactose as a fuel for energy production (Resnick and Hechter, 1957; Dvornik, 1987; Heidenreich et al., 1993), however, replacing glucose with galactose in tissue culture media was introduced as a method to enhance mitochondrial respiration and to reveal mitochondrial dysfunction in human primary myotubes (Aguer et al., 2011), which I discussed in detail in the Introduction (1.4.2).

In a trial to interpret the confusion about the use of galactose with skeletal muscle, we hypothesized that the observed changes in the galactose-treated muscle cells are primarily due to glucose deprivation. In order to distinguish the differences between galactose-treated and glucose-deprived cells, we created a set of different metabolic phenotypes by incubating C2C12 myoblasts in the presence or absence of various sugars for at least 3 successive generations, and we used the following generations with subculture numbers from 4-8 for experiments. The phenotypes included cells adapted to a low concentration (1 g/l) of glucose (**LG**) or galactose (**GAL**), a carbohydrate-free environment phenotype (**CF**) and a high concentration (5 g/l) of glucose (**HG**).

3.1 C2C12 cells do not substitute glucose with galactose as energy substrate

We first compared the growth rates of the different metabolic phenotypes of C2C12 myoblasts. The fastest growth rate occurred in the LG phenotype where the cells achieved a doubling time ≈17.16 h, 95% CI[15.19, 19.70]. The presence of galactose did not seem to provide the GAL phenotype with any advantage and both GAL and CF phenotypes maintained a similar, slower growth rate: GAL ≈24.24 h, 95% CI[21.40, 27.93] and CF ≈23.44 h, 95% CI[21.79, 25.36] (Figure 3.1 A,B).

Based on these observations, it is clear that no significant difference can be found in the growth rate between cells incubated with galactose and cells deprived of glucose, and that galactose is not to replace glucose for C2C12 cells *in vitro*. In order to find out whether C2C12 cells can utilize galactose as a source of energy, it was necessary to estimate the consumption rate of galactose in this growth condition by measuring the concentration of galactose in the incubation medium with time intervals, aiming to conclude the gradual decline in media galactose level.

To avoid possible errors due to the persistent heating and evaporation during the incubation time, a control was created of incubated medium in wells without

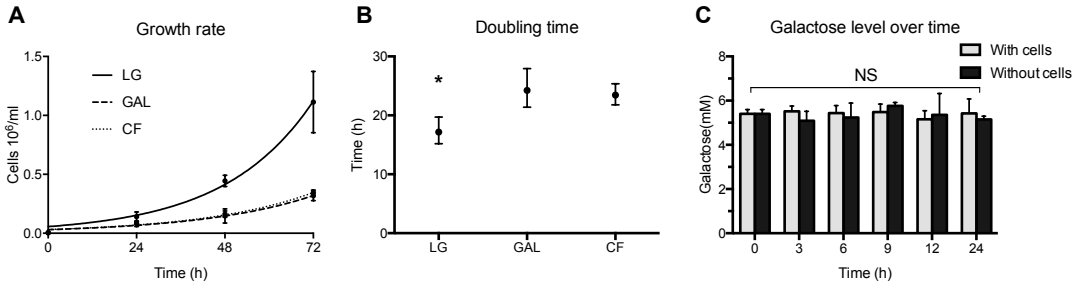

Figure 3.1: **A.** Growth rate of C2C12 myoblasts over 3 days in LG, 1 g/l glucose; GAL, 1 g/l galactose, CF, carbohydrate-free showing the higher rate of growth when glucose is available. **B.** The doubling time was concluded from a regression analysis of the cell counting data. **C.** Galactose concentration in incubation media did not change over time. Results are presented as means ±95% CI, * indicates $p<0.05$, (n=3, each experiment was performed in triplicate).

cells. The concentration of galactose in the initial time point (0 hour) was considered as a reference, and these samples were taken before the incubation. Further samples were then taken from the control wells simultaneously at similar time points. The colorimetric assay (2.3.1.1) indicated that galactose concentration in the incubation medium did not change over time in either wells containing cells or control, cell-free wells (Figure 3.1 C), suggesting that C2C12 cells cannot use galactose as a major metabolic substrate.

3.2 C2C12 myoblasts fail to differentiate without glucose

We then looked at the ability of C2C12 myoblasts to differentiate into myotubes by replacing the growth medium with the differentiation induction medium containing low serum and the relevant sugar according to each phenotype.

Under the light microscope, we could observe the ability of LG phenotype

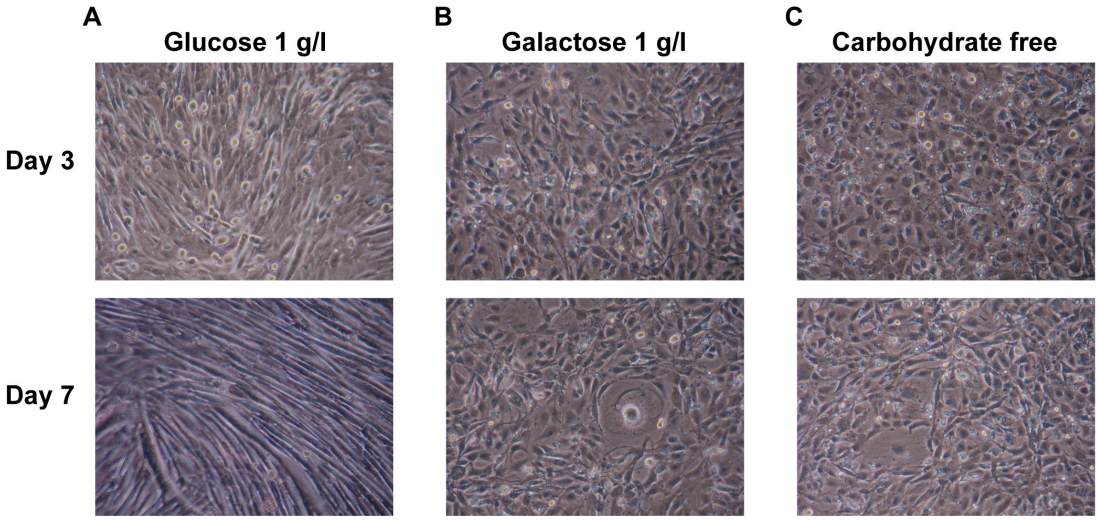

Figure 3.2: Images taken under light microscope of confluent C2C12 myoblasts exposed to low-serum medium to differentiate into myotubes.**A.** Cells in low-glucose (1 g/l) medium fused to form myotubes after 7 days in a differentiation induction medium. **B,C.** In galactose (5 g/l) and carbohydrate free media cells failed to differentiate after 7 days and few scattered large cells can be noticed in both conditions.

to differentiate by fusing into spindle shaped cells, which continued to enlarge along the course of differentiation process (Figure 3.2 A). In contrast to the LG phenotype, the other phenotypes did not show signs of differentiation or fusion. This observation was consistent with the previous findings that galactose is not a suitable consumable substrate for this type of cells (Figure 3.2 B,C). We also observed the formation of giant rounded cells in both GAL and CF phenotypes, which was never observed in the glucose exposed cells, suggesting enhanced cell senescence in absence of glucose.

3.2.1 Expression of skeletal myosin heavy chain

Skeletal muscle differentiation process is characterized by the expression of contractile protein markers such as myosin heavy chain (MHC), which is considered as a marker for the terminally differentiated myotubes (Schiaffino et al., 1986). We investigated the expression of MHC by immunofluorescence staining in all

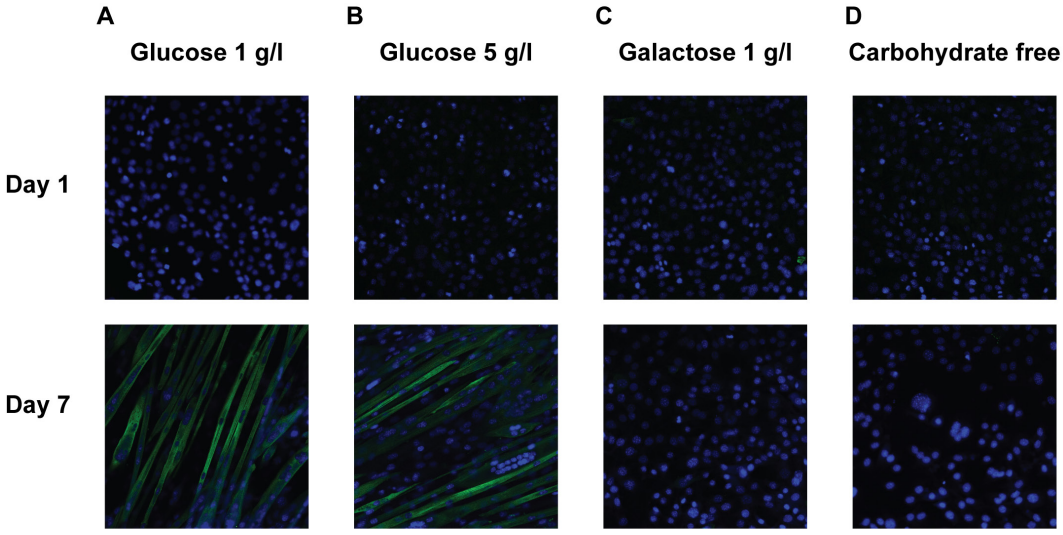

Figure 3.3: Fluorescence imaging of C2C12 before and after induction of differentiation into myotubes to follow MHC expression. Nuclei were stained with DAPI to demonstrate the presence of multi-nucleated myotubes. **A, B.** Cells in low-glucose (1 g/l) as well as in high glucose (5 g/l) media fused to form multi-nucleated myotubes after 7 days in a differentiation medium and expressed MHC. **C, D.** In galactose (1 g/l) and carbohydrate free media cells failed to differentiate after 7 days and show no sign of MHC expression.

phenotypes, including these that failed to differentiate. We tested also the HG phenotype, treated with 5 g/l glucose during the growth and differentiation, for MHC expression in order to compare the rate of differentiation in relation to glucose level.

The expression of MHC does not occur in the early stages of differentiation, and on the first day of differentiation induction, no signal of could be detected in any of the examined phenotypes. At the end of the 7 days differentiation course, well formed MHC-positive multinucleated myotubes were observed (Figure 3.3 A,B) in both LG and HG phenotypes with a similar level. When glucose was not available, there was not any positive sign of MHC expression (Figure 3.3 C,D).

3.2.2 Expression of MyoD

MyoD is a transcriptional factor belonging to the myogenic regulatory factors family (MRFs). Its expression in the undifferentiated myoblasts following the

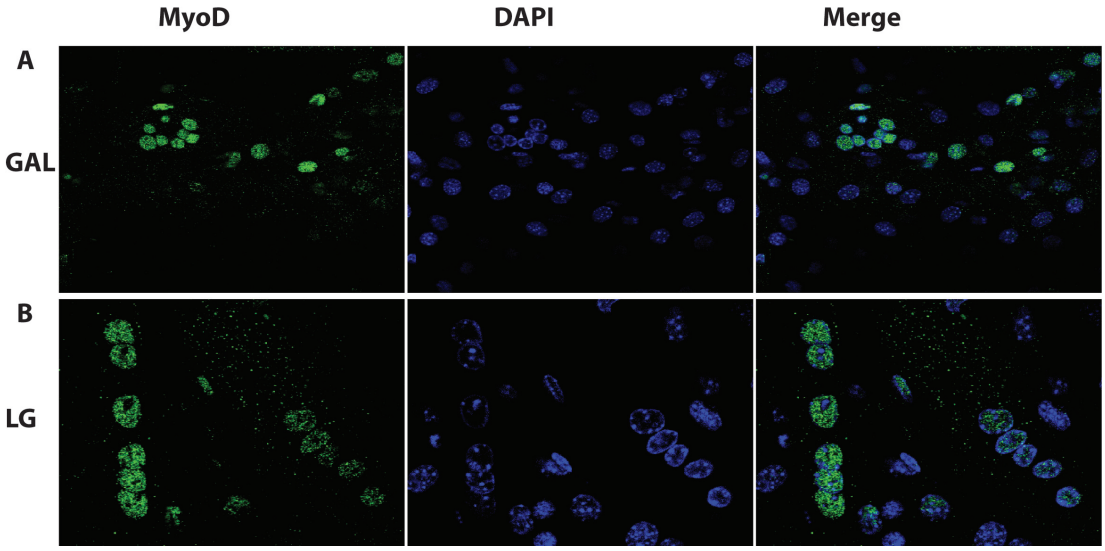

Figure 3.4: Expression of MyoD after 6 days of the differentiation induction. The nuclei are stained with DAPI to facilitate the localization the expressed MyoD. **A.** In the galactose (1 g/l) supplemented medium, the expression of MyoD can be observed in some non aligned nuclei indicating the activation of the differentiation pathway. **B.** The cells in the low-glucose (1 g/l) medium show MyoD expression in aligned nuclei.

induction of differentiation is considered an indicator of cellular differentiation activation in the early stages of myogenic differentiation pathway (Tapscott et al., 1988; Davis et al., 1989).

We used immunofluorescent staining to detect MyoD expression after six days of differentiation induction in LG and GAL phenotypes. The expression of MyoD was observed in some nuclei indicating the initiation of the differentiation pathway. The expression of MyoD occurred in both conditions, including GAL phenotype (Figure 3.4 A) where non-aligned nuclei of the C2C12 undifferentiated myoblasts showed signals indicating MyoD expression. However, its expression in the GAL phenotype was not followed by any evidence of cell fusion as observed by the light microscope (Figure 3.2 B,C). In the LG phenotype and after six days of differentiation induction, MyoD expression was observed with various signal intensities in the aligned nuclei of the differentiating myotubes. We also observed a number of nuclei that did not show signs of expression (Figure 3.4 B).

3.3 Changes in glucose availability affect mitochondrial respiratory capacity

In order to identify the changes in mitochondrial parameters due to growth conditions, and to avoid the confusion resulting from the different composition of the assay medium, we measured the mitochondrial respiration of the different phenotypes under three distinct conditions. Firstly, the initial bioenergetic state of each phenotype was examined in assay media containing sugars at concentrations equal to that of the growth medium of each phenotype, which is essentially a replication of the study performed by Aguer et al. 2011, but using murine C2C12 instead of human primary myoblasts.

The next step was to compare mitochondrial respiration of the different phenotypes in an identical assay environment. Since the availability of glucose in the culture media was the main factor, we performed the mitochondrial respiratory analysis in the presence and absence of glucose, once in the standard assay medium with 1 g/l glucose and another in an assay medium not supplemented with glucose.

3.3.1 Respiratory parameters in growth conditions

We first assessed the mitochondrial performance under assay conditions identical to that of the culture conditions. We observed marked differences in the maximum and the spare respiratory capacities (Table 1 on page 99). Compared to no glucose, the presence of glucose in either concentration, 1 or 5 g/l, led to a significant increase in the maximal respiration and spare respiratory capacity of the glucose treated phenotypes (Figure 3.5). However, a further increase of glucose concentration over 1 g/l in the long-term culture medium caused a relative decrease in the maximal respiration and in the spare respiratory capacity of the HG phenotype, which can be translated as an aspect of mitochondrial dysfunction associated with hyperglycemic incubation. Other respiratory parameters showed no significant difference.

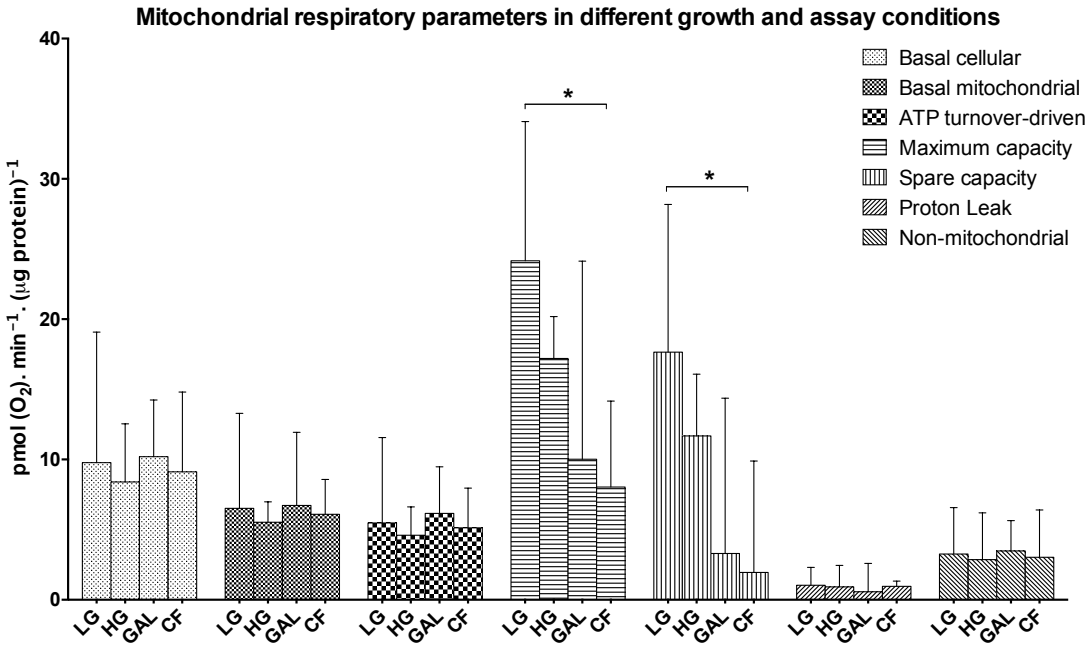

Figure 3.5: Bioenergetic profile of 4 different C2C12 metabolic phenotypes showing the mitochondrial respiratory parameters in assay media containing the same concentrations of growth medium substrates. Results are presented as means ±95% CI, * indicates $p<0.05$, (n=3, each experiment was performed in triplicate).

3.3.2 Respiratory parameters in 1 g/l glucose

When we used only one assay medium supplemented with 1 g/l glucose, cells deprived of glucose during growth exhibited a lower maximal respiration and spare respiratory capacity (Table 2 on page 100). Despite the presence of similar concentration of glucose, pyruvate and glutamine in the assay medium, the GAL and CF phenotypes maintained a significant lower respiratory capacity (Figure 3.6), which once again is an indicator of an established defect in the respiratory machinery.

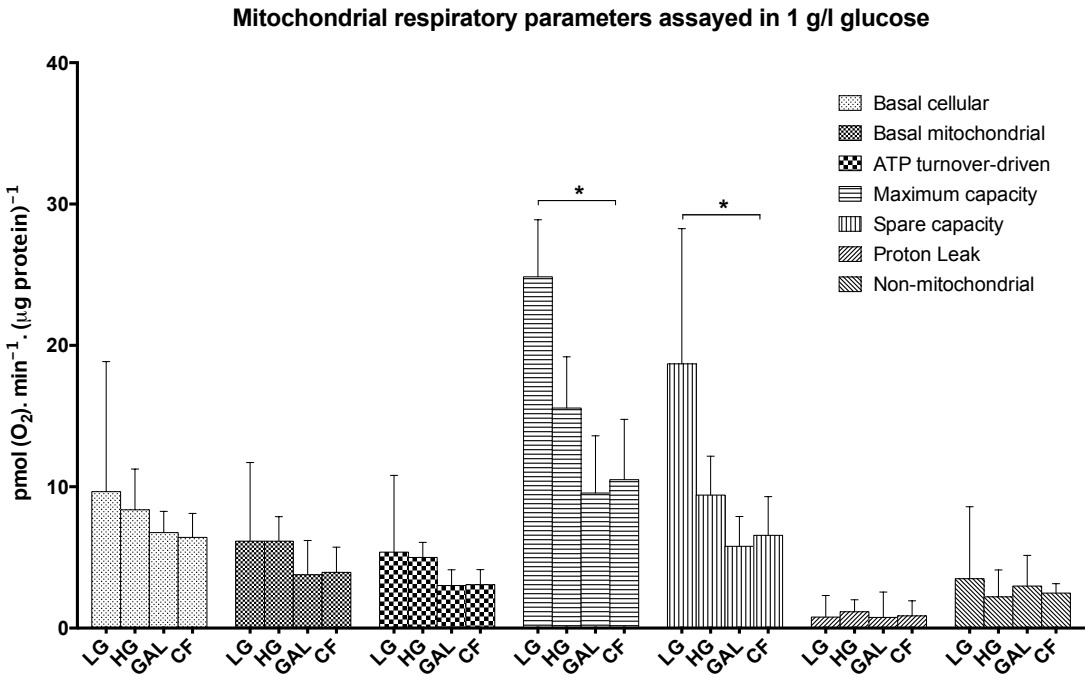

Figure 3.6: Bioenergetic profile of 4 different C2C12 metabolic phenotypes showing the mitochondrial respiratory parameters in assay media supplemented with 1 g/l glucose. Results are presented as means ±95% CI, * indicates $p<0.05$, (n=3, each experiment was performed in triplicate).

We expected that the GAL and the CF phenotypes will maintain a higher basal oxygen consumption, but in contrast to the expected outcome of cell incubation in glucose-free media, there was a slightly higher basal mitochondrial and ATP turnover-driven respiration in the two glucose phenotypes compared to glucose-deprived cells. This may refer to a slower metabolic rate of these

phenotypes. The differences in other mitochondrial parameters were negligible.

The differences between LG and HG phenotypes continued to persist even at a different glucose level in the assay medium. Going over 1 g/l glucose in the culture medium of the LG phenotype to 5 g/l in the HG case caused more decrease in the maximal respiration and spare respiratory capacity of the HG cells (Table 2 on page 100).

Decreasing glucose concentration in the assay environment induced a higher reliance on mitochondrial respiration in the HG phenotype, however, probably due to defects in the mitochondrial respiratory machinery the cells failed to cope with the sudden energy requirement. This shows that lowering glucose concentration in the assay environment can reveal a relative mitochondrial dysfunction.

3.3.3 Respiratory parameters in the absence of glucose

While the outcome of testing glucose-deprived phenotypes, GAL and CF, was already obtained in the first set of measurements (3.3.1), the main idea of performing the mitochondrial respiratory test in a glucose-free condition was to examine the behavior of the cells, especially the LG phenotype, when glucose is eliminated from the environment and to see whether these cells exhibit a higher dependence on oxidative respiration in such case, also prompting a state of glucose-starvation to LG and HG cells can activate the consumption of the stored substrates and drive the cells to depend on the exogenous substrates found in the assay medium.

Since the assay medium contained beside its content of amino acids other mitochondrial substrates such as pyruvate (1 mM) and glutamine (4 mM), in the absence of glucose the assayed cells will probably rely on mitochondria to synthesise ATP. Furthermore, we can conclude the contribution of glucose metabolism to mitochondrial respiration by comparing the results of in the previous set of experiments where glucose was in the assay medium, especially following stress induction.

The results obtained from running the assay in this condition were similar to a great extent (Figure 3.7), and there were only very small differences among all four phenotypes (Table 3 on page 100). However, a comparison of respiratory parameters between assay media with and without glucose showed dramatically

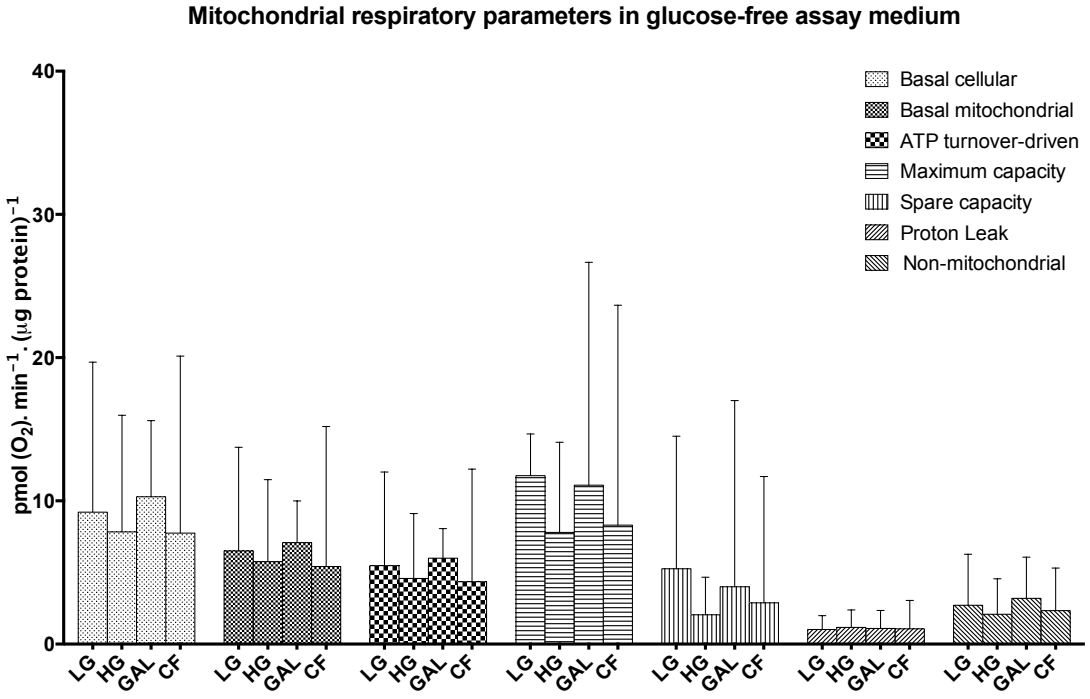

Figure 3.7: Bioenergetic profile of 4 different C2C12 metabolic phenotypes showing the mitochondrial respiratory parameters in a glucose-free assay medium. Results are presented as means ±95% CI, (n=3, each experiment was performed in triplicate).

lower respiratory capacities of the two glucose phenotypes in the no-glucose environment, which indicates that glucose utilization is probably preferred by C2C12 cells despite the presence of other oxidizable mitochondrial substrates. One possible explanation for this observation is that the available substrates in this experiment limit achievable maximal respiration, but the fact that basal respiration and ATP turnover-driven respiration are virtually at the same level regardless of glucose availability during the assay argues against the possibility of an adverse reaction to sudden glucose withdrawal.

3.4 Uniformity of mitochondrial mass markers

In order to study a possible relationship between the observed changes in the respiratory capacity and mitochondrial mass, we measured citrate synthase (CS)

activity in whole cell lysates and estimated the mitochondrial yield (μg mitochondrial protein/μg total cellular protein) in all phenotypes as indicators of mitochondrial mass (Holloszy et al., 1970; Williams et al., 1986; Hood et al., 1989).

Growing cells in different metabolic conditions did not lead to any significant change in the mitochondrial mass and we found no significant differences in CS activity among the substrate phenotypes (Table 6 on page 102). This indicates that the observed changes in mitochondrial respiratory parameters were not a result of lower mitochondrial mass, but most likely resulted from changes in the respiratory machinery within the mitochondria, either in the form of low expression or lower activity of the electron transport chain enzymes (Figure 3.8).

3.5 Effect on respiratory chain complexes

The previously described differences in the respiratory capacity indicated malfunction in the ATP production machinery and to identify the nature of these defects we analyzed the activity of the respiratory chain complexes. The activity of complexes I, II and III (Table 7 on page 102) tended to be higher in the glucose-starved phenotypes GAL and CF compared to LG and HG but without statistical significance. The activity of complex IV was significantly higher in GAL and CF phenotypes than in LG and HG ones. We also observed that no significant differences were observed within the glucose starved (GAL and CF) group nor the glucose exposed (LG and HG) group (Figure 3.8).

3.6 Impact on glycolytic activity

Since the presence of glucose in both low and high concentration provides a continuous input for glycolysis, we expected to observe differences between the glucose-fed cells and the glucose-starved phenotypes. However, in the presence of 1 g/l glucose in the assay medium we found no significant differences in any of the measured glycolytic criteria among the substrate phenotypes (Table 5 on page 101).

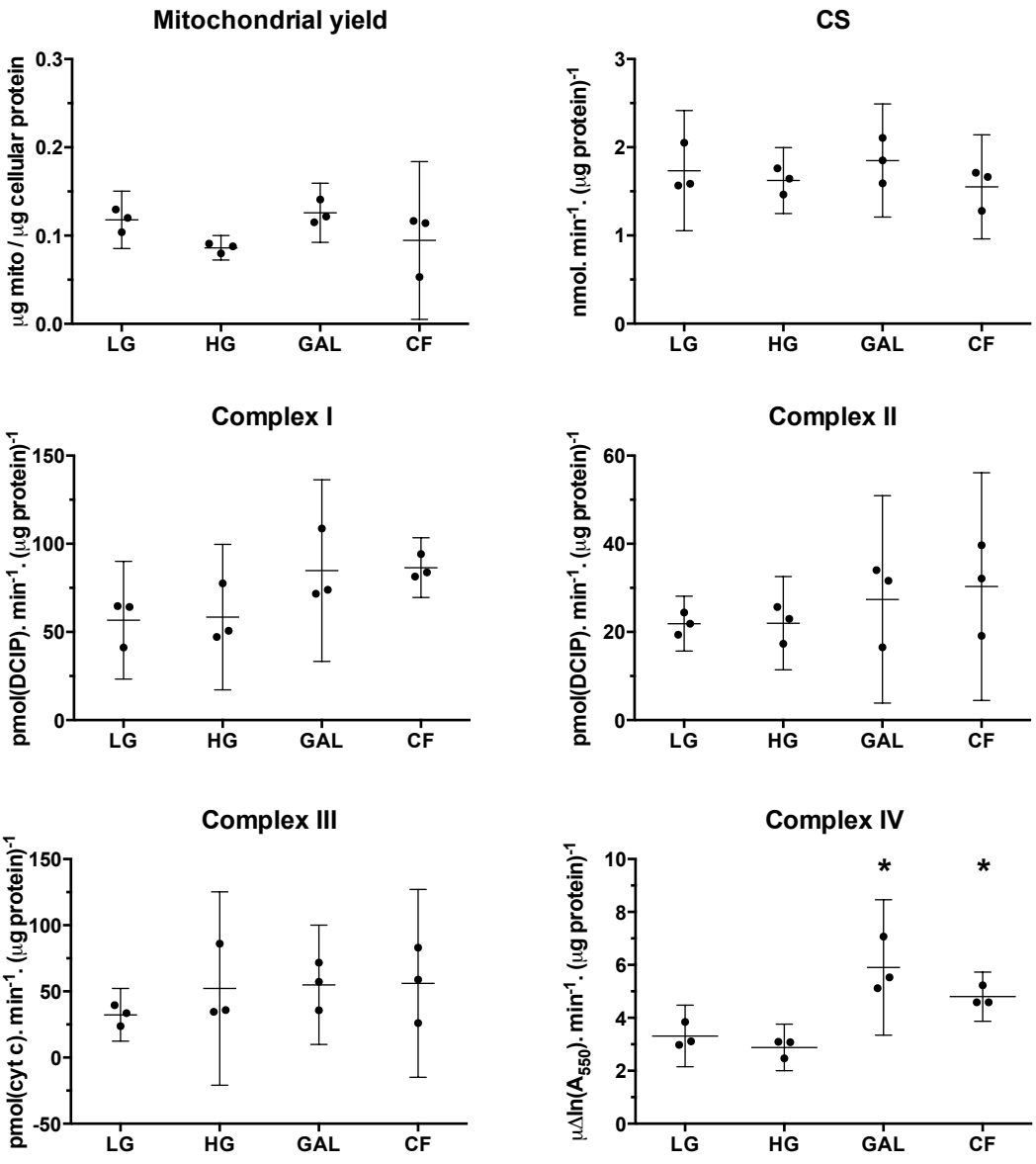

Figure 3.8: Mitochondrial mass markers and respiratory enzymatic activity of 4 different C2C12 metabolic phenotypes. Results are presented as means ±95% CI, * indicates $p<0.05$, (n=3, each experiment was performed in triplicate).

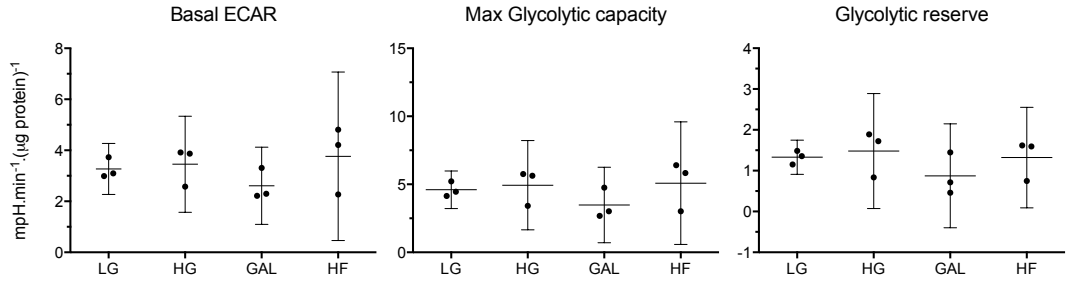

Figure 3.9: Glycolytic activity of different phenotypes of C2C12 myoblasts in 1 g/l glucose. Results are presented as means ±95% CI, (n=3, each experiment was performed in triplicate).

Under basal conditions before using any of the mitochondrial inhibitors to induce stress, all phenotypes maintained similar extracellular acidification rate ECAR (Figure 3.9), which indicates a comparable efflux of lactate and CO_2. To exclude the acidification by CO_2 as a product of Krebs cycle, the ECAR was measured after inhibiting the ATP synthase by oligomycin in order to shift the ATP production completely towards the glycolytic pathway and inhibit mitochondrial CO_2 production. Oligomycin-stimulated ECAR indicates the maximum activity of the glycolytic pathway to produce lactate by anaerobic glycolysis. By subtracting the value of basal ECAR from the maximum glycolytic capacity we get the glycolytic reserve.

3.7 Discussion

The results shown in this chapter shed some more light on the controversial use of galactose in skeletal muscle culture media. The first finding was that growing myoblasts do not utilize available galactose in the medium and had a growth rate indistinguishable from cells grown in a carbohydrate-free environment. The cellular growth rate is an important parameter that reflects the availability of nutrients within the cells, and the presence of a potentially favorable environment for cell division.

This result matches with previous publications reporting that the entry of galactose into the cells of isolated diaphragm muscle is limited, and galactose that

enters the skeletal muscle remains essentially unmodified (Resnick and Hechter, 1957) and that myoblasts do not possess enzymes necessary for galactose metabolism (Heidenreich et al., 1993). Therefore, it is reasonable to assume that C2C12 cells in the absence of glucose rely on the metabolism of pyruvate and amino acids in the growth medium irrespective of the presence or absence of galactose.

We obtained more evidence by testing the ability of C2C12 myoblasts to differentiate with galactose, pyruvate and other amino acids in the culture medium as a source of energy. The course of myogenic differentiation includes a series of processes that results in cell fusion and terminal expression of the characteristic skeletal muscle proteins, and as previously mentioned, glucose starvation is known to impair the differentiation process (Nedachi et al., 2008; Fulco et al., 2008), therefore, to investigate whether galactose can be substituted for glucose, differentiation was induced in all different phenotypes by shifting to the differentiation induction media supplemented with the relevant substrate.

Due to lack of sufficient published data describing different respiratory parameters, we performed a detailed study of mitochondrial respiration of C2C12 cells grown in media with different levels of glucose or galactose. Previous similar studies measured fewer parameters (Mailloux and Harper, 2010) or used different assay media for different phenotypes(Aguer et al., 2011). Therefore we used more experimental designs, which included analyses in the same assay medium for all phenotypes and further extended previous publications through performing experiments in different metabolic environments.

In an experimental setup directly comparable to Aguer et al. 2011, we observed the lower maximal and spare respiratory capacities of the GAL and CF phenotypes, without further differences in basal or ATP turnover-driven mitochondrial respiration. This suggests that glucose-starved C2C12 cells do not increase their oxidative metabolism. The disagreement between these results and the published study may be explained by hypothetical metabolic differences between primary human myoblasts and the C2C12 cell line.

When glucose was available in the assay environment, GAL and CF cells exhibited lower basal and maximal respiration, which goes against the hypothesis that glucose-deprivation or glucose replacement by galactose can stimulate oxidative metabolism. Both LG and HG cells exhibited a higher basal

and ATP turnover-driven respiration suggesting a stronger reliance on oxidative metabolism. However, HG cells had lower respiratory capacity than LG cells, which suggests an optimal respiratory phenotype of C2C12 cells is achieved at moderate glucose concentration. Interestingly, we could see the difference between the two glucose phenotypes in the stimulated mitochondrial respiration, which points less to a generally glycolytic metabolism in the high glucose phenotype and more to a kind of mitochondrial dysfunction(Brand and Nicholls, 2011) caused by the incubation with supraphysiological glucose concentration (5 g/l).

In the glucose-free assay medium, the differences observed in other assay conditions when glucose was available diminished, and absence of glucose masked the changes in maximal and spare respiratory capacities. However, a comparison of experiments in the presence or absence of glucose shows that in the sudden absence of glucose in the assay medium caused the two glucose phenotypes (LG, HG) to exhibit a significantly lower maximal respiration and spare capacity compared to their response in the presence of 1 g/l glucose, with similar values for other mitochondrial parameters. The glucose-deprived cells GAL and CF on the other hand had similar values of maximal and spare respiration in the absence of glucose as in the presence of glucose, but with higher basal mitochondrial respiration and ATP turnover-driven respiration.

Trying to interpret these differences, the assessment of respiratory chain activities presents a complicated picture. The glucose-starved phenotypes appeared to have a higher activity across the complexes compared to cells grown in the presence of glucose, although the differences were small and statistically insignificant except with complex IV. This suggests that the observed differences in oxidative capacity are not linked to respiratory chain capacity in any simple way, but are possibly complicated by changes in regulatory or transport pathways.

Despite of that complicated picture, none of the respiratory parameters suggested the use of galactose to enhance oxidative respiration, and all of the results showed great similarity between the GAL and CF phenotypes. Based on the results we recommend the use of low glucose during cell incubation, and in mitochondrial assay conditions in order to detect the differences between different metabolic phenotypes, and at the same time to provide an alternative (glycolytic) fuel, towards which the cells can shift upon stress induction.

Chapter 4

High glucose induces mitochondrial dysfunction in differentiated muscle cells

The detrimental effects of the persistent exposure to high glucose level (in the extracellular environment) can be found clinically in uncontrolled diabetes, where mitochondrial dysfunction presents a large subject for researchers. The relation between mitochondrial dysfunction and the development of diabetes has been a subject of extensive research. It has been suggested that insulin-resistance develops due to defects in mitochondrial function, that lead to insufficient ATP production for the hexokinase as well as other reactions requiring phosphorylation (Gerbitz et al., 1996). Mitochondrial dysfunction in diabetic cases was manifested as impaired mitochondrial capacity for fat oxidation during fasting conditions (Kelley and Mandarino, 2000).

Several studies have reported the impairment of mitochondrial activity and the significant morphological and functional differences between samples taken from diabetic and control healthy individuals (Kelley et al., 2002; Petersen et al., 2004; Ritov et al., 2005; Mogensen et al., 2007; Schrauwen-Hinderling et al., 2007; Szendroedi et al., 2007). In contrast to these studies, another study has reported no marked difference in mitochondrial function between the diabetic and the healthy control samples (Boushel et al., 2007).

The consequences of sustained high glucose level *in vivo* is highly complicated due to the interaction with manifestations and/or causes of diabetes and insulin resistance. Therefore, testing simply the effect of high glucose environment on mitochondrial performance *in vitro* may partially interpret an aspect of the intricate picture found in diabetes.

The results of the previous chapter showed that carbohydrate availability influenced the respiratory capacity of the examined phenotypes. The undifferentiated myoblasts that were exposed to a high level of glucose (5 g/l) acquired a lower respiratory capacity than that treated with a lower level of glucose (1 g/l) in the culture media. This difference was more vivid when the assay medium contained a lower concentration of glucose. Using the ability of C2C12 cells to differentiate and aiming to obtain more data about glucose level interaction with cellular bioenergetics, in this chapter we tested the response of the differentiated muscle cells to high glucose level during differentiation. We compared the bioenergetic characteristics in two types of myotubes, the first was grown and differentiated in a normoglycemic concentration of glucose 1 g/l (**LG**), and the second was exposed to a hyperglycemic concentration of glucose 5 g/l (**HG**) along the course of differentiation.

4.1 Respiratory activation in the basal state

Unlike the undifferentiated myoblasts (3.3.2), the differentiated HG myotubes exhibited a significantly higher respiration than the LG ones in the basal state prior to the addition of any of the mitochondrial inhibitors (Figure 4.1). This finding suggests a higher dependence on oxidative glucose metabolism in the HG phenotype under basal conditions (Figure 4.1), in particular, when the glucose concentration in the assay medium was 1 g/l.

The factors mediating basal respiration, after excluding the non-mitochondrial oxygen requirement, are the respiration devoted to ATP production and the proton leak. While the difference in the leak respiration and non-mitochondrial respiration was found to be negligible, the HG cells had a significantly higher ATP turnover-driven respiration (Table 4 on page 101).

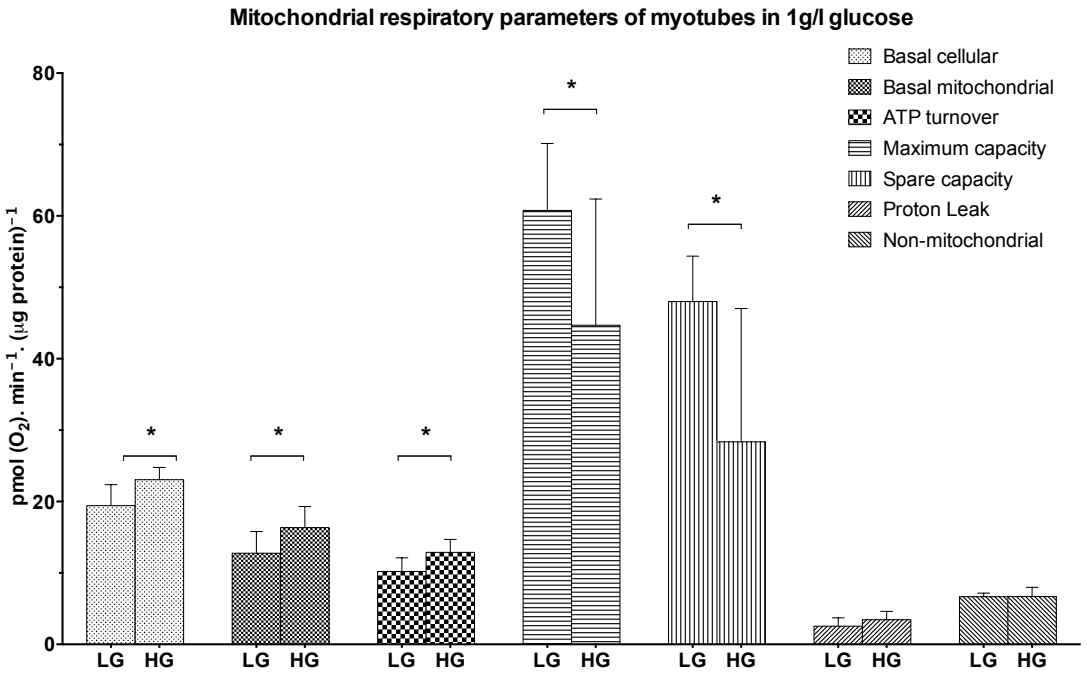

Figure 4.1: Mitochondrial respiratory parameters of C2C12 myotubes in assay medium supplemented with 1 g/l glucose, 1 mM pyruvate and 4 mM L-glutamine. The LG myotubes were grown and allowed to differentiate in medium containing 1 g/l glucose, while the HG cells were in a 5 g/l glucose containing medium. Results are presented as means ±95% CI, *indicates $p<0.05$, (n=3, each experiment was performed in triplicate).

4.2 Decreasing respiratory capacity

Stimulation of the mitochondrial respiration by an uncoupling agent induces a state of stress, that revealed significantly higher maximal respiration and spare respiratory capacity in the LG phenotype (Figure 4.1). This finding agrees with the results of a previous study that used the same cell line, where C2C12 cells were allowed to grow and differentiate in a high concentration (25 mM) of glucose condition (Mailloux and Harper, 2010).

This decrease in the maximum respiratory capacity of the HG cells (Figure 4.1) indicates a defect in the mitochondrial respiratory pathway, which became observable following stress induction. The spare respiratory capacity was also decreased in the HG cells, and this decrease was not due to the higher basal

respiration but mainly due to the lower maximal capacity of the HG cells. The presence of equal concentration of mitochondrial substrates in the assay medium excludes a shortage of substrate in the assay medium as a possible reason for the observable difference between both phenotypes, but refers to a probable defect in mitochondrial respiratory pathway.

4.3 Decreasing mitochondrial mass

As with myoblasts, we analyzed the mitochondrial yield of each phenotype (μg mitochondrial protein/μg total cellular protein) and estimated the activity of the citrate synthase (CS) as mitochondrial mass markers. LG cells exhibited a higher mitochondrial content than the HG ones (Figure 4.2), which probably can be the reason for the higher respiratory capacity of the LG phenotype. Unlike the mitochondrial protein yield, the CS activity did not show any difference (Table 6 on page 102), which indicates no functional changes in mitochondrial matrix enzymes.

We observed another marked difference between undifferentiated myoblasts and differentiated myotubes due to bioenergetic changes during the differentiation process. By comparing the mitochondrial mass markers of both, we could see a significant shift in the metabolic phenotype in the form of higher CS activity and mitochondrial yield in myotubes, which could account for their higher respiratory rate .

4.4 Respiratory chain enzymatic activity

The LG phenotype exhibited significantly higher activities of complex I and complex III (Figure: 4.2), while the activity of complexes II and IV tended to be higher but without a statistical significance (Table 7 on page 102). The equal activity of complex IV is once again consistent with the results of (Mailloux et al., 2011) who observed no differences in complex IV expression in either phenotype. The differences in the activity of complex I and III can probably be the cause of the lower respiratory capacity of the HG cells.

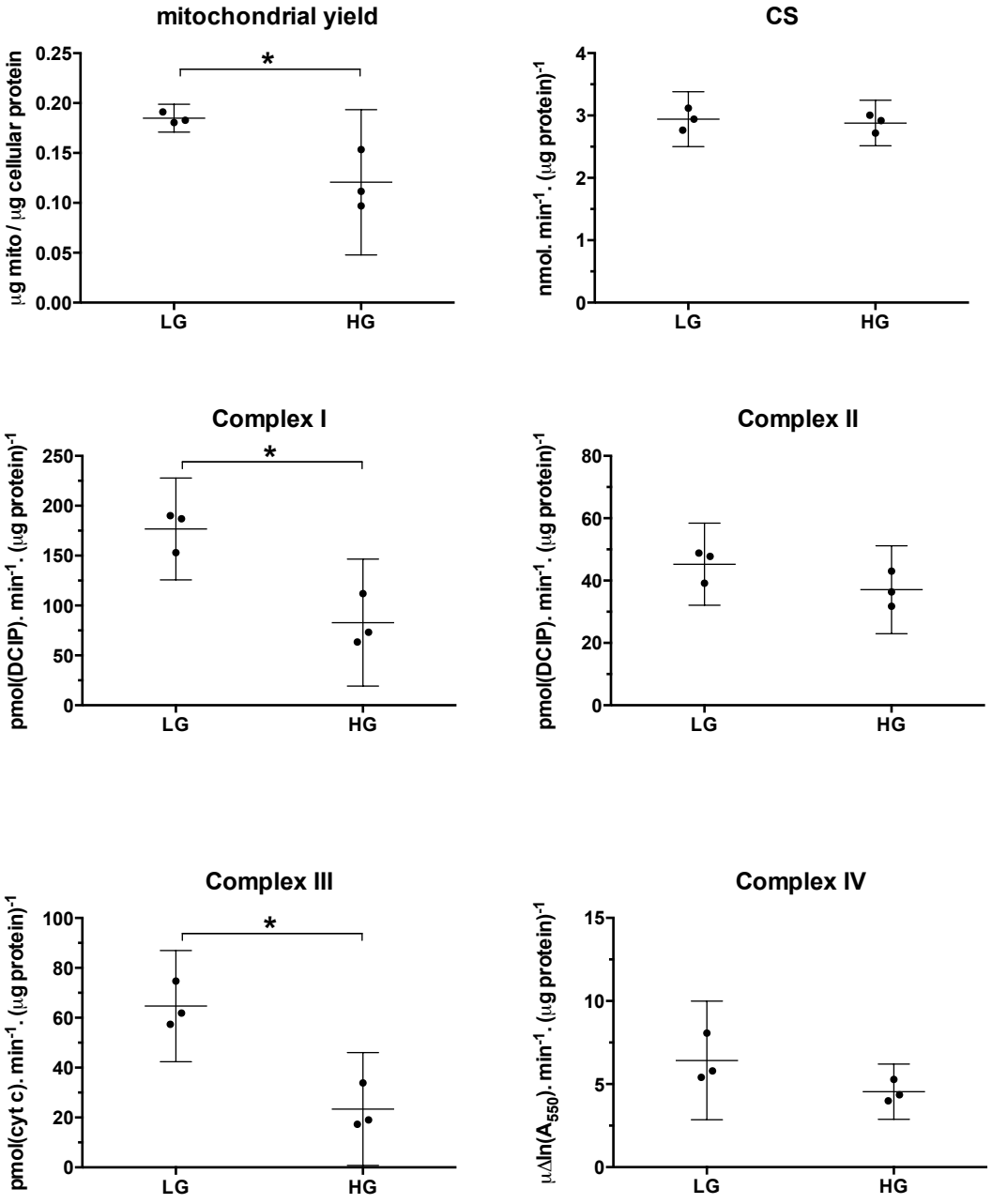

Figure 4.2: Mitochondrial mass markers and respiratory enzymatic activity of C2C12 myotubes grown and differentiated in low glucose (1 g/l) or high glucose (5 g/l) conditions. Results are presented as means ±95% CI, * indicates $p<0.05$, (n=3, each experiment was performed in triplicate).

4.5 No changes in the glycolytic activity

The glycolytic parameters of both LG and HG phenotypes were with no observed differences in the basal, oligomycin-stimulated rate (maximum glycolytic capacity), and the glycolytic reserve (Figure: 4.3). This finding comes in contrast to what was described by Mailloux et al., where the HG phenotype had $\approx 1.5\times$ higher ECAR in the basal state.

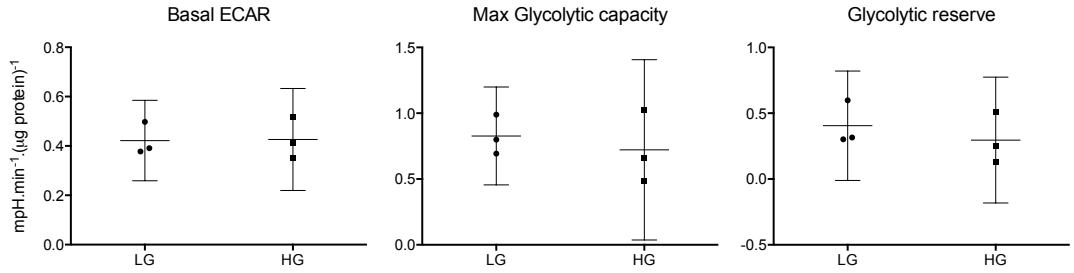

Figure 4.3: Glycolytic activity of C2C12 myotubes in 1 g/l glucose assay medium. Results are presented as means ±95% CI, (n=3, each experiment was performed in triplicate).

The ECAR values showed the less glycolytic nature of differentiated C2C12 cells, and the severe decrease in glycolytic activity induced by myogenic differentiation when compared to the glycolytic parameters of the undifferentiated myoblasts of both the LG and HG phenotypes (Table 5 on page 101).

4.6 No changes in free palmitate oxidation

The study of mitochondrial function in diabetes is complicated by the interference of lipid metabolism. The inverse relation between fatty acids availability and glucose utilization was initially reported (Randle et al., 1963), and the alteration in lipid and carbohydrate metabolism in skeletal muscles became a well known feature of diabetes (Kelley and Simoneau, 1994; Kelley et al., 1996). Manifestations of such changes are in the form of accumulation of intramuscular lipid intermediates and a subsequent abnormal lipid oxidation, combined with a decrease in the level of free fatty acid binding proteins in plasma (Goodpaster et al.,

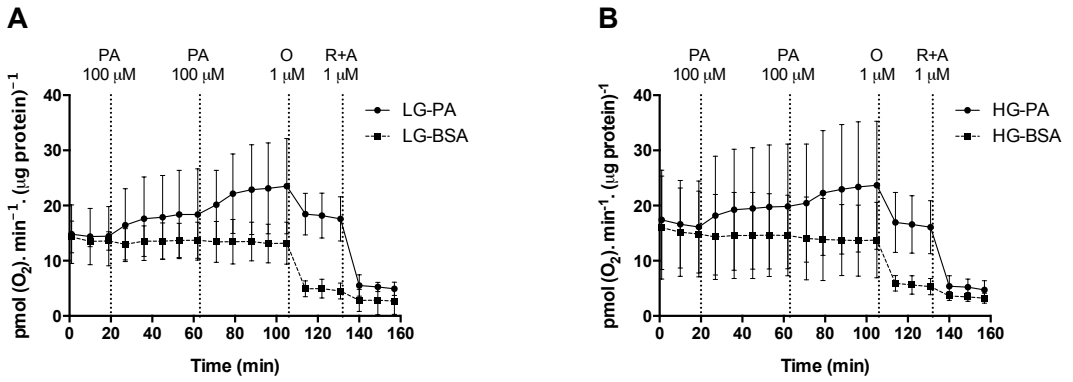

Figure 4.4: C2C12 myotubes respiration in KHB, then 100 μM of BSA-conjugated palmitate (PA) was injected, followed by another dose of 100 μM PA to reach a final concentration of 200 μM. The control groups were treated with BSA concentration similar to that present in the PA samples. 1 μM oligomycin (O) was then injected in all wells followed by 1 μM of rotenone-antimycin A (R+A) mixture. **A.** The LG phenotype. **B.** The HG phenotype. n=3, each experiment was performed in quintuplicate.

2000; Blaak et al., 2000). A sudden rise of plasma free fatty acids was proved to induce insulin resistance in skeletal muscle (Boden, 1999), and an acute decrease in their level was found to lower insulin resistance in both diabetic and non-diabetic individuals (Santomauro et al., 1999). Several studies observed the direct relation between triacylglycerol accumulation in skeletal muscle and the degree of insulin resistance (Pan et al., 1997; Krssak et al., 1999; Perseghin et al., 1999). More recent studies demonstrated that long-chain fatty acyl-CoA, diacylglycerol and ceramide are responsible for the development of insulin resistance (Schmitz-Peiffer, 2000; Itani et al., 2002; Cooney et al., 2002; Summers, 2006).

We tried to test the impact of high glucose on exogenous palmitic acid oxidation, and we found that the differences between LG and HG phenotypes did not include an observable change in the utilization of the acutely added palmitate (Table 8 on page 103). We observed a lower basal oxygen consumption in the basal state than in the previous setting when the assay was performed in DMEM supplemented with pyruvate and L-glutamine (4.1), while fatty acid oxidation is assayed in modified Krebs-Henseleit buffer (KHB) containing low concentration of glucose (2.5 mM).

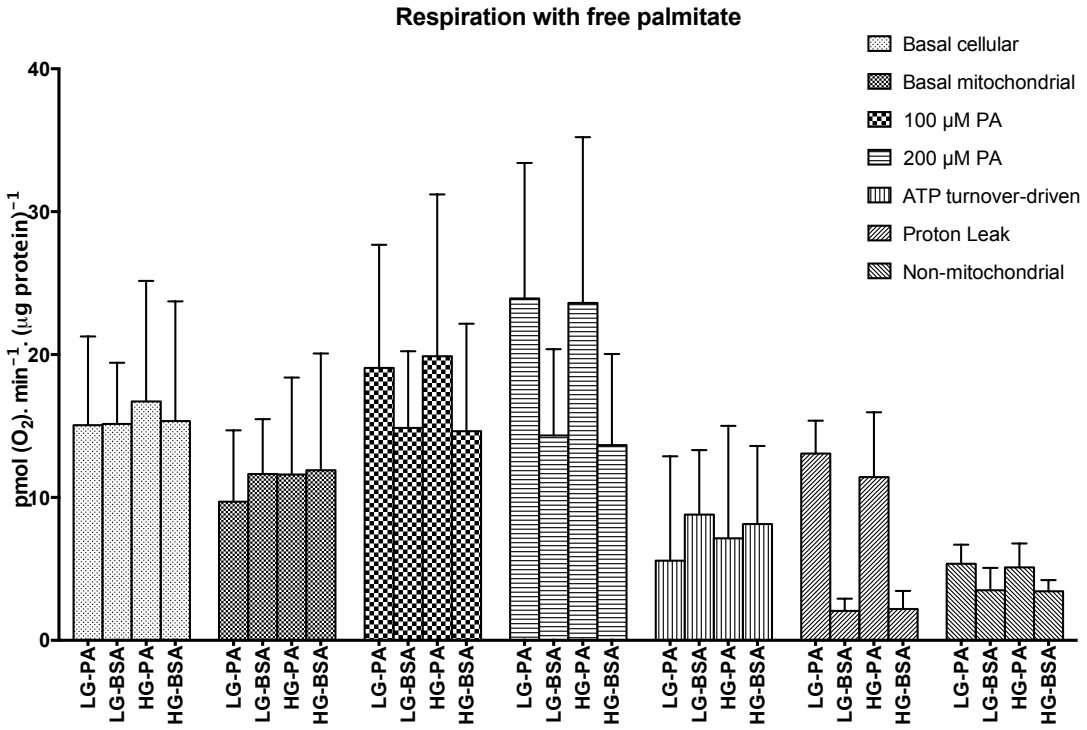

Figure 4.5: Effect of acutely added exogenous BSA-conjugated palmitate on the mitochondrial respiration of differentiated C2C12 myotubes. Both LG and HG phenotypes maintained a similar response to the added palmitate. The rise in OCR after palmitate addition is due to the uncoupling effect of the free palmitate. The leak respiration increased in both phenotypes and a marked difference can be observed when compared to the control BSA treated groups. Results are presented as means ±95% CI, (n=3, each experiment was performed in quintuplicate).

Both phenotypes responded equally to the addition of 100 μM palmitate by gradually increasing their OCR (Figure 4.5). Another palmitate addition to reach a final concentration of 200 μM caused a further increase in the OCR without an observable difference between the two phenotypes. However, this increase in the OCR does was not due to an actual increase in the oxidative respiration. The ATP-turnover driven respiration of the palmitate treated (LG-PA or HG-PA) and the vehicle treated (LG-BSA or HG-BSA) did not show any significant difference.

This finding shows that the rise in respiration following palmitate addition was mainly due to the uncoupling effect of palmitate, which was demonstrated

by the increase in proton leak respiration in both phenotypes, compared to the control groups treated with BSA (Figure 4.5). Another modest contributor to the higher respiration after palmitate addition was the non-mitochondrial respiration, which increased in both phenotypes equally.

4.7 Discussion

A persistent and uncontrolled hyperglycemia is most commonly found in diabetic patients, where the development of insulin resistance impairs glucose metabolism in different sites, such as a decrease in the rates of glucose transport, phosphorylation and glycogen synthesis (Shulman et al., 1990). In addition, the development of diabetic complications has been related to the level of glucose in blood (Brownlee, 2001). The crucial role of mitochondria in cellular metabolism attracted researchers to investigate the cellular bioenergetic system in diabetic individuals. In a leading report about impaired mitochondrial oxidative function in the skeletal muscles of diabetic patients, a reduction of enzymatic activity of the oxidative pathway was observed (Simoneau and Kelley, 1997). Later, these changes were described as lower enzymatic activity of complex I and citrate synthase (Kelley et al., 2002), which was then specified in the subsarcolemmal fraction of mitochondria (Ritov et al., 2005). This was confirmed later by respirometric measurements of the ETC enzymatic capacity, that showed a significant impairment in diabetic samples (Mogensen et al., 2007).

The results showed that incubating and allowing the C2C12 cells to differentiate in a high level of glucose led to the development of mitochondrial dysfunction, which was manifested by the lower maximum and spare respiratory capacity of the HG phenotype when compared to the LG cells differentiated in a normoglycemic environment. The mitochondrial respiratory chain complexes activity revealed the significant decrease in the activity of complex I and III in the HG phenotype. Other complexes were not affected, which raises another question about the role of glucose level in the regulation of the respiratory chain complexes, in an intact respiratory chain and separately. The mitochondrial yield also decreased in the HG phenotype, however the citrate synthase activity was similar in both LG and HG phenotypes, which indicates that the dysfunction is mainly confined to

mitochondrial membrane complexes rather than the matrix enzymes.

These findings suggests a lower efficiency to produce energy from all available mitochondrial substrates, so we tried to investigate the ability to oxidize free fatty acids, such as palmitate. We encountered a difficulty due to the strong uncoupling effect of the free palmitic acid. The difference in utilizing exogenous palmitate between the two phenotypes was not distinguishable and both LG and HG phenotypes responded equally to palmitate addition by increasing their respiration, however this increase was not caused by a real oxidative respiration. The Leak respiration increased ≈5-6 folds in the palmitate treated cells than in the BSA treated ones, which explains the rise in oxygen demand in order to maintain the accelerated respiration. The coupled (ATP-driven) respiration used to produce ATP was equal in both phenotypes and in the BSA-treated control, indicating absence of any change in the fatty acid oxidative function. An actual difference in fatty acid oxidation might be present, however, this last finding raises doubts about the validity of this method as an accurate estimation of free fatty acid oxidation in intact cells.

Chapter 5

Adverse effects of the highly lipophilic triphenylphosphonium cations

Triphenylphosphonium moieties (TPP^+) are charged molecules that are used to target mitochondria by several probes in order to facilitate the study of mitochondrial function or the delivery of bioactive compounds to mitochondria (Murphy, 1997). The positive charge of these molecules allows the TPP^+ conjugated moiety to accumulate inside the mitochondrial matrix, thanks to the driving forces created by the mitochondrial membrane potential. In addition, the hydrophobic nature of these molecules facilitates the uptake and the binding to biological membranes (Ross et al., 2005, 2008). This hydrophobic character is mediated in inactive alkylTPP^+ compounds by the length of the hydrophobic alkyl side chain. This provides the TPP^+ moiety with a higher affinity to cross the phospholipid bilayer, and bind to the mitochondrial membrane.

The rate of mitochondrial uptake of TPP^+ cations follows the Nernstian distribution, which allows an approximate thousand fold higher mitochondrial concentration than the used extracellular concentration. Although the TPP^+ conjugated molecules are widely used, the mechanism of action of such compounds is not well described and their effect on the different mitochondrial functions is partially understood. Recently, it was observed that the highly hydrophobic TPP^+

compounds, including the biologically inactive alkylTPP$^+$ salts, can inhibit mitochondrial respiration with various degrees (Reily et al., 2013). We therefore tried in this chapter to investigate the mechanism of the inhibitory action of the more hydrophobic TPP$^+$ moieties.

5.1 Impairment of mitochondrial respiration in intact cells

We evaluated the effect of TPP$^+$ compounds on mitochondrial respiration of intact cells by testing the bioenergetic performance of C2C12 cells after treatment with 1 μM of different alkylTPP$^+$ compounds. We treated the cells with propyl-, heptyl-, decyl- and dodecylTPP$^+$ before performing a mitochondrial stress test (2.7.1) and followed the changes in oxygen consumption rate (Figure 5.1) and extracellular acidification rate (Figure 5.2). We observed that the more hydrophobic TPP$^+$ derivatives affected mitochondrial respiration by inducing proton leak respiration and reducing the maximal respiratory capacity. We also observed an increase in ECAR, which reflects the induction of glycolysis and the shift from oxidative respiration to glycolytic metabolism.

5.1.1 Induction of proton leak

Mitochondrial respiration in the basal state is mediated by two respiratory parameters, the first is the mitochondrial ATP-driven production and the other is the physiologically occurring proton leak respiration. A qualitative estimation of proton leak in intact cells can be concluded via blocking the ATP synthase activity by oligomycin, thus eliminating the mitochondrial ATP production contribution in mitochondrial respiration and shift cellular ATP synthesis towards the glycolytic pathway.

The presence of 1 μM decyl- or dodecylTPP$^+$ led to $\approx$ 10 fold increase in proton leak-driven (oligomycin-inhibited) respiration, compared to controls treated with the DMSO vehicle alone. The less hydrophobic heptylTPP$^+$ exhibited a more modest effect than the more hydrophobic ones, and caused an $\approx$ 5 fold

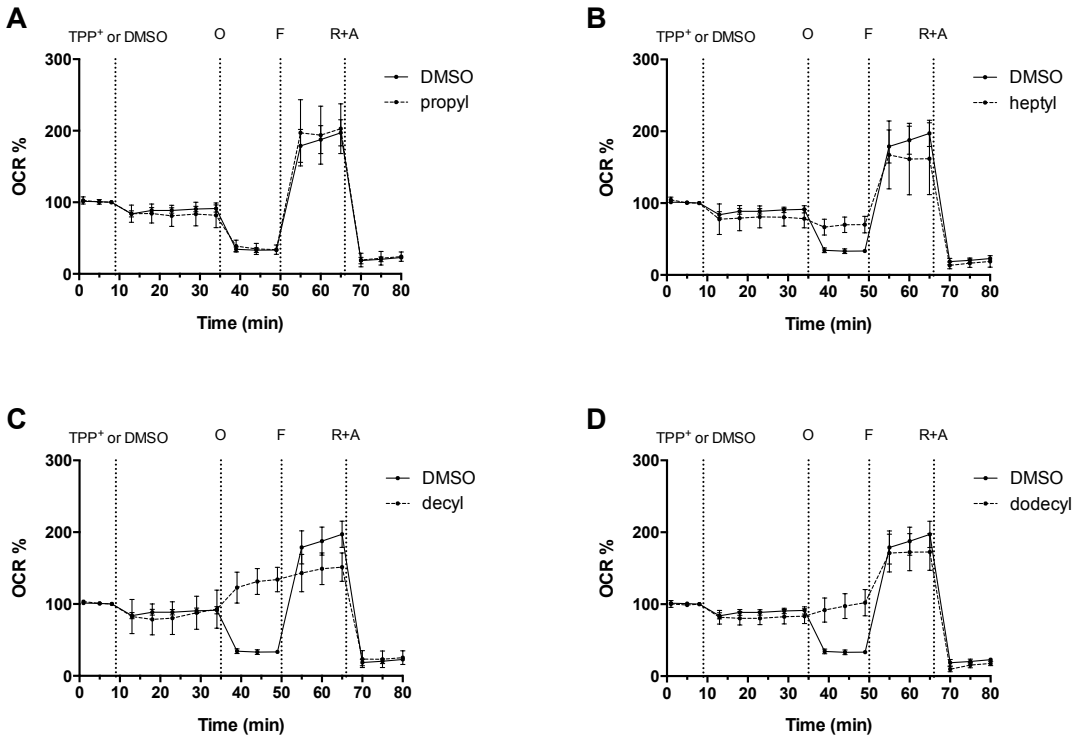

Figure 5.1: **The acute response of cellular respiration to various alkylTPP$^+$ compounds in intact C2C12 myoblasts.** Traces of mitochondrial stress test performed using the XF-24 analyzer. After measuring the respiration in basal conditions, cells were treated with different alkylTPP$^+$ at a final concentration of 1 μM or vehicle (DMSO 0.02%). Oligomycin (O) 1 μM, FCCP (F) 0.5 μM rotenone-antimycin A (R+A) 1 μM were injected successively to perform a mitochondrial stress test. Cellular oxygen consumption rate (OCR) is expressed as the percentage of basal OCR (OCR%) and presented as means ± 95% CI, n=3–6.

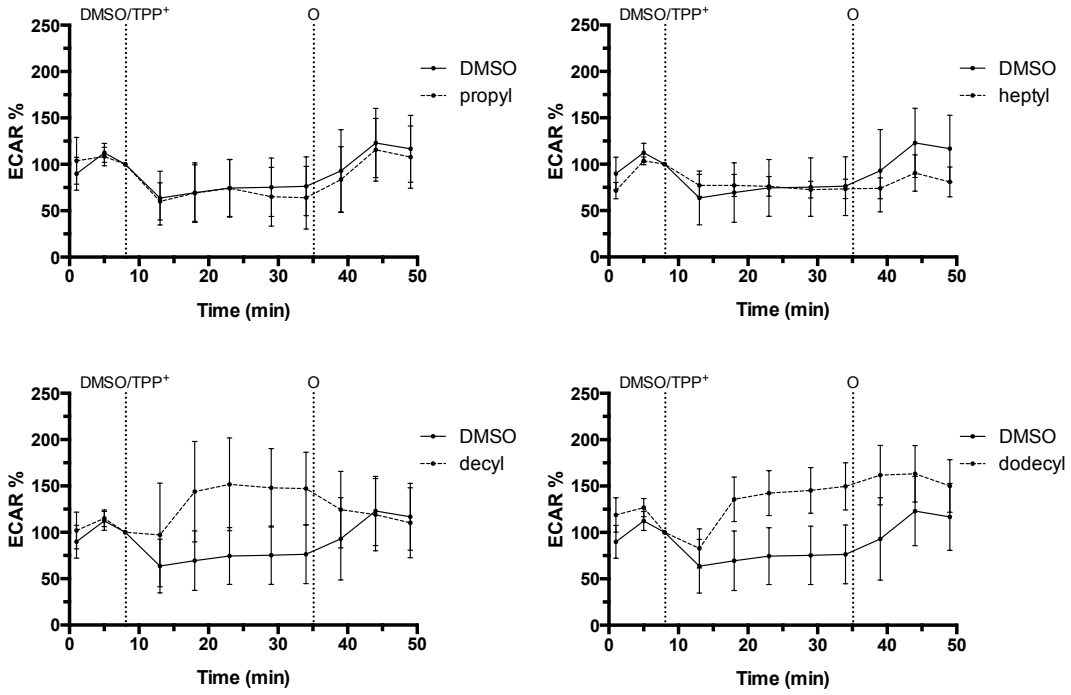

Figure 5.2: **Changes in glycolytic rate in response to various alkylTPP$^+$ compounds in intact C2C12 myoblasts.** As in figure 5.1, cells were treated with different alkylTPP$^+$ at a final concentration of 1 μM or vehicle (DMSO 0.02%). The addition of oligomycin (O) stimulates the maximum glycolytic capacity. The extracellular acidification rate (ECAR) is expressed as the percentage of basal ECAR (ECAR%) and presented as means ± 95% CI, n=3–6.

increase in the leak respiration. The least hydrophobic derivative propylTPP^+ had no observable effect at this concentration (Figure 5.3 A).

5.1.2 Reduction of maximal respiration

Inducing an energy crisis deliberately by a highly effective protonophore (FCCP) allows to measure the maximal respiratory rate at a given substrate availability, which tests the efficiency of the mitochondrial respiratory pathway. While the effect on maximal respiration was not as pronounced as on the proton leak at the 1 μM concentration, it was observed that there is a tendency to have an inhibitory effect with increasing the alkyl chain length. This was apparent (Figure 5.3 B) with only decyl- and dodecylTPP^+, and both derivatives exhibited a significant inhibitory effect.

Both FCCP and the highly hydrophobic TPP^+ derivatives are inducers of proton leak through different mechanisms. FCCP is a protonophore that leads to a state of complete uncoupling and neutralization of the mitochondrial membrane potential. Therefore, it is most likely that the effective concentrations of TPP^+ derivatives inside mitochondria are much lower than under basal conditions with intact membrane potential. Another considerable factor is the possible leakage of the TPP^+ compounds from mitochondria following the dissociation of the membrane potential and removal of its regulatory effect that drives the TPP^+ accumulation. This suggests that the impact of TPP^+ on the mitochondrial respiratory machinery during measurement might be underestimated, and a more inhibition of the activity of the respiratory enzymes can be expected.

5.1.3 Enhancement of glycolytic metabolism

When mitochondrial respiration is interrupted, energy production shifts instantly to glycolytic metabolism to compensate for ATP shortage. This is translated as an increase in the extracellular acidification rate (ECAR) due to the increase in lactate production and release to the extracellular environment.

We found the effect of the alkylTPP^+ on the ECAR corresponding to the previous findings (Figure 5.3 C), which once again follows the same relationship between alkyl chain length and the effect magnitude. The addition of oligomycin

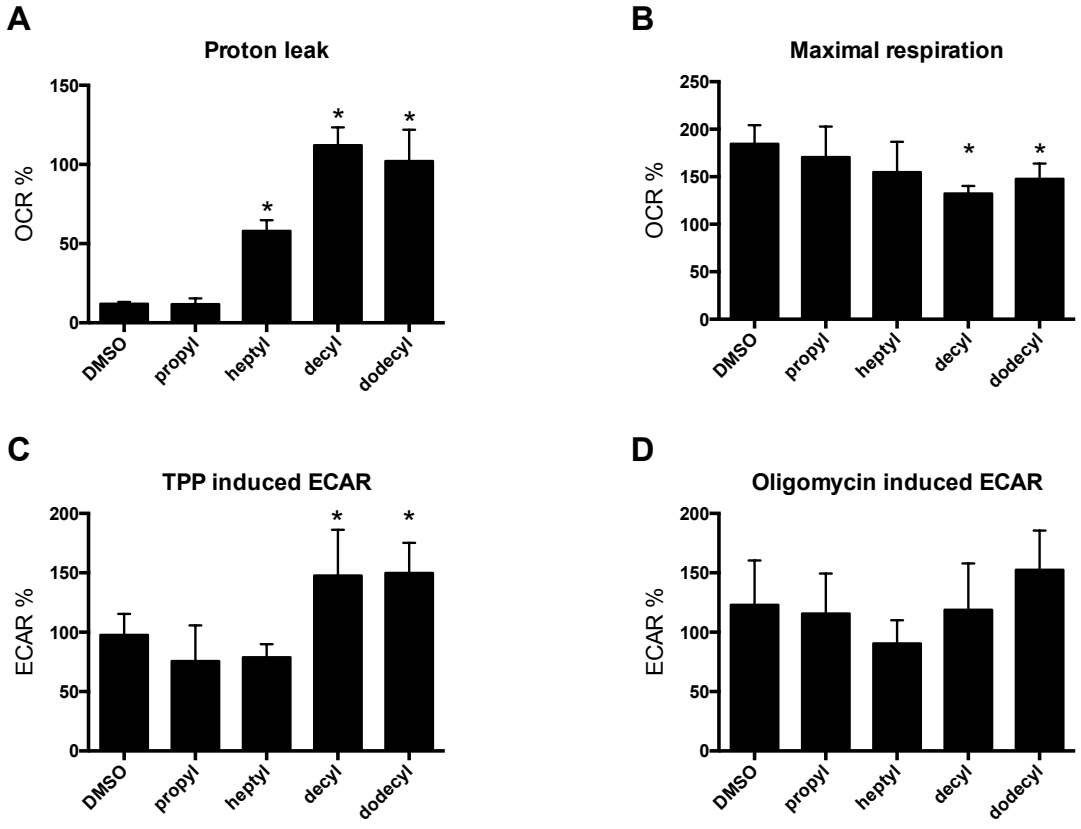

Figure 5.3: **Effect of alkylTPP$^+$ compounds (1 μM) on mitochondrial metabolism in intact cells. A.** Long alkyl chain TPP$^+$ derivatives cause an increase in proton leak-driven respiration. **B.** Decyl- and dodecylTPP$^+$ cause an inhibition of maximal respiration. **C.** Cells respond to alkylTPP$^+$ addition by shifting ATP production to the glycolytic pathway as indicated by an increase in extracellular acidification rate (ECAR). **D.** No significant effect of alkylTPP$^+$ compounds on maximum glycolytic capacity induced by oligomycin. All results are expressed as a percentage of basal cellular OCR or basal ECAR and are presented as means ± 95% CI, n=3–6. * indicates $p<0.05$ when compared to the DMSO treated group.

completely blocks oxidative phosphorylation and leads to a further increase in the ECAR under basal conditions, which allows to detect the maximum glycolytic capacity of the tested cells. Since all the cells are from the same phenotype, it is expected to possess a similar glycolytic activity, given that the alkylTPP$^+$ derivatives have no reported interference with the process of glycolysis (Figure 5.3 D).

5.1.4 Direct relation between TPP$^+$ concentration and the respiratory response

The nature of the relation between the inhibitory effects of alkylTPP$^+$ derivatives and the used concentration was found to be dose-dependent. The C2C12 cells responded to the gradual increase in the extracellular concentration of the most potent dodecylTPP$^+$ by increasing the rate of proton leak respiration and the maximum respiratory capacity decreased accordingly. Figure 5.4 shows the relationship between both effects and the tested concentration of dodecylTPP$^+$ to which cells were exposed.

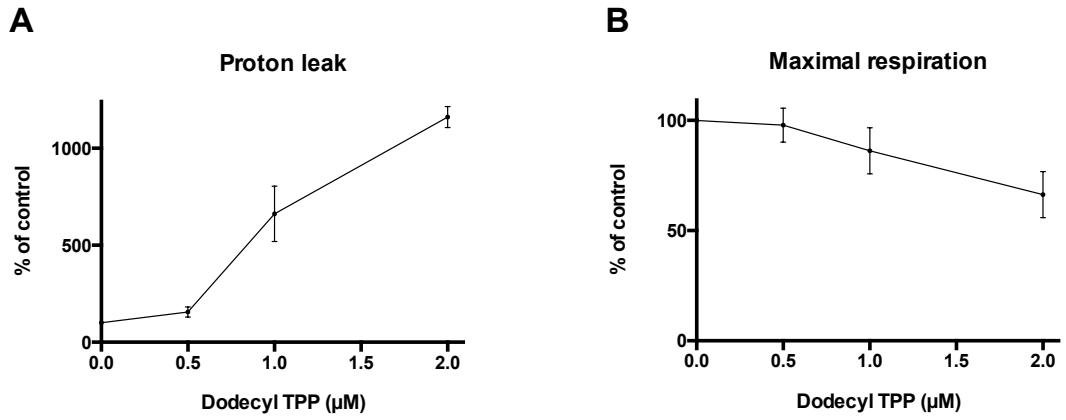

Figure 5.4: **Dose-dependence of the effect of dodecylTPP$^+$ on mitochondrial metabolism. A.** Proton leak-driven respiration increases substantially with an increasing extracellular concentration of dodecylTPP$^+$. **B.** A simultaneous decrease in maximal respiration due to increasing doses of dodecylTPP$^+$. All results are expressed as the percentage of OCR of the DMSO treated control and are presented as means ± 95% CI, n=3–6.

We observed that the proton leak stimulation appears to be much stronger than the control than the inhibitory effect on maximal respiration. At an extracellular concentration of 2 μM dodecylTPP$^+$ proton leak respiration increased ≈10 folds, while the respiratory capacity decreased by ≈35%.

5.2 Effect on respiratory chain complexes

While increasing the proton leak can be assumed to be due to disruption of the mitochondrial membrane and the subsequent collapse of the inner membrane potential, the decrease of maximal respiration is not interpreted in the same manner. The factors mediating maximum respiratory capacity are the availability of consumable substrates and the presence of functioning electron transfer system. Therefore, the study extended to investigate whether respiratory complexes are inhibited by the TPP$^+$ alkyl derivatives, and to measure directly their effect on the mitochondrial membrane potential.

We measured the effect of alkylTPP$^+$ compounds on the enzymatic activity of individual mitochondrial respiratory chain complexes using samples from freeze-thawed rat skeletal muscle homogenate enriched in the mitochondrial fraction (2.1.3.1). This model allows a direct access to the respiratory chain in the absence of a mitochondrial membrane potential, due to complete depolarization of mitochondrial membrane after freezing. This eliminates the contribution of the membrane potential in the observed manifestations with intact cells, and ensures the presence of a stable concentration of TPP$^+$ without the possibility of leakage following the addition of the uncoupling agent. Considering the Nernstian distribution of TPP$^+$ cations, we used a concentration of 1 mM of each alkylTPP$^+$, which is equivalent to 1 μM of extracellular concentration*.

5.2.1 General inhibition of ETC

All of the four complexes of the electron transport chain were non-specifically inhibited by the long chain TPP$^+$ derivatives (Figure 5.5) with various degrees

*Due to interaction with the reaction components, the homogenate was treated with 1 mM alkylTPP$^+$ before measuring the enzymatic activity (2.3.2.10).

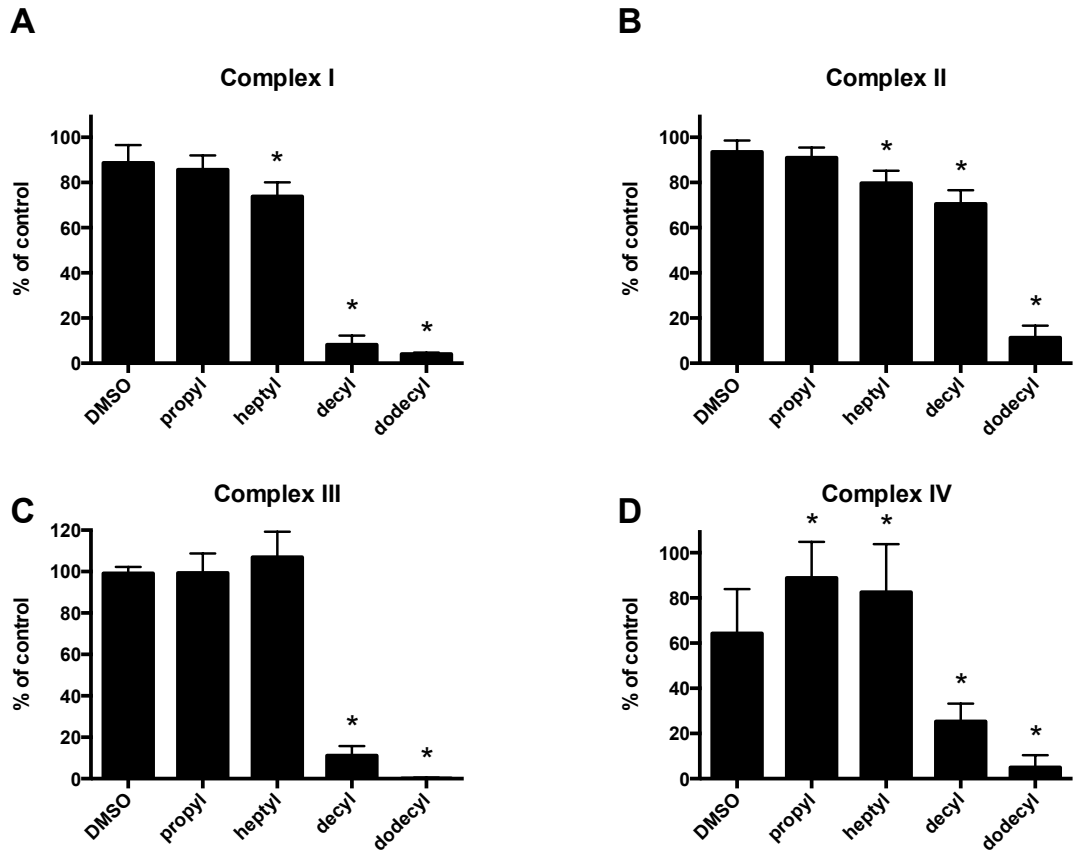

Figure 5.5: **Activity of mitochondrial respiratory chain complexes in rat skeletal muscle homogenate is inhibited by longer-chain alkylTPP$^+$ compounds.** Muscle homogenate was preincubated with 1 mM TPP$^+$ compounds on ice. **A.** Complex I activity was slightly affected by DMSO alone and longer-chain TPP$^+$ derivatives caused a marked inhibition. **B.** Complex II activity was less affected with only significant inhibition caused by by dodecylTPP$^+$. **C.** Complex III activity was affected in a similar manner as complex I. **D.** DMSO decreased the activity of complex IV by about 40%, and TPP$^+$ compounds with shorter chains appear to alleviate this inhibition. Longer chain derivatives, however, caused a marked inhibition of complex IV activity. All results are expressed as the percentage of the activity of the untreated control and are presented as means ± 95% CI, n=3. * indicates $p<0.05$ when compared to the DMSO treated group.

after being exposed to a concentration of 1 mM of the different alkylTPP$^+$. We found dodecylTPP$^+$ to be a very potent inhibitor of all complexes and the enzymatic activity dropped down to less than 20 % of the control. Complexes I and III appeared to be the most sensitive to decyl- and dodecylTPP$^+$ inhibition. Complex II was relatively resistant especially to decylTPP$^+$, which caused a moderate decrease in complex II activity.

The effect of TPP$^+$ derivatives on complex IV activity is rather curious. The vehicle (1 % DMSO during preincubation, 0.05 % during assay) inhibited the activity of complex IV significantly, and decyl- and dodecylTPP$^+$ dramatically potentiated this inhibitory effect. Surprisingly, the shorter chain derivatives, propyl- and heptylTPP$^+$, on the other hand, appear to alleviate the toxic effect of DMSO, which further complicates our understanding of the real mechanism of action of these compounds.

Inhibition of complexes I, III, and IV reveals the major cause of lowering maximum respiratory capacity in intact cells, since most electron flux to ETC is via complex I. In addition, these complexes are the main proton pumps responsible for maintaining the proton gradient across the inner membrane, which is another indicator of indirect interference with membrane potential.

5.2.2 Dose-response relation

The relation between the concentration of the most hydrophobic tested alkylTPP$^+$, decyl- and dodecylTPP$^+$, and the rate of inhibition of each enzymatic activity can indicate the range of the extracellular effective concentrations that can directly interfere with mitochondrial respiration. Therefore, we assessed the enzymatic activity of each complex after preincubation with different concentrations of decyl- and dodecylTPP$^+$.

DodecylTPP$^+$ virtually inhibited complexes I, III and IV completely at a 0.5 mM concentration (equivalent to 0.5 μM of extracellular concentration), while the activity of complex II was only reduced by about 50 % at this concentration. DecylTPP$^+$ exhibited a similar pattern with a substantially lower potency, however a lower concentration of 100 μ decylTPP$^+$ (equivalent to 0.1 μM of extracellular concentration) was found to potentiate the activity of complex IV

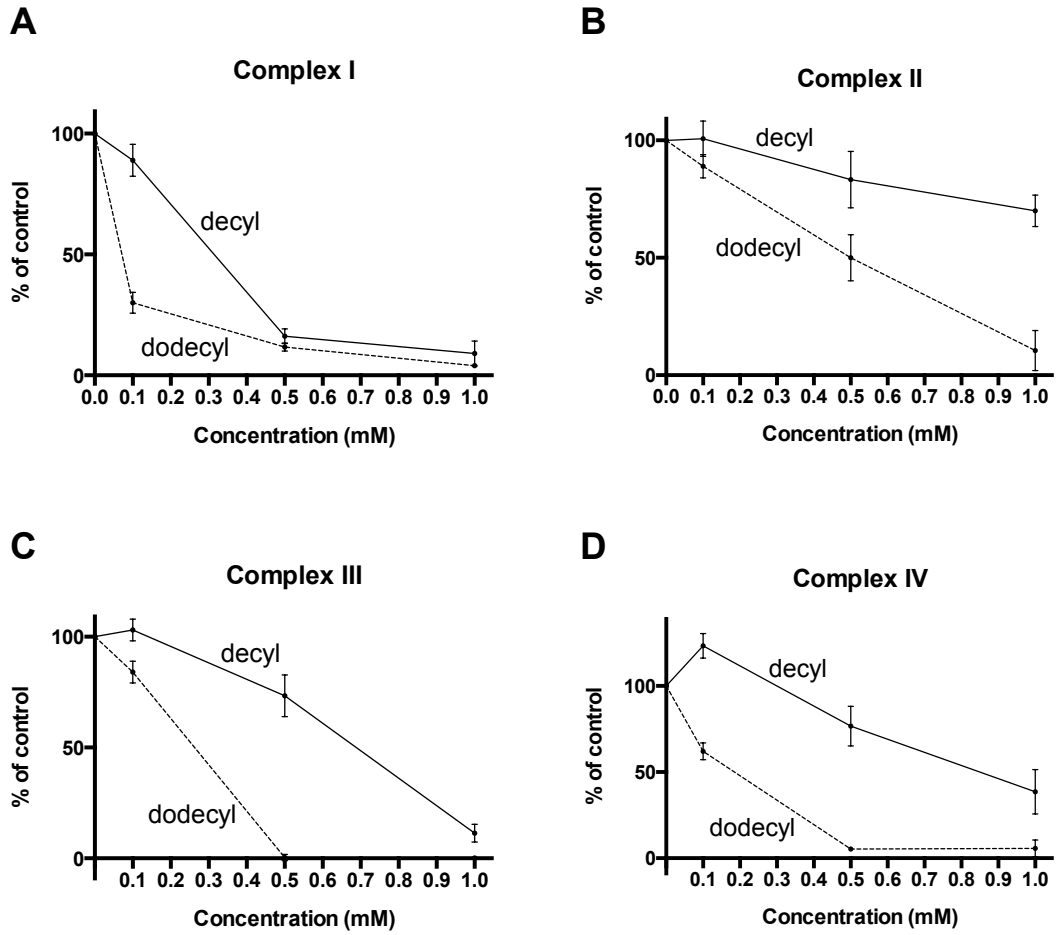

Figure 5.6: **The inhibition of mitochondrial respiratory chain complex activity by longer chain TPP$^+$ compounds is dose dependent.** Samples of rat skeletal muscle homogenate were incubated with various concentrations of decylTPP$^+$ and dodecylTPP$^+$ prior to the assay. **A, B, and C.** Complexes I, II, and III show a gradual decrease in activity proportionate with the dose of the TPP$^+$ compounds. DodecylTPP$^+$ exhibits a stronger inhibitory effect than decylTPP$^+$. **D.** A low concentration of decylTPP (100 μM) appears to cause a slight 'activation' of complex IV activity, while higher concentrations caused inhibition. DodecyTPP$^+$ is once again the more potent inhibitor. All results are expressed as the percentage of the activity of the DMSO treated sample and are presented as means ± 95% CI, n=3.

(Figure 5.6), which indicates a possible detergent effect of decylTPP$^+$ that solubilized mitochondrial membrane fragments.

5.3 The highly hydrophobic TPP$^+$ derivatives decrease $\Delta\psi_m$

We performed an independent measurement of mitochondrial membrane potential in intact C2C12 cells using flow cytometry to present an unbiased method demonstrating the effect of alkylTPP$^+$ derivatives. In addition, a detection of membrane potential changes following the exposure to TPP$^+$ derivatives might strengthen our findings on proton leak respiration. We used the negatively charged, membrane-permeable fluorescent dye tetramethylrhodamine methyl ester (TMRM). The dye accumulates in mitochondria proportionately to the membrane potential and therefore cells with a higher membrane potential will fluoresce with a higher intensity.

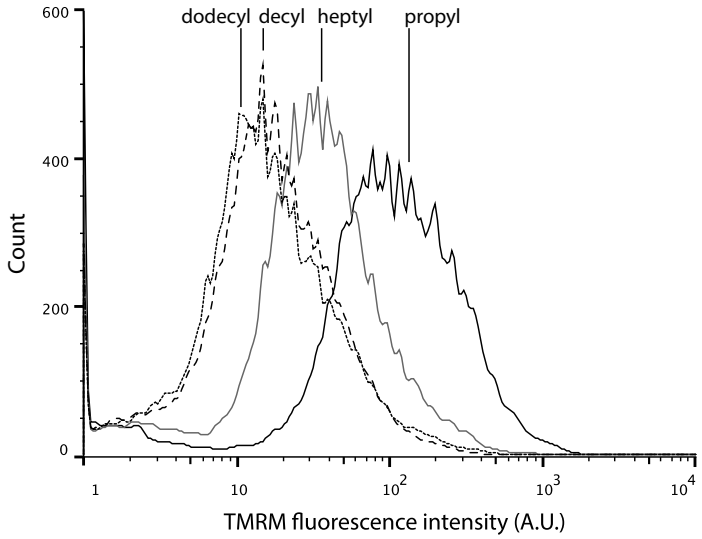

Figure 5.7: **TPP$^+$ derivatives decrease mitochondrial membrane potential.** A typical TMRM fluorescence intensity histogram from a flow cytometry experiment with C2C12 cells in the presence of 1 μM TPP$^+$ compounds. Lower fluorescence intensity corresponds to a lower membrane potential ($\Delta\psi_m$).

As expected, there is a clear trend towards lower fluorescence intensities as the alkyl chain length increases (Figure 5.7). PropylTPP^+ at a concentration of 1 μM did not affect the membrane potential, and the fluorescence intensity was similar to that treated with the vehicle (DMSO). Heptyl-, decyl- and dodecylTPP^+ at the same concentration decreased the intensity significantly, indicating a lower value of $\Delta\psi_m$ in cells treated with these salts.

We observed that the two longest chain derivatives appeared to collapse the mitochondrial membrane potential even more effectively than an equal concentration of the uncoupler FCCP (Table 9), and both diminished the fluorescence intensity in the treated cells. This could potentially be explained by the combined action of a strong uncoupling effect and respiratory chain inhibition.

5.4 Discussion

TPP^+ compounds are well known and their use is common due to their high affinity to the biological membranes (Murphy, 1997). This affinity will further increase with an increasing hydrophobicity of the derivative (Ross et al., 2005, 2008) resulting in larger accumulation of the positively charged TPP^+ molecule in mitochondria. The high intramitochondrial concentration most likely interferes with one or more of the several mitochondrial functions, however, the adverse reactions of such compounds including the theoretically inactive derivatives is partially studied, and the available data about the mechanism of action of these compounds have not reached a satisfying level. The TPP^+ moiety of mitochondrially targeted compounds is often considered to be without a significant biological activity. Our results show a clear evidence that increasing the hydrophobic character of TPP^+ derivatives conjugated with chemically inactive alkyl chains in place of the 'active' moieties significantly affect mitochondrial bioenergetics.

All TPP^+ compounds are positively charged, and the highly lipophilic compounds can achieve a higher accumulation rate due to their easier diffusion through the phospholipid membranes. Therefore, we expected that the magnitude of these side effects may correlate with the alkyl side chain length which mediate the hydrophobicity of the compounds. The main findings of this chapter are the significant potentiation of proton leak with a subsequent decrease in the

mitochondrial membrane potential. Another adverse reaction was the inhibitory effect on the mitochondrial respiratory chain complexes.

Although the mechanism of action is not yet clearly revealed, a plausible explanation of these observations therefore may be that both the increase in proton leak and the inhibition of respiratory chain complexes is mediated by an incorporation of alkylTPP$^+$ molecules into the inner mitochondrial membrane and the resulting disruption of its normal function. This conclusion is strongly supported by data available about the nature and structure of each enzyme complex. The respiratory complexes are known to be sensitive to their lipid environment and require phospholipid molecules for their activity (Cerletti et al., 1965; Fry and Green, 1980, 1981). Therefore, a high concentration of alkylTPP$^+$ molecules in the membrane could interfere with the membrane properties and integrity, allowing the leak of protons from the intermembrane space back to the matrix, and most likely alters the membrane structure and subsequently the function of the membrane bound enzymes.

The observed effect of the more lipophilic alkylTPP$^+$ on the respiration of intact C2C12 is strongly compatible with previously published results on different cell lines (Reily et al., 2013). The nearly similar response of intact cells to alkylTPP$^+$ is useful to identify broad effects on mitochondrial bioenergetics, however, additional investigations are required to pinpoint more precise mechanisms of action of TPP$^+$ derivatives.

We therefore assessed the activity of mitochondrial respiratory chain enzymes after being targeted with the alkylTPP$^+$. Although the function of each complex is highly regulated in intact cells by the ratio of substrates and products, trying to conclude the activity of each enzyme within an intact electron transfer system can be masked by the inhibition of other complexes. For that reason we performed distinct assays for each enzyme in a completely uncoupled system.

Highlt hydrophobic alkylTPP$^+$ caused a non-specific inhibition of all complexes, and complex II appeared to be the least sensitive from all complexes. This finding was augmented by trying several concentrations of the strongest inhibitors, and the dose-dependency of these inhibitory effects was demonstrated. Although the inhibitory effect of the hydrophobic alkylTPP$^+$ could be demonstrated, the exact mechanism of respiratory chain inhibition can only be specu-

lated about based on these data. The fact that the inhibitory effect is not specific to any derivative nor to any complex suggests a non-specific binding of the TPP^+ derivates to the inner mitochondrial membrane, which affects membrane integrity causing both the breakdown of its insulating properties and impairment of the phospholipid milieu faced by the respiratory complexes.

We must mention that the study could not estimate the actual rate of inhibition when it comes to investigate the effect on intact cells. When an assumed concentration approximately near to that found in mitochondria of treated cells, it was not possible to perform the enzymatic reaction due to interference of alkylTPP^+ with the reaction components (2.3.2.10). It is therefore possible that the effects observed in our study underestimate the real effects in intact cells.

Lastly, the inhibition of complex I, III and IV led to interruption of mitochondrial membrane potential, being essentially the sites of proton pumping that create the electrochemical potential difference. We confirmed this interference independently by determining the drop in mitochondrial membrane potential following exposure to the longer chain TPP^+ compounds. Based on these results we recommend to consider the effect of the hydrophobic nature of the mitochondrially targeted molecules when used as diagnostic probes or therapeutic agents.

Chapter 6

Methyltriphenylphosphonium targeting of 2-oxoglutarate dehydrogenase complex

Accumulating data have shown that TPP^+ derivatives in general exert some undesirable effects on mitochondrial metabolism due to non-specific binding to membranes (Plecitá-Hlavatá et al., 2009; Severin et al., 2010; Antonenko et al., 2013), such as the potentiation of proton leak across the inner mitochondrial membrane, which are largely independent of the biologically-active moiety and become more pronounced with increasing hydrophobicity of the molecule as seen in the previous chapter.

The strongest adverse responses were induced by the highly lipophilic alkylTPP^+ compounds, and the less hydrophobic propylTPP^+ did not exert any negative effect on cellular respiration nor on the activity of the respiratory chain complexes. However, the least hydrophobic derivative, methyltriphenylphosphonium (TPMP), was found to inhibit mitochondrial respiration in the basal state and induce glycolytic metabolism of glucose (Reily et al., 2013). This valuable observation demonstrated by the study of Reily et al. was not supported by more data about the possible mechanism of action of TPMP.

TPMP is the most used alkylTPP^+, and its main application is the direct measurement of mitochondrial membrane potential, using the TPMP-sensitive

electrodes (Liberman et al., 1969; Grinius et al., 1970; Brown and Brand, 1985). Its inhibitory effect when used with high extra-mitochondrial concentrations was reported in studies with isolated mitochondria (Brand, 1995; Ojovan et al., 2011). Unlike the highly lipophilic alkylTPP$^+$ derivatives, A direct interference with the mitochondrial membrane potential is most unlikely to be the reason of TPMP inhibitory effect. A possible explanation of this effect can be demonstrated by recognizing the available binding sites where TPMP molecules may exert an adverse reaction.

In order to explore the effects of TPP$^+$ compounds in more detail, we first investigated the respiratory response and bioenergetic changes to TPMP in intact C2C12 cells using the Seahorse XF-24 analyzer and compared the response of this cell line to the previously published report (Reily et al., 2013). The next step was to test respiration of the permeabilized cells in the presence of different respiratory substrates requiring different metabolism so as to pinpoint, if possible, the specific enzymatic sites of TPMP action. In this step and to avoid unnecessary mitochondrial membrane permeabilization, we decided to selectively permeabilize the plasma membrane of the C2C12 cells using the XF plasma membrane permeabilizer from Seahorsebio.

Finally we examined the major enzymes responsible for the metabolism of each substrate after treatment with TPMP. We assayed the enzymes in skeletal muscle homogenate isolated from Wistar rats. In addition, treatment with the more hydrophobic propyl- and pentylTPP$^+$ was examined to find out a possible role of hydrophobicity in binding to the sites of interest.

6.1 Response of intact C2C12 cells to TPMP

The initial step in investigating the effect of TPMP was to examine the response of C2C12 intact cells respiring on substrates as that found in the growth medium to an acute addition of 1 μM TPMP (Figure 6.1). As previously discussed, the Nernstian distribution of these ions will result in an accumulation of approximately 1000-fold concentration inside the mitochondrial matrix. We found that TPMP at this concentration induces inhibition of respiration and simultaneously activates glycolytic metabolism.

6.1.1 Changes in cellular bioenergetics

Cells in the basal state responded to an acute addition of TPMP (1 μM final concentration) by a gradual decrease in oxygen consumption rate. We observed that the extent of this decrease in respiration was time-dependent and reached 36.93% [33.58-40.28%] of basal OCR after one hour of the initial treatment (Figure 6.1 B).

Due to this time-dependent course, the calculation of each respiratory parameter had to be time-related. After 20 minutes of treatment during which we obtained 3 cycles of measurement, the mitochondrial ATP turnover-driven respiration was reduced by ≈30% than the untreated control. This indicates a decrease in the reliance on oxidative phosphorylation to liberate the required energy.

The maximum respiratory capacity and proton leak respiration were also reduced following TPMP treatment (Figure 6.1 C). We have observed the reduction in maximal uncoupled respiration with the highly lipophilic alkylTPP$^+$ derivatives, however, a remarkable difference in the mechanism of respiratory inhibition between the more lipophilic alkylTPP$^+$ and TPMP was in proton leak respiration. Unlike the highly lipophilic TPP$^+$ compounds which caused a large increase in proton leak, the leak respiration in the TPMP treated cells was less than that of the untreated control cells, which is probably due to less flux of electrons to the respiratory chain. It is also an indicator that the mitochondrial membrane potential is intact after TPMP treatment. The reduction of all these respiratory parameters can be explained by an overall reduction in mitochondrial respiration, in which the mitochondria maintains an intact proton translocation driving force and subsequently intact electron transport chain, which directed us towards investigating the pathways that feeds electrons to the respiratory chain, which are mainly the enzymes of Krebs cycle.

6.1.2 Increase in glycolytic activity

Corresponding to the decrease in reliance on mitochondria respiration, TPMP treatment caused an increase in the glycolytic activity in the basal state. The increase in most likely to compensate for impaired mitochondrial ATP synthesis. The extracellular acidification rate started to increase immediately after TPMP

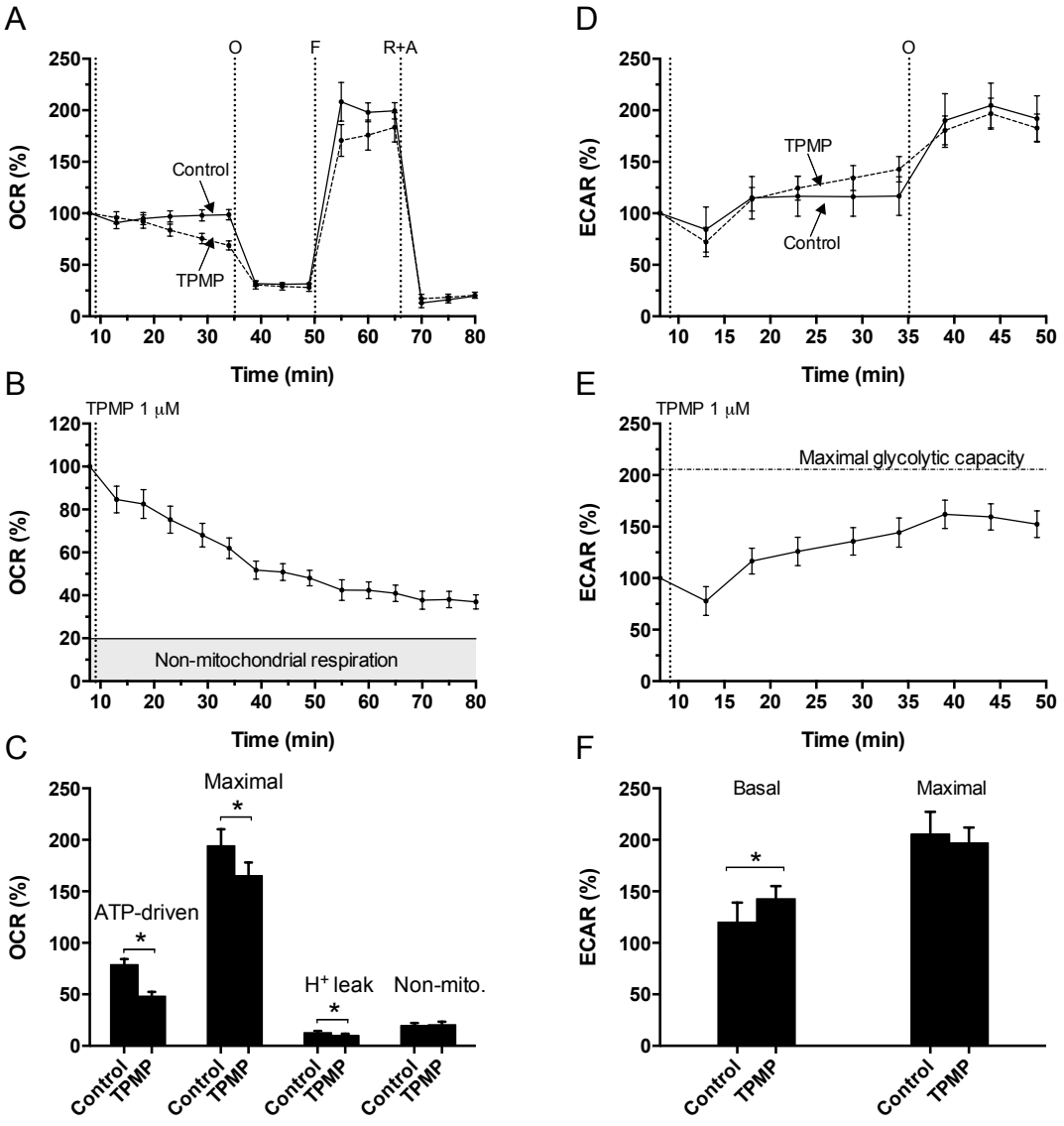

Figure 6.1: **TPMP inhibits mitochondrial respiration and increase glycolytic activity in intact cells. A.** A metabolic analysis of cellular respiration in intact C2C12 myoblasts. Cells were treated with 1 μM TPMP or vehicle, followed by sequential injection of 1 μM oligomycin (O), 1 μM FCCP (F), then 1 μM rotenone and antimycin A (R+A) mixture. The TPMP treated cells showed a decrease in oxygen consumption rate (OCR) following the TPMP addition. **B.** Cellular OCR decreases gradually after TPMP treatment. The level of non-mitochondrial respiration was found to be 19.76% [17.33-22.18%]. **C.** Mitochondrial respiratory parameters calculated from A were reduced. **D**, **E** & **F.** ECAR increases simultaneously with the decrease in OCR. Data is expressed as the percentage of basal OCR (OCR%) and is presented as means $\pm$95% CI, n=4. * indicates significant $p<0.05$ when compared to the control untreated group.

injection, and achieved the highest level after 40 minutes (Figure 6.1 E). As the rest of alkylTPP$^+$ derivatives, the maximum glycolytic capacity was not affected.

6.2 Response of permeabilized cells

The decrease in respiratory capacity of intact cells after TPMP treatment can be explained by a defect in the electron transport chain, or in the presence of sufficient concentrations of electron donors to feed the respiratory chain. In order to pinpoint the actual site of inhibition, it was suggested to test mitochondrial respiration in permeabilized cell. To maintain mitochondrial coupled respiration, we decided to selectively permeate the plasma membrane before using different respiratory substrates.

An important advantage of measuring mitochondrial respiration in permeabilized cells is the broad selection of plasma membrane impermeable substrates that can reach mitochondria, which enable researchers to examine different segments of the respiratory pathways. A functional citric acid cycle enzymes are essential to provide the electron transport chain with enough NADH and $FADH_2$ to maintain ATP production.

We assessed the activity of Krebs cycle by using different substrates. The used substrates included NADH-linked substrates (pyruvate/malate and glutamate/malate) which feed into the Krebs cycle and via complex I into the respiratory chain. The $FADH_2$-linked substrate was succinate, which is metabolized solely by the respiratory complex II. The metabolism of these different substrates guarantees scanning of all of the citric acid cycle enzymes (Figure 6.2).

In permeabilized C2C12 myoblasts an exposure to 10 μM TPMP (approximate equivalent of 1 μM TPMP extracellular concentration in the presence of plasma membrane potential) caused a rapid decrease of respiration in both NADH-linked substrates to an equal rate. Respiration on pyruvate/malate dropped to 26.17% [23.21-29.12%] and on glutamate/malate respiration decreased to 26.08% [24.66-27.50%] of basal respiration (Figure 6.3 A, B & C). When succinate was used as a substrate, the respiratory rate following a TPMP addition decreased to 89.17% [87.54-90.79%]. As in intact cells, adding an uncoupler (FCCP) removes the regulatory role of membrane potential and it caused a moderate increase

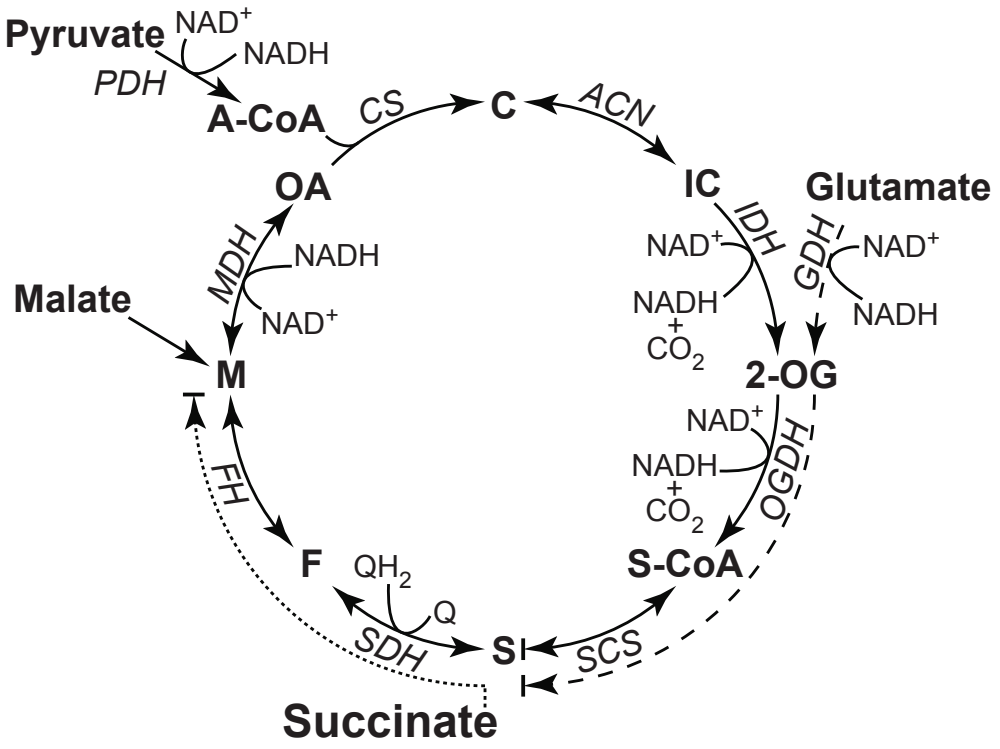

Figure 6.2: **Metabolic flux in permeabilized cells.** A schematic presentation of Krebs cycle showing the active enzymes when different mitochondrial substrates are used. NADH produced is re-oxidized by the respiratory complex I. The role of malate in pyruvate/malate respiration is to provide oxaloacetate which is further metabolized to citrate in the presence of acetyl-CoA. In glutamate/malate respiration, malate takes part in the malate aspartate shuttle. OGDH is a meeting point for pyruvate/malate and glutamate/malate metabolism. The presence of high concentration of malate inhibits succinate dehydrogenase by equilibrating with fumarate, which eventually prevents the flux from succinate to fumarate. PDH, pyruvate dehydrogenase complex; A-CoA, acetyl-CoA; CS, citrate synthase; C, citrate; ACN, aconitase; IC, isocitrate; IDH, isocitrate dehydrogenase; GDH, glutamate dehydrogenase; 2-OG, 2-oxoglutarate; OGDH, 2-oxoglutarate dehydrogenase complex; S-CoA, succinyl-CoA; SCS, succinyl-CoA synthase; S, succinate; SDH, succinate dehydrogenase; F, fumarate; FH, fumarate hydratase; M, malate; MDH, malate dehydrogenase; OA, oxaloacetate; Q, ubiquinone; QH_2, ubiquinol.

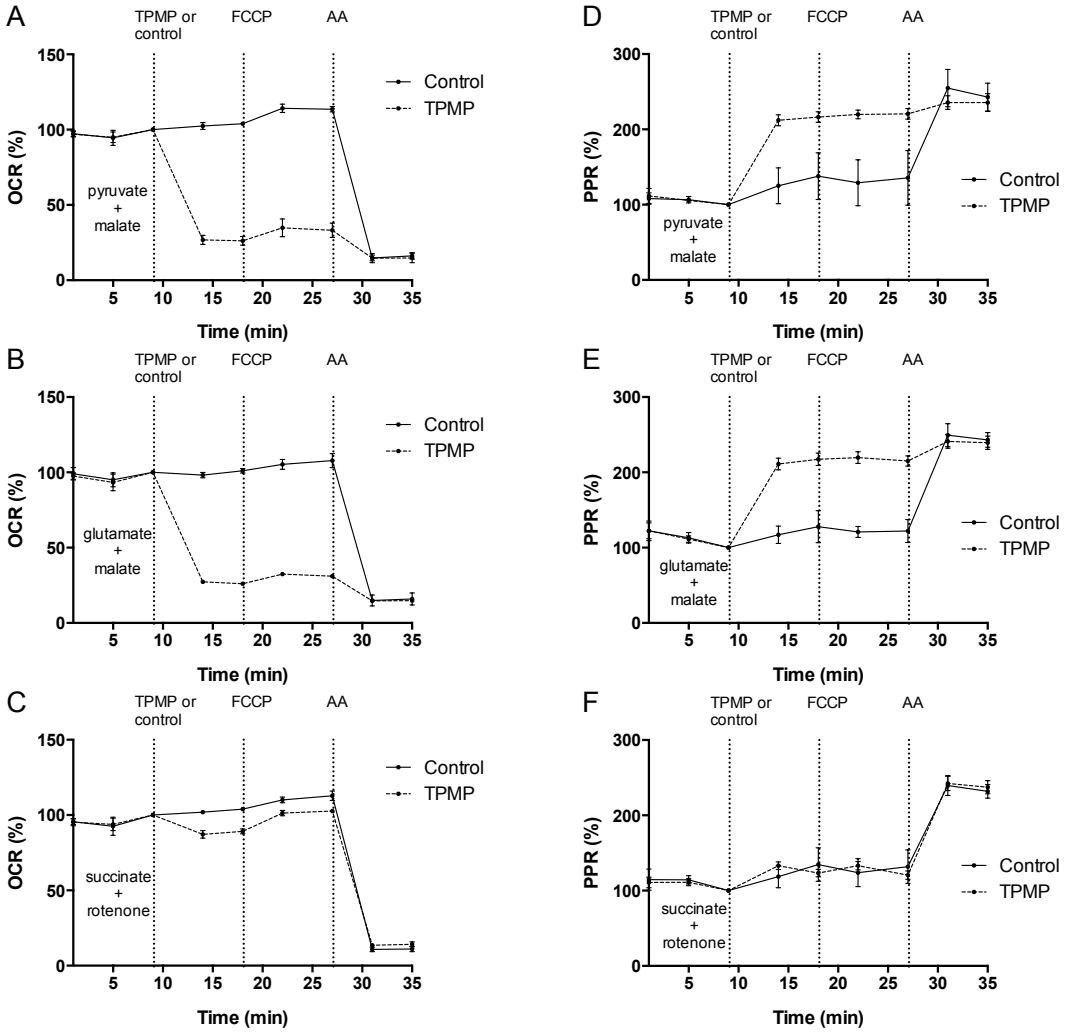

Figure 6.3: **Substrate driven respiration in selectively permeabilized plasma membrane.** Respiration was induced by the addition of ADP in the presence of the relative substrate. Cells were treated with TPMP10 μM or vehicle (deionized H_2O), followed by 1 μM FCCP, then 1 μM AA to block the flow of electrons in the respiratory chain. **A.** Respiration on 5mM pyruvate/ 2.5 mM malate. **B.** Respiration on 5 mM glutamate / 2.5 mM malate. **C.** Respiration on 10 mM succinate. **D & E.** The acidification rate (PPR) increased following TPMP treatment in pyruvate/malate and glutamate/malate cases. **F.** In the presence of succinate, the increase in PPR occurred after AA addition. Data is expressed as the percentage of basal OCR (OCR%) and is presented as means $\pm$95% CI, n=4. AA, antimycin A; OCR, oxygen consumption rate; PPR, proton production rate.

in respiration, which confirms the inhibitory effect of TPMP. The inhibition of respiration was associated with an increase in the proton production rate (PPR), which is analogous to ECAR in intact cells (Figure 6.3 D, E & F). TPMP caused an increase in PPR in pyruvate/malate and glutamate/malate cases equally, while the change in succinate case was not detectable. When respiration is completely inhibited by antimycin A, we observed the rise in PPR in all cases.

6.3 TPMP selectively inhibits 2–oxoglutarate dehydrogenase complex

We assessed the enzymatic activity of some mitochondrial enzymes including the complexes of the respiratory chain in skeletal muscle homogenate (except

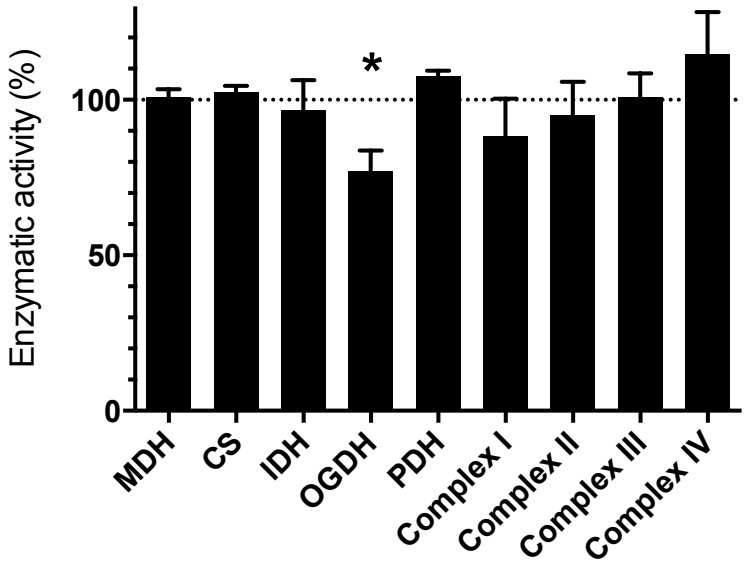

Figure 6.4: **Selective TPMP inhibitory effect on OGDH.** The enzymatic activities of pyruvate dehydrogenase, Krebs cycle and electron transport chain were not affected by the presence of 1 mM TPMP, except the OGDH, which was significantly reduced. Data is presented as means ±95% CI, n=3. * indicates significant $p<0.05$ when compared to the control untreated group. MDH, malate dehydrogenase; CS, citrate synthase; IDH, isocitrate dehydrogenase; OGDH, 2-oxoglutarate dehydrogenase complex; PDH, pyruvate dehydrogenase complex.

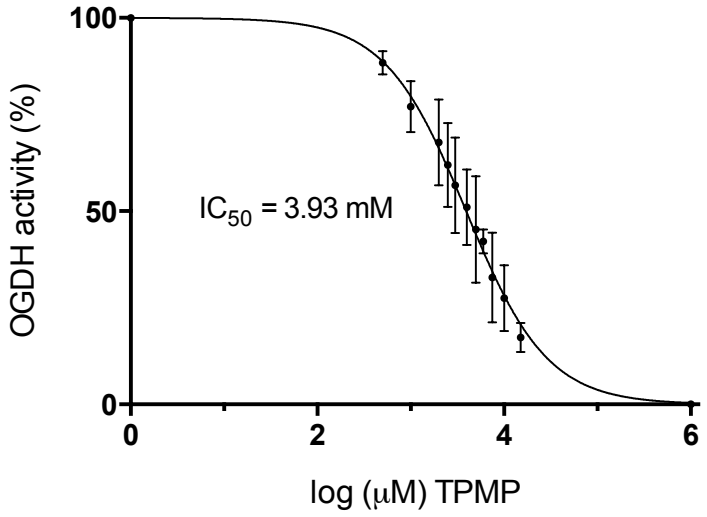

Figure 6.5: **IC_{50} of intramitochondrial TPMP.** IC_{50} of TPMP was found to be 3.93 [3.70-4.17] mM. Data is presented as means ±95% CI, n=3.

pyruvate dehydrogenase which was obtained purified from porcine heart) so as to identify the most affected site. The reaction condition contained 1 mM TPMP (approximate equivalent of 1 μM extracellular concentration).

The activity of OGDH complex was effectively reduced to 77.00% [70.34-83.66%] of the untreated control (Figure 6.4) in the presence of 1 mM of TPMP. The IC_{50} of TPMP was estimated to be 3.93 [3.70-4.17] mM (Figure 6.5). Other enzymes were resistant to TPMP with a minor non significant reduction in the activity of complex I.

6.4 TPP^+ hydrophobicity and OGDH inhibition are directly related

The activity of OGDH was measured after treatment with other more hydrophobic alkylTPP^+ derivatives using an equal concentration as that of TPMP. It was found that increasing the length of the alkyl side chain appears to enhance the inhibitory effect on OGDH activity. Activities of the pyruvate dehydrogenase complex and other Krebs cycle enzymes were not affected by the more

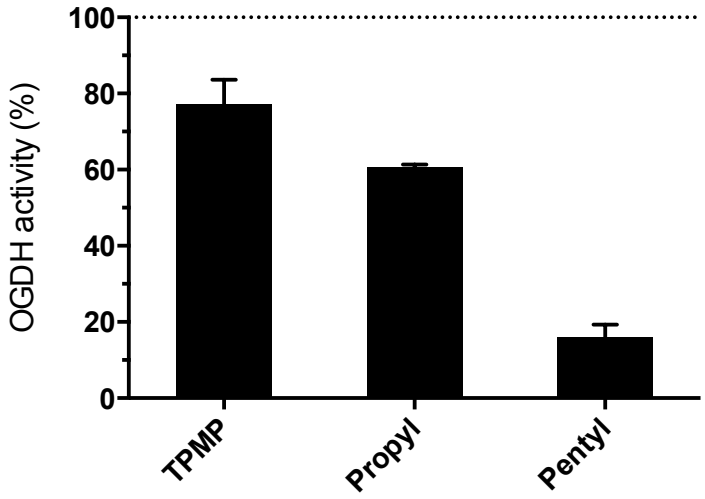

Figure 6.6: **More lipophilic TPP$^+$ derivates are more potent inhibitors of OGDH.** Longer chain alkylTPP$^+$ compounds have higher inhibitory effect. OGDH showed less activity in the presence of 1 mM concentration of the more lipophilic TPP$^+$ moieties in the assay mixture. The rate of inhibition was proportional to the increase in the length of the alkyl side chain. Data is presented as means ±95% CI, n=3. TPMP, methyltriphenylphosphonium; Propyl, propyltriphenylphosphonium; Pentyl, pentyltriphenylphosphonium.

hydrophobic TPP$^+$ moieties, and only OGDH was selectively affected. 1 mM propylTPP$^+$ reduced the activity to 60.70% [60.09-61.31%] of the untreated control, and pentylTPP$^+$ caused even more inhibition to reach 15.87% [12.44-19.30%] of the control activity (Figure 6.6).

6.5 Discussion

The results of this chapter show that one of the simplest and most widely used TPP$^+$ derivatives also inhibit Krebs cycle. The use of the mitochondriotropic TPP$^+$ derivatives has expanded to study mitochondria as ell as to influence its various functions including the production of reactive oxygen species (Smith et al., 2012). Despite their use on large scale, the unidentified effects of TPP$^+$ derivatives due to their chemical structure are much less understood (Asin-Cayuela et al., 2004).

We tried to answer the unexplained inhibitory effect of TPMP on mitochondrial respiration, which was observed in intact cells (Reily et al., 2013) and in isolated mitochondria (Brand, 1995; Ojovan et al., 2011). The data obtained from intact cells (Figure 6.1) show a general inhibitory effect of TPMP on cellular respiration, which is considerably slower to develop compared to more lipophilic derivatives discussed in the previous chapter. Another observed difference was the diminished proton leak respiration, which is together with the decrease in ATP-turnover driven and maximal respiration show a generalized drop in mitochondrial respiration. This was augmented by an immediate shift to glycolytic metabolism and an increase in ECAR.

The response of permeabilized C2C12 cells to TPMP inhibitory effect was much faster. A probable explanation is the easier transport of the relatively hydrophilic TPMP across the permeabilized plasma membrane (Ross et al., 2008) and the direct access to mitochondria. The inhibitory effect of TPMP was specific to the NADH-linked respiratory substrates. The rate of inhibition of pyruvate/malate respiration was nearly identical to that of glutamate/malate. Given that respiration on pyruvate/malate requires the presence of mitochondrial pyruvate carrier and an active pyruvate dehydrogenase complex beside a functional Krebs cycle, while glutamate/malate respiration requires a functioning glutamate dehydrogenase and oxoglutarate dehydrogenase complex, we could identify the possible site of inhibition to be linked to OGDH.

The OGDH is one of the rate limiting steps of the Krebs cycle, and it is required for both pyruvate/malate and glutamate/malate respiration, and since TPMP inhibited respiration of NADH-linked substrates equally, we directed the investigation towards the activity of OGDH in response to TPMP treatment. Bypassing OGDH step in the Krebs cycle by using succinate as a substrate confirmed the importance of OGDH as the site of action of TPMP. Respiration on succinate was minimally affected by TPMP and the cells maintained a high rate of respiration (Figure 6.3).

With exception of complex I, a negative effect of TPMP on the complexes of the respiratory chain and ATP synthase was excluded also by the results obtained from respiration of the permeabilized cells. NADH-linked substrates require active complexes I, III and IV, while succinate respiration requires complexes II,

III and IV. In the coupled state the ATP synthase maintains the production of ATP depending on the membrane potential in creating the essential driving force to maintain the process of oxidative phosphorylation. TPMP did not affect succinate respiration which reflects the continuous function of complexes II, III and IV in addition to ATP synthase.

Although OGDH was found to be the enzyme of interest, we performed a more detailed study of the enzymatic activity of major Krebs cycle enzymes in addition to pyruvate dehydrogenase complex and enzymes of the electron transport chain to reveal any other possible site of action of TPMP. Except OGDH, none of the examined enzymes was inhibited by TPMP (Figure 6.4), propylTPP$^+$ nor by pentylTPP$^+$. The function of OGDH is to oxidize and decarboxylate 2-oxoglutarate and attach coenzyme A to the product to form succinyl-CoA (Sheu and Blass, 1999; Qi et al., 2011). This function was increasingly affected by the length of the alkyl side chain of the alkylTPP$^+$ (Figure 6.6). This raises a question about OGDH structure and the possible attraction force to more harmful hydrophobic probes.

TPMP was quite potent in inhibiting the respiration of permeabilized cells, and 1 mM of it was sufficient to reduce the activity of OGDH by ≈23%. The estimated IC50 was therefore in the millimolar range (Figure 6.5), which appears high compared to other inhibitory substances. Considering the Nernstian distribution of cations, we can conclude that an accumulation of such high concentrations is very likely to occur in intact cells due to the negative plasma/mitochondrial membrane potentials, which allows TPMP and other TPP$^+$ derivatives to accumulate up to 1000 times higher concentration. Treating the cells with a micromolar concentration of TPP$^+$ moieties can induce its inhibitory response, and if TPMP is used, an inhibition of Krebs cycle can be expected. This inhibition can lead to accumulation of some of the citric acid cycle intermediates, which as a consequence may influence intracellular signaling and gene expression via the role of 2-oxoglutarate in prolyl hydroxylation of HIF-1 alpha (Semenza, 2007) and other signaling processes (Loenarz and Schofield, 2008; Chin et al., 2014).

The results of this chapter and the previous one raise a question about the distribution of different alkylTPP$^+$ derivatives in intact cells. While in the previous chapter we found no sign of interference of propylTPP$^+$ with mitochondrial

respiration, we observed that it is a more potent inhibitor of the activity of OGDH enzyme than TPMP at equal concentrations. However, TPMP could inhibit mitochondrial respiration of the intact cells. A probable explanation is that the concentration of the more hydrophobic propylTPP$^+$ in mitochondrial matrix, where it is needed to interfere with OGDH, would be lower than that of TPMP due to its preferential association with mitochondrial membranes.

The data of this chapter demonstrates the side effect of TPMP on mitochondrial respiration, and clarify the mechanism of action by selectively inhibiting the OGDH. This finding should be taken into account when interpreting data from experiments using TPP$^+$ salts. The results also show the importance of OGDH in mediating mitochondrial respiration, and its liability to the hydrophobic mitochondrial probes.

Chapter 7

Conclusions

The primary aim of this work was designed to investigate the energy metabolism of skeletal muscle. This general topic presented a large field of various research subjects, and it was initiated by investigating the mitochondrial respiratory function in an *in vitro* model of skeletal muscle, cultured in different conditions with various consumable substrates. The study also included the correlation between glucose level in culture media and mitochondrial function/dysfunction, targeting mitochondria, and the ability of the skeletal muscles to metabolize different energy substrates. This work partially increases our understanding of skeletal muscle metabolism, and allows us to develop a better model for studying mitochondria of skeletal muscle.

Galactose is not a suitable fuel for skeletal muscle

The use of galactose with skeletal muscles was proved in chapter 3 to be inappropriate. C2C12 cells do not utilize galactose even when cultured in glucose free media. The growth rate of cells treated with galactose was similar to those deprived of glucose, and both phenotypes possessed a significant lower growth rate than glucose fed cells. The level of media galactose was not changed when incubated with the cultured cells. The undifferentiated myoblasts failed to differentiate when supplemented with galactose and the presence of glucose is essential for C2C12 to differentiate. Cells lack of glucose failed to express the differentiation marker MHC, however, evidence of activation of the differentiation pathway was observed by expressing the MyoD transcriptional factor.

Oxidative respiration is enhanced by lowering glucose

The results of chapter 3 also show that using galactose or no glucose in the cell growth medium fails as a simple method to enhance the oxidative metabolism of C2C12 cells. Observable changes in mitochondrial respiratory parameters associated with the use of galactose were basically due to glucose deprivation. The effects of glucose deprivation are complex and depend, among other things, on the cell type used. For C2C12 cells, these results support a recommendation to use a moderate glucose concentration for cultivation and avoid high-glucose growth media. Different culture media may have a significant effect on the capacity of the mitochondrial respiratory chain, but the link of such a change to the extent of oxidative metabolism of the cultured cells cells remains unclear. In addition mitochondrial mass markers were not different among all groups of cells, and so were the glycolytic capabilities of the cells treated with normal, high or complete absence of glucose.

Glucose level optimization is essential to reveal the variation between different bioenergetic profiles

Assessment of mitochondrial parameters showed a marked variation when the glucose level was changed. Differences in respiratory capacity were best observed when the assay condition included 1 g/l glucose. When assessed in a glucose free medium supplemented with the mitochondrial substrates pyruvate and glutamine, the previously observed differences were masked. These observations recommend the use of a unified medium with identical composition and supplements for a proper comparison of mitochondrial parameters among different phenotypes.

High glucose decreased mitochondrial respiratory capacities

The data obtained from chapter 4 confirms the direct relation between high glucose level and mitochondrial dysfunction. Allowing the C2C12 cells to grow and differentiate in a high glucose environment caused a lower respiratory capacity when compared to myotubes treated with normal glucose concentration. The differences includes also a lower mitochondrial mass yield, and lower activity of

complex I and complex III. The differences did not include any change in glycolytic profiles. A major limitation to test the ability to oxidize free palmitic acid is due to the uncoupling effect of palmitate, which resulted in a large increase in leak respiration.

The hydrophobicity of mitochondrial targeting molecules negatively affect respiratory efficiency

The widely used mitochondriotropic triphenylphosphonium (TPP^+) derivatives were shown to interfere with mitochondrial bioenergetics in chapter 5. Although facilitating mitochondrial targeting, high hydrophobicity of the TPP^+ molecule alters the bioenergetic performance by markedly increasing the proton leak respiration and significantly decrease the coupling efficiency in intact cells. In isolated mitochondrial preparations, the more hydrophobic TPP^+ moieties inhibited the enzymatic activity of the mitochondrial respiratory chain. The mechanism of inhibition is not completely revealed, and disruption of the mitochondrial phospholipid membrane remains the most plausible explanation, due to the non-specific inhibition on all respiratory complexes. The hydrophobic mitochondrial targeting molecules are recommended to be tested for the adverse respiratory inhibition when designing new ones for use as diagnostic probes or therapeutic agents.

Methyltriphenylphosphonium inhibits Krebs cycle

Another adverse response of TPP^+ moieties is discussed in chapter 6. The least hydrophobic alkylTPP^+, methyltriphenylphosphonium (TPMP), inhibits mitochondrial respiration by directly inhibiting Krebs cycle. It selectively targets the 2-oxoglutarate dehydrogenase complex and interferes with the complex function, which declined markedly when treated with more hydrophobic alkyl TPP^+ compounds. The IC_{50} of TPMP is 3.93 mM in isolated mitochondrial fractions (3.93 μM extra-cellular). The enzyme 2-oxoglutarate dehydrogenase complex showed less activity when treated with more hydrophobic alkylTPP^+ derivatives, which draws the attention towards the importance of this enzyme, and also towards the distribution and binding of mitochondrial targeting molecules to mitochondrial matrix and membrane structures.

Supplementary tables

Throughout tables 1–8, the different metabolic phenotypes were given abbreviations. Phenotypes myoblasts or myotubes were given abbreviations according to their growth or differentiation conditions. LG, in 1 g/l glucose; HG, in 5 g/l glucose; GAL, in 1 g/l galactose; CF, in no carbohydrate supplement.

Table 1: Respiratory parameters of different metabolic phenotypes of C2C12 myoblasts in assay media containing growth medium substrates ($pmol(O_2).min^{-1}.(\mu g\ protein)^{-1}$). Data are shown as means and 95% CI, n=3.

	LG	HG	GAL	CF
Basal respiration	9.78 [0.48,19.08]	8.39 [4.25,12.54]	10.20 [6.17,14.24]	9.18 [3.42,14.81]
Basal mitochondrial respiration	6.52 [-0.25,13.29]	5.52 [4.06,6.99]	6.73 [1.52,11.93]	6.09 [3.61,8.57]
ATP turnover-driven respiration	5.48 [-0.06,11.57]	4.60 [2.57,6.63]	6.15 [2.83,9.47]	5.13 [2.30,7.97]
Maximum respiratory capacity	24.17 [14.24,34.09]	17.20 [14.21,20.18]	10.03 [-4.08,24.13]	8.04 [1.91,14.17]
Spare respiratory capacity	17.65 [7.11,28.18]	11.67 [7.27,16.08]	3.30 [-7.77,14.37]	1.95 [-6.00,9.90]
H^+ Leak	1.04 [-0.23,2.31]	0.92 [-0.60,2.45]	0.57 [-1.45,2.60]	0.96 [0.58,1.34]
Non-mitochondrial respiration	3.26 [-0.06,6.58]	2.87 [-0.45,6.19]	3.48 [1.31,5.65]	3.03 [-0.36,6.41]

Table 2: Respiratory parameters of C2C12 myoblasts in glucose 1 g/l assay medium (pmol(O_2).min^{-1}.(μg protein)$^{-1}$). Data are shown as means and 95% CI, n=3.

	LG	HG	GAL	CF
Basal respiration	9.65 [0.45,18.85]	8.37 [5.49,11.26]	6.76 [5.25,8.26]	6.42 [4.73,8.12]
Basal mitochondrial respiration	6.16 [0.60,11.71]	6.16 [4.43,7.89]	3.78 [1.35,6.21]	3.94 [2.16,5.73]
ATP turnover-driven respiration	5.37 [-0.06,10.8]	5.00 [3.93,6.06]	3.02 [1.90,4.13]	3.08 [2.01,4.15]
Maximum respiratory capacity	24.86 [20.83,28.89]	15.57 [11.93,19.2]	9.56 [5.51,13.61]	10.51 [6.25,14.77]
Spare respiratory capacity	18.70 [9.15,28.25]	9.41 [6.65,12.17]	5.78 [3.67,7.89]	6.56 [3.83,9.30]
H^+Leak	0.79 [-0.74,2.31]	1.16 [0.31,2.01]	0.76 [-1.03,2.55]	0.87 [-0.19,1.93]
Non-mitochondrial respiration	3.50 [-1.59,8.59]	2.22 [0.32,4.11]	2.98 [0.81,5.15]	2.48 [1.81,3.14]

Table 3: Respiratory parameters of C2C12 myoblasts in glucose-free assay medium (pmol(O_2).min^{-1}.(μg protein)$^{-1}$). Data are shown as means and 95% CI, n=3.

	LG	HG	GAL	CF
Basal respiration	9.21 [-1.26,19.69]	7.83 [-0.31,15.97]	10.29 [4.97,15.60]	7.75 [-4.60,20.11]
Basal mitochondrial respiration	6.50 [-0.74,13.74]	5.75 [0.02,11.48]	7.09 [4.18,10.00]	5.42 [-4.36,15.19]
ATP turnover-driven respiration	5.48 [-1.05,12.02]	4.58 [0.05,9.11]	6.00 [3.93,8.07]	4.35 [-3.52,12.22]
Maximum respiratory capacity	11.76 [8.85,14.67]	7.80 [1.50,14.09]	11.09 [-4.48,26.66]	8.31 [-7.05,23.66]
Spare respiratory capacity	5.26 [-3.99,14.51]	2.05 [-0.58,4.67]	4.00 [-9.00,17.00]	2.89 [-5.92,11.70]
H^+ Leak	1.02 [0.05,1.99]	1.17 [-0.04,2.38]	1.09 [-0.17,2.34]	1.07 [-0.91,3.05]
Non-mitochondrial respiration	2.71 [-0.85,6.27]	2.08 [-0.41,4.56]	3.20 [0.33,6.07]	2.33 [-0.64,5.31]

Table 4: Respiratory parameters of myotubes in glucose 1 g/l assay medium (pmol(O_2).min^{-1}.(μg protein)$^{-1}$). Data are shown as means and 95% CI, n=3.

	LG	HG
Basal respiration	19.43 [16.49,22.37]	23.05 [21.31,24.79]
Basal mitochondrial respiration	12.76 [9.73,15.79]	16.34 [13.37,19.31]
ATP turnover-driven respiration	10.22 [8.31,12.13]	12.89 [11.09,14.70]
Maximum respiratory capacity	60.77 [51.37,70.16]	44.70 [27.03,62.36]
Spare respiratory capacity	48.01 [41.64,54.37]	28.36 [9.68,47.03]
H^+ Leak	2.54 [1.38,3.70]	3.45 [2.28,4.62]
Non-mitochondrial respiration	6.67 [6.17,7.17]	6.71 [5.44,7.98]

Table 5: Glycolytic activity of C2C12 myoblasts and myotubes represented as the extracellular acidification rate (ECAR) in 1 g/l glucose environment (mpH.min^{-1}.(μg protein)$^{-1}$). Data are shown as means and 95% CI, n=3.

	Basal	Oligomycin-stimulated	Glycolytic reserve
Myoblasts			
LG	3.27 [2.27,4.27]	4.60 [3.22,5.98]	1.33 [0.91,1.75]
HG	3.46 [1.57,5.34]	4.94 [1.66,8.22]	1.48 [0.07,2.89]
GAL	2.61 [1.10,4.12]	3.48 [0.71,6.26]	0.87 [-0.40,2.15]
CF	3.77 [0.46,7.07]	5.09 [0.58,9.59]	1.32 [0.09,2.55]
Myotubes			
LG	0.42 [0.26,0.59]	0.83 [0.46,1.20]	0.41 [-0.01,0.82]
HG	0.43 [0.22,0.63]	0.72 [0.04,1.41]	0.30 [-0.18,0.77]

Table 6: Mitochondrial mass markers in C2C12 myoblasts and myotubes. Data are shown as means and 95% CI, n=3. Citrate synthase activity (CS) is expressed as (nmol.min^{-1}.(μg protein)$^{-1}$). Mitochondrial yield was determined as μg of mitochondrial protein content per μg of total cellular protein.

	CS	Mitochondrial yield
Myoblasts		
LG	1.73 [1.05,2.42]	0.12 [0.09,0.15]
HG	1.62 [1.25,2.00]	0.09 [0.07,0.10]
GAL	1.85 [1.21,2.49]	0.13 [0.09,0.16]
CF	1.55 [0.96,2.14]	0.09 [0.01,0.18]
Myotubes		
LG	2.94 [2.50,3.38]	0.18 [0.17,0.20]
HG	2.88 [2.52,3.24]	0.12 [0.05,0.19]

Table 7: Respiratory chain enzymatic activity in C2C12 myoblasts and myotubes. Data are shown as means and 95% CI, n=3.

	Complex I†	Complex II†	Complex III¶	Complex IV§
Myoblasts				
LG	56.70 [23.33,90.07]	21.89 [15.57,28.12]	32.29 [12.34,52.24]	3.31 [2.15,4.48]
HG	58.44 [17.19,99.69]	22.00 [11.40,32.59]	26.35 [-11.83,64.53]	2.88 [2.00,3.76]
GAL	84.78 [33.26,136.30]	27.39 [3.85,50.93]	54.94 [9.85,100.03]	5.91 [3.35,8.47]
CF	86.49 [69.58,103.40]	30.31 [4.48,56.14]	56.07 [-14.94,127.07]	4.80 [3.87,5.73]
Myotubes				
LG	176.72 [125.70,227.75]	45.25 [32.09,58.42]	64.67 [42.36,86.99]	6.42 [2.85,9.99]
HG	82.89 [19.22,146.55]	37.08 [22.98,51.18]	23.40 [0.75,46.05]	4.55 [2.88,6.21]

Activities were expressed as †pmol(DCIP).min^{-1}.(μg protein)$^{-1}$, ¶pmol(cytochrome c).min^{-1}.(μg protein)$^{-1}$, $^{\S}\mu\Delta\ln(A_{550})$.min^{-1}.($\mu$g protein)$^{-1}$.

Table 8: Testing palmitate oxidation in C2C12 myotubes (pmol(O_2).min^{-1}.(μg protein)$^{-1}$). Data are shown as means and 95% CI, n=3.

	LG-PA	LG-BSA	HG-PA	HG-BSA
Basal respiration	15.06 [8.86,21.26]	15.15 [10.86,19.43]	16.72 [8.27,25.16]	15.35 [6.97,23.72]
Basal mitochondrial respiration	9.70 [4.70,14.70]	11.64 [7.79,15.48]	11.61 [4.83,18.39]	11.91 [3.75,20.08]
100 μM palmitate or vehicle	19.07 [10.45,27.68]	14.87 [9.50,20.23]	19.89 [8.57,31.21]	14.64 [7.13,22.15]
200 μM palmitate or vehicle	23.93 [14.45,33.41]	14.34 [8.31,20.37]	23.62 [12.02,35.21]	13.66 [7.28,20.04]
ATP turnover-driven respiration	5.58 [-1.73,12.89]	8.80 [4.29,13.31]	7.14 [-0.73,15.01]	8.14 [2.68,13.60]
H^+Leak	13.07 [10.77,15.37]	2.07 [1.22,2.92]	11.43 [6.89,15.97]	2.19 [0.93,3.45]
Non-mitochondrial respiration	5.36 [4.03,6.69]	3.50 [1.94,5.07]	5.11 [3.43,6.78]	3.43 [2.65,4.21]

PA, indicates treatment with palmitate during the measurement; BSA, indicates treatment with a BSA vehicle.

Table 9: Mean fluorescence intensity of TMRM as indicator of qualitative changes in mitochondrial membrane potential of C2C12 myoblasts treated with 1 μM TPP^+ derivatives or DMSO control. Data are geometrical means of fluorescence intensity, and expressed as the percentage of the untreated control and 95% CI, n=4.

Treatment	Fluorescence intensity (% of untreated control)
DMSO	94,50 [87.56,101.4]
propylTPP^+	93,75 [88.18,99.32]
hepty$lTPP^+$	35,50 [25.07,45.93]
decylTPP^+	19,25 [2.39,36.11]
dodecylTPP^+	18,00 [0.71,35.29]
FCCP	43,50 [25.47,61.53]

References

Acosta, P. B. and Gross, K. C. (1995). Hidden sources of galactose in the environment. *European Journal of Pediatrics*, 154(7):S87–92. 16

Affourtit, C. and Brand, M. D. (2008). Uncoupling protein-2 contributes significantly to high mitochondrial proton leak in INS-1E insulinoma cells and attenuates glucose-stimulated insulin secretion. *Biochemical Journal*, 409(1):199–204. 10

Affourtit, C. and Brand, M. D. (2009). Measuring mitochondrial bioenergetics in INS-1E insulinoma cells. *Methods in Enzymology*, 457:405–424. 11

Aguer, C., Gambarotta, D., Mailloux, R. J., Moffat, C., Dent, R., McPherson, R., and Harper, M.-E. (2011). Galactose enhances oxidative metabolism and reveals mitochondrial dysfunction in human primary muscle cells. *PloS One*, 6(12):e28536. 2, 15, 16, 43, 56

Ainscow, E. K. and Brand, M. D. (1999). Top-down control analysis of ATP turnover, glycolysis and oxidative phosphorylation in rat hepatocytes. *European Journal of Biochemistry*, 263(3):671–685. 10

Amo, T., Yadava, N., Oh, R., Nicholls, D. G., and Brand, M. D. (2008). Experimental assessment of bioenergetic differences caused by the common European mitochondrial DNA haplogroups H and T. *Gene*, 411(1-2):69–76. 10

Anglin, R. E., Garside, S. L., Tarnopolsky, M. A., Mazurek, M. F., and Rosebush, P. I. (2012a). The psychiatric manifestations of mitochondrial disorders: a case and review of the literature. *J Clin Psychiatry*, 73(4):506–512. 1

Anglin, R. E., Mazurek, M. F., Tarnopolsky, M. A., and Rosebush, P. I. (2012b). The mitochondrial genome and psychiatric illness. *Am. J. Med. Genet. B Neuropsychiatr. Genet.*, 159B(7):749–759. 1

Antonenko, Y. N., Khailova, L. S., Knorre, D. A., Markova, O. V., Rokitskaya, T. I., Ilyasova, T. M., Severina, I. I., Kotova, E. A., Karavaeva, Y. E., Prikhodko, A. S., Severin, F. F., and Skulachev, V. P. (2013). Penetrating cations enhance uncoupling activity of anionic protonophores in mitochondria. *PLoS ONE*, 8(4):e61902. 21, 83

Asin-Cayuela, J., Manas, A. R., James, A. M., Smith, R. A., and Murphy, M. P. (2004). Fine-tuning the hydrophobicity of a mitochondria-targeted antioxidant. *FEBS Lett.*, 571(1-1):9–16. 92

Bakeeva, L. E., Grinius, L. L., Jasaitis, A. A., Kuliene, V. V., Levitsky, D. O., Liberman, E. A., Severina, I. I., and Skulachev, V. P. (1970). Conversion of biomembrane-produced energy into electric form. II. Intact mitochondria. *Biochim Biophys Acta.*, 216(1):13–21. 20

Baron, A. D., Brechtel, G., Wallace, P., and Edelman, S. V. (1988). Rates and tissue sites of non-insulin- and insulin-mediated glucose uptake in humans. *American Journal of Physiology. Endocrinology and Metabolism*, 255(6):E769–774. 13

Beal, F. M. (2000). Energetics in the pathogenesis of neurodegenerative diseases. *Trends in neurosciences*, 23(7):298–304. 14

Berry, G. T. (1995). The role of polyols in the pathophysiology of hypergalactosemia. *European Journal of Pediatrics*, 154(7):S53–64. 18

Berry, G. T., Moate, P. J., Reynolds, R. A., Yager, C. T., Ning, C., Boston, R. C., and Segal, S. (2004). The rate of de novo galactose synthesis in patients with galactose-1-phosphate uridyltransferase deficiency. *Mol Genet Metab*, 81(1):22–30. 16

Berry, G. T., Nissim, I., Gibson, J. B., Mazur, A., Lin, Z., Elsas, L. J., Singh, R. H., Klein, P. D., and Segal, S. (1997). Quantitative assessment of whole body galactose metabolism in galactosemic patients. *European Journal of Pediatrics*, 156(1):S43–49. 16

Berry, G. T., Nissim, I., Lin, Z., Mazur, A., Gibson, J. B., and Segal, S. (1995). Endogenous synthesis of galactose in normal men and patients with hereditary galactosaemia. *Lancet*, 346(8982):1073–1074. 16

Berry, G. T., Palmieri, M., Gross, K. C., Acosta, P. B., Henstenburg, J. A., Mazur, A., Reynolds, R., and Segal, S. (1993). The effect of dietary fruits and

vegetables on urinary galactitol excretion in galactose-1-phosphate uridyltransferase deficiency. *Journal of Inherited Metabolic Disease*, 16(1):91–100. 16

Blaak, E. E., Wagenmakers, A. J. M., Glatz, J. F. C., Wolffenbuttel, B. H. R., Kemerink, G. J., Langenberg, C. J. M., Heidendal, G. A. K., and Saris, W. H. M. (2000). Plasma FFA utilization and fatty acid-binding protein content are diminished in type 2 diabetic muscle. *American Journal of Physiology. Endocrinology and Metabolism*, 279:E146–E154. 64

Blake, R. and Trounce, I. A. (2014). Mitochondrial dysfunction and complications associated with diabetes. *Biochim Biophys Acta.*, 1840(4):1404–1412. 1

Boden, G. (1999). Free Fatty Acids, Insulin Resistance, and Type 2 Diabetes Mellitus. *Proceedings of the Association of American Physicians*, 111(3):241–248. 64

Bogardus, C., Thuillez, P., Ravussin, E., Vasquez, B., Narimiga, M., and Azhar, S. (1983). Effect of muscle glycogen depletion on in vivo insulin action in man. *The Journal of Clinical Investigation*, 72(5):1605–1610. 13

Boushel, R., Gnaiger, E., Schjerling, P., Skovbro, M., Kraunsøe, R., and Dela, F. (2007). Patients with type 2 diabetes have normal mitochondrial function in skeletal muscle. *Diabetologia*, 50:790–796. 58

Brand, M. D. (1990). The contribution of the leak of protons across the mitochondrial inner membrane to standard metabolic rate. *Journal of Theoretical Biology*, 145(2):267–286. 12

Brand, M. D. (1995). *Bioenergetics – A practical approach*, chapter 3– Measurement of mitochondrial protonmotive force, pages 39–62. IRL PRESS. 21, 84, 93

Brand, M. D., Chien, L. F., Ainscow, E. K., Rolfe, D. E., and Porter, R. K. (1994). The causes and functions of mitochondrial proton leak. *Biochimica et Biophysica Acta*, 1187(2):132–139. 12

Brand, M. D. and Nicholls, D. G. (2011). Assessing mitochondrial dysfunction in cells. *Biochemical Journal*, 435(2):297–312. 9, 11, 57

Brown, G. C. and Brand, M. D. (1985). Thermodynamic control of electron flux through mitochondrial cytochrome bc1 complex. *Biochem. J.*, 225(2):399–405. 84

Brown, G. C., Lakin-Thomas, P. L., and Brand, M. D. (1990). Control of respiration and oxidative phosphorylation in isolated rat liver cells. *European Journal of Biochemistry*, 192(2):355–362. 10

Brown, S. E., Ross, M. F., Sanjuan-Pla, A., Manas, A. B., Smith, R. A., and Murphy, M. P. (2007). Targeting lipoic acid to mitochondria: synthesis and characterization of a triphenylphosphonium-conjugated alpha-lipoyl derivative. *Free Radic Biol Med.*, 42(12):1766–1780. 20

Brownlee, M. (2001). Biochemistry and molecular cell biology of diabetic complications. *Nature*, 414(6865):813–820. 66

Cameron, N. E., Cotter, M. A., Robertson, S., and Cox, D. (1992). Muscle and nerve dysfunction in rats with experimental galactosaemia. *Exp Physiol*, 77(1):89–108. 14, 18

Cerletti, P., Strom, R., and Giordano, M. G. (1965). Reactivation of succinic dehydrogenase by phospholipids. *Biochem. Biophys. Res. Commun.*, 18:259–263. 81

Chen, R. F. and Plaut, G. W. (1963). Activation and inhibition of DPN-linked isocitrate dehydrogenase of heart by certain nucleotides. *Biochemistry*, 2:1023–1032. 32

Chin, R. M., Fu, X., Pai, M. Y., Vergnes, L., Hwang, H., Deng, G., Diep, S., Lomenick, B., Meli, V. S., Monsalve, G. C., Hu, E., Whelan, S. A., Wang, J. X., Jung, G., Solis, G. M., Fazlollahi, F., Kaweeteerawat, C., Quach, A., Nili, M., Krall, A. S., Godwin, H. A., Chang, H. R., Faull, K. F., Guo, F., Jiang, M., Trauger, S. A., Saghatelian, A., Braas, D., Christofk, H. R., Clarke, C. F., Teitell, M. A., Petrascheck, M., Reue, K., Jung, M. E., Frand, A. R., and Huang, J. (2014). The metabolite α-ketoglutarate extends lifespan by inhibiting ATP synthase and TOR. *Nature*, 510(7505):397–401. 94

Choi, S. W., Gerencser, A. A., and Nicholls, D. G. (2009). Bioenergetic analysis of isolated cerebrocortical nerve terminals on a microgram scale: spare respiratory capacity and stochastic mitochondrial failure. *Journal of neurochemistry*, 109(4):1179–1191. 12

Chrissobolis, S., Miller, A. A., Drummond, G. R., Kemp-Harper, B. K., and Sobey, C. G. (2011). Oxidative stress and endothelial dysfunction in cerebrovascular disease. *Frontiers in Bioscience (Landmark Ed)*, 16:1733–1745. 1

Cochemé, H. M., Quin, C., McQuaker, S. J., Cabreiro, F., Logan, A., Prime, T. A., Abakumova, I., Patel, J. V., Fearnley, I. M., James, A. M., Porteous, C. M., Smith, R. A., Saeed, S., Carré, J. E., Singer, M., Gems, D., Hartley, R. C., Partridge, L., and Murphy, M. P. (2011). Measurement of H2O2 within living Drosophila during aging using a ratiometric mass spectrometry probe targeted to the mitochondrial matrix. *Cell Metab.*, 13(3):340–350. 20

Cogan, D. G., Kinoshita, J. H., Kador, P. F., Robison, G., Datilis, M. B., Cobo, L. M., and Kupfer, C. (1984). NIH conference. Aldose reductase and complications of diabetes. *Ann Intern Med*, 101(1):82–91. 18

Constable, S. H., Favier, R. J., Cartee, G. D., Young, D. A., and Holloszy, J. O. (1988). Muscle glucose transport: interactions of in vitro contractions, insulin, and exercise. *Journal of Applied Physiology*, 64(6):2329–2332. 13

Cooney, G. J., Thompson, A. L., Furler, S. M., Ye, J., and Kraegen, E. W. (2002). Muscle Long-Chain Acyl CoA Esters and Insulin Resistance. *Annals of the New York Academy of Sciences*, 967:169–207. 64

Cooperstein, S. J. and Lazarow, A. (1951). A microspectrophotometric method for the determination of cytochrome oxidase. *The Journal of Biological Chemistry*, 189(2):665–670. 34

Cumming, G. (2012). *The new statistics: effect sizes, confidence intervals and meta-analysis*. Routledge, New York. 41

Cunniff, B., Benson, K., Stumpff, J., Newick, K., Held, P., Taatjes, D., Joseph, J., Kalyanaraman, B., and Heintz, N. H. (2013). Mitochondrial-targeted nitroxides disrupt mitochondrial architecture and inhibit expression of peroxiredoxin 3 and FOXM1 in malignant mesothelioma cells. *J. Cell. Physiol.*, 228(4):835–845. 20

Davidson, W. S. and Murphy, D. G. (1985). Aldehyde reductases and their involvement in muscular dystrophy. *Progress in Clinical and Biological Research*, 174:251–263. 18

Davis, R. L., Cheng, P. F., Lassar, A. B., Thayer, M., Tapscott, S., and Weintraub, H. (1989). MyoD and achaete-scute: 4-5 amino acids distinguishes myogenesis from neurogenesis. *Int. Symp. Princess Takamatsu Cancer Res. Fund*, 20:267–278. 48

DeFronzo, R. A. (1988). The triumvirate: B-cell, muscle, liver-A collusion responsible for NIDDM. *Diabetes*, 37:667–687. 13

Dela, F. and Helge, J. W. (2013). Insulin resistance and mitochondrial function in skeletal muscle. *Int. J. Biochem. Cell Biol.*, 45(1):11–15. 1

Duggleby, R. G., Chao, Y. C., Huang, J. G., Peng, H. L., and Chang, H. Y. (1996). Sequence differences between human muscle and liver cDNAs for UDPglucose pyrophosphorylase and kinetic properties of the recombinant enzymes expressed in Escherichia coli. *European Journal of Biochemistry*, 235(1-2):173–179. 17

Dvornik, D. (1987). *Aldose reductase inhibition: an approach to the prevention of diabetic complications*. Biomedical Information Corp. 15, 18, 43

Fiaschi, T., Chiarugi, P., Buricchi, F., Giannoni, E., Taddei, M. L., Talini, D., Cozzi, G., Zecchi-Orlandini, S., Raugei, G., and Ramponi, G. (2001). Low molecular weight protein-tyrosine phosphatase is involved in growth inhibition during cell differentiation. *J. Biol. Chem.*, 276(52):49156–49163. 14

Filipovska, A., Kelso, G. F., Brown, S. E., Beer, S. M., Smith, R. A., and Murphy, M. P. (2005). Synthesis and characterization of a triphenylphosphonium-conjugated peroxidase mimetic. Insights into the interaction of ebselen with mitochondria. *J Biol Chem.*, 280(25):24113–24126. 20

Flewelling, R. F. and Hubbell, W. L. (1986). The membrane dipole potential in a total membrane potential model. Applications to hydrophobic ion interactions with membranes. *Biophys. J.*, 49(2):541–552. 19

Floryk, D. and Houstěk, J. (1999). Tetramethyl rhodamine methyl ester (TMRM) is suitable for cytofluorometric measurements of mitochondrial membrane potential in cells treated with digitonin. *Biosci. Rep.*, 19(1):27–34. 37

Fry, M. and Green, D. E. (1980). Cardiolipin requirement by cytochrome oxidase and the catalytic role of phospholipid. *Biochem. Biophys. Res. Commun.*, 93(4):1238–1246. 81

Fry, M. and Green, D. E. (1981). Cardiolipin requirement for electron transfer in complex I and III of the mitochondrial respiratory chain. *J. Biol. Chem.*, 256(4):1874–1880. 81

Fulco, M., Cen, Y., Zhao, P., Hoffman, E. P., Mcburney, M. W., Sauve, A., and Sartorelli, V. (2008). Glucose restriction inhibits skeletal myoblast differentiation by activating SIRT1 through AMPK-mediated regulation of Nampt. *Developmental Cell*, 14(5):661–673. 56

Gardner, M. and Altman, D. (1986). Confidence intervals rather than P values : estimation rather than hypothesis testing. *British Medical Journal*, 292:746–750. 41

Garetto, L. P., Richter, E. A., Goodman, M. N., and Ruderman, N. B. (1984). Enhanced muscle glucose metabolism after exercise in the rat: the two phases. *American Journal of Physiology. Endocrinology and Metabolism*, 246(6):E471–475. 13

Gerbitz, K. D., Gempel, K., and Brdiczka, D. (1996). Mitochondria and diabetes. Genetic, biochemical, and clinical implications of the cellular energy circuit. *Diabetes*, 45(2):113–126. 58

Goncalves, S., Paupe, V., Dassa, E. P., Briere, J. J., Favier, J., Gimenez-Roqueplo, A. P., Benit, P., and Rustin, P. (2010). Rapid determination of tricarboxylic acid cycle enzyme activities in biological samples. *BMC Biochem.*, 11:5. 32, 33

Goodpaster, B. H., Theriault, R., Watkins, S. C., and Kelley, D. E. (2000). Intramuscular lipid content is increased in obesity and decreased by weight loss. *Metabolism*, 49(4):467–472. 63

Grinius, L. L., Jasaitis, A. A., Kadziauskas, Y. P., Liberman, E. A., Skulachev, V. P., Topali, V. P., Tsofina, L. M., and Vladimirova, M. A. (1970). Conversion of biomembrane-produced energy into electric form. I. Submitochondrial particles. *Biochim Biophys Acta.*, 216(1):1–12. 20, 84

Guyton, A. C. and Hall, J. E. (2006). *Textbook of medical physiology*. Elsevier Saunders, Philadelphia,, 11th edition edition. 13

Hardy, M., Rockenbauer, A., Vásquez-Vivar, J., Felix, C., Lopez, M., Srinivasan, S., Avadhani, N., and Kalyanaraman, B. (2007). Detection, characterization, and decay kinetics of ROS and thiyl adducts of mito-DEPMPO spin trap. *Chem Res Toxicol.*, 20(7):1053–1060. 20

Heidenreich, R., Mallee, J., Rogers, S., and Segal, S. (1993). Developmental and tissue-specific modulation of rat galactose-1-phosphate uridyltransferase steady state messenger RNA and specific activity levels. *Pediatric Research*, 34(4):416–419. 15, 43, 56

Holden, H. M., Rayment, I., and Thoden, J. B. (2003). Structure and Function of Enzymes of the Leloir Pathway for Galactose Metabolism. *The Journal of Biological Chemistry*, 278:43885–43888. 17

Holloszy, J. O. J., Oscai, B. L., Don, J. I., and Mole, A. P. (1970). Mitochondrial citric acid cycle and related enzymes: Adaptive response to excercise. *Biochemical and Biophysical Research Communications*, 40(6):1368–1373. 53

Hood, A. D., Zak, R., and Pette, D. (1989). Chronic stimulation of rat skeletal muscle induces coordinate increases in mitochondrial and nuclear mRNAs of cytochrome-c-oxidase subunits. *European Journal of Biochemistry*, 179(2):275–280. 53

Ibsen, K. H. (1961). The Crabtree effect: a review. *Cancer Research*, 21(7):829–841. 2

Ichiki, T. and Sunagawa, K. (2014). Novel roles of hypoxia response system in glucose metabolism and obesity. *Trends Cardiovasc Med.* 1

Itani, S. I., Ruderman, N. B., Schmieder, F., and Boden, G. (2002). Lipid-induced insulin resistance in human muscle is associated with changes in diacylglycerol, protein kinase C, and IkappaB-alpha. *Diabetes*, 51(7):2005–2011. 64

James, A. M., Cochemé, H. M., Smith, R. A., and Murphy, M. P. (2005). Interactions of mitochondria-targeted and untargeted ubiquinones with the mitochondrial respiratory chain and reactive oxygen species. Implications for the use of exogenous ubiquinones as therapies and experimental tools. *J Biol Chem.*, 280(22):21295–21312. 20

Janssen, A., Trijbels, F., Sengers, R., Smeitink, J., Heuvel, L., Wintjes, L., Stoltenborg-Hogenkamp, B., and Rodenburg, R. (2007). Spectrophotometric assay for complex I of the respiratory chain in tissue samples and cultured fibroblasts. *Clinical Chemistry*, 53(4):729–734. 33

Jarrett, S. G., Lewin, A. S., and Boulton, M. E. (2010). The Importance of Mitochondria in Age-Related and Inherited Eye Disorders. *Ophthalamic Research*, 44(3):179–190. 1

Jekabsons, M. B. and Nicholls, D. G. (2004). In situ respiration and bioenergetic status of mitochondria in primary cerebellar granule neuronal cultures exposed continuously to glutamate. *Journal of Biological Chemistry*, 279(31):32989–33000. 10

Jelenik, T. and Roden, M. (2013). Mitochondrial plasticity in obesity and diabetes mellitus. *Antioxid. Redox Signal.*, 19(3):258–268. 1

Kang, H. C., Lee, Y. M., and Kim, H. D. (2013). Mitochondrial disease and epilepsy. *Brain Dev.*, 35(8):757–761. 1

Kelley, D. E. and Mandarino, L. J. (2000). Fuel Selection in Human Skeletal Muscle in Insulin Resistance. *Diabetes*, 49(5):677–683. 58

Kelley, D. E., Menshikova, E. V., and Ritov, V. B. (2002). Dysfunction of mitochondria in human skeletal muscle in type 2 diabetes. *Diabetes*, 51(10):2944–2950. 58, 66

Kelley, D. E., Minutun, M. A., Watkins, S. C., Simoneau, J.-A., Jadali, F., and Fredrickson, A. (1996). The Effect of Non–Insulin-dependent Diabetes Mellitus and Obesity on Glucose Transport and Phosphorylation in Skeletal Muscle. *The Journal of Clinical Investigation*, 97(12):2705–2713. 63

Kelley, D. E. and Simoneau, J.-A. (1994). Impaired FFA utilization by skeletal muscle in NIDDM. *The Journal of Clinical Investigation*, 94:2349–2356. 63

Kelso, G. F., Maroz, A., Cochemé, H. M., Logan, A., Prime, T. A., Peskin, A. V., Winterbourn, C. C., James, A. M., Ross, M. F., Brooker, S., Porteous, C. M., Anderson, R. F., Murphy, M. P., and Smith, R. A. (2012). A mitochondria-targeted macrocyclic Mn(II) superoxide dismutase mimetic. *Chem Biol.*, 19(10):1237–1246. 20

Kelso, G. F., Porteous, C. M., Coulter, C. V., Hughes, G., Porteous, W. K., Ledgerwood, E. C., Smith, R. A., and Murphy, M. P. (2001). Selective targeting of a redox-active ubiquinone to mitochondria within cells: antioxidant and antiapoptotic properties. *J Biol Chem.*, 276(7):4588–4596. 20

Kraegen, E. W., James, D. E., Jenkins, A. B., and Chisholm, D. J. (1985). Dose-response curves for in vivo insulin sensitivity in individual tissues in rats. *American Journal of Physiology. Endocrinology and Metabolism*, 248(3):E353–362. 13

Krssak, M., Falk Petersen, K., Dresner, A., DiPietro, L., Vogel, S. M., Rothman, D. L., Roden, M., and Shulman, G. I. (1999). Intramyocellular lipid concentrations are correlated with insulin sensitivity in humans: a 1H NMR spectroscopy study. *Diabetologia*, 42(1):113–116. 64

Kus, V., Prazak, T., Brauner, P., Hensler, M., Kuda, O., Flachs, P., Janovska, P., Medrikova, D., Rossmeisl, M., Jilkova, Z., Stefl, B., Pastalkova, E., Drahota, Z., Houstek, J., and Kopecky, J. (2008). Induction of muscle thermogenesis by high-fat diet in mice: association with obesity-resistance. *Am. J. Physiol. Endocrinol. Metab.*, 295(2):E356–367. 12

Leary, S. C., Battersby, B. J., Hansford, R. G., and Moyes, C. D. (1998). Interactions between bioenergetics and mitochondrial biogenesis. *Biochimica et Biophysica Acta*, 1365(3):522–530. 14, 15

Leo, S., Szabadkai, G., and Rizzuto, R. (2008). The mitochondrial antioxidants MitoE(2) and MitoQ(10) increase mitochondrial Ca(2+) load upon cell stimulation by inhibiting Ca(2+) efflux from the organelle. *Ann. N. Y. Acad. Sci.*, 1147:264–274. 20

Li, H. and Yu, X. (2013). Emerging role of JNK in insulin resistance. *Curr Diabetes Rev*, 9(5):422–428. 1

Liberman, E. A., Topaly, V. P., Tsofina, L. M., Jasaitis, A. A., and Skulachev, V. P. (1969). Mechanism of coupling of oxidative phosphorylation and the membrane potential of mitochondria. *Nature*, 222(5198):1076–1078. 84

Lillioja, S., Mott, D. M., Zawadzki, J. K., Young, A. A., Abbott, W. G., and Bogardus, C. C. (1986). Glucose storage is a major determinant of in vivo "insulin resistance" in subjects with normal glucose tolerance. *The Journal of Clinical Endocrinology and Metabolism*, 62(5):922–927. 13

Loenarz, C. and Schofield, C. J. (2008). Expanding chemical biology of 2-oxoglutarate oxygenases. *Nat. Chem. Biol.*, 4(3):152–156. 94

Luo, C., Long, J., and Liu, J. (2008). An improved spectrophotometric method for a more specific and accurate assay of mitochondrial complex III activity. *Clinica Chimica Acta*, 395:38–41. 34

Lyons, C. N., Leary, S. C., and Moyes, C. D. (2004). Bioenergetic remodeling during cellular differentiation: changes in cytochrome c oxidase regulation do not affect the metabolic phenotype. *Biochemistry and Cell Biology*, 82(3):391–399. 14

Mailloux, R. J. and Harper, M.-E. (2010). Glucose regulates enzymatic sources of mitochondrial NADPH in skeletal muscle cells; a novel role for glucose-6-phosphate dehydrogenase. *FASEB J*, 24(7):2495–2506. 15, 30, 56, 60

Marazziti, D., Baroni, S., Picchetti, M., Landi, P., Silvestri, S., Vatteroni, E., and Catena Dell'Osso, M. (2012). Psychiatric disorders and mitochondrial dysfunctions. *Eur Rev Med Pharmacol Sci*, 16(2):270–275. 1

Marroquin, L. D., Hynes, J., Dykens, J. A., Jamieson, J. D., and Will, Y. (2007). Circumventing the Crabtree effect: replacing media glucose with galactose increases susceptibility of HepG2 cells to mitochondrial toxicants. *Toxicological Sciences*, 97(2):539–547. 2, 15

Martín, M. G., Turk, E., Lostao, P. M., Kerner, C., and Wright, E. M. (1996). Defects in Na+/glucose cotransporter (SGLT1) trafficking and function cause glucose-galactose malabsorption. *Nature Genetics*, 12:216–220. 16

Martin, S. D. and McGee, S. L. (2014). The role of mitochondria in the aetiology of insulin resistance and type 2 diabetes. *Biochim. Biophys. Acta*, 1840(4):1303–1312. 1

Martins, A. R., Nachbar, R. T., Gorjao, R., Vinolo, M. A., Festuccia, W. T., Lambertucci, R. H., Cury-Boaventura, M. F., Silveira, L. R., Curi, R., and Hirabara, S. M. (2012). Mechanisms underlying skeletal muscle insulin resistance induced by fatty acids: importance of the mitochondrial function. *Lipids Health Dis*, 11:30. 1

McPherson, J. D., Shilton, B., and Walton, D. J. (1988). Role of fructose in glycation and cross-linking of proteins. *Biochemistry*, 27(6):1901–1907. 16

Miyake, T., McDermott, J. C., and Gramolini, A. O. (2011). A method for the direct identification of differentiating muscle cells by a fluorescent mitochondrial dye. *PloS One*, 6(12):e28628. 30

Mogensen, M., Sahlin, K., Fernström, M., Glintborg, D., Vind, B. F., Beck-Nielsen, H., and Højlund, K. (2007). Mitochondrial Respiration Is Decreased in Skeletal Muscle of Patients With Type 2 Diabetes. *Diabetes*, 56(6):1592–1599. 58, 66

Mohanty, A. and McBride, H. M. (2013). Emerging roles of mitochondria in the evolution, biogenesis, and function of peroxisomes. *Front Physiol*, 4:268. 1

Morava, E. and Kozicz, T. (2013). Mitochondria and the economy of stress (mal)adaptation. *Neurosci Biobehav Rev*, 37(4):668–680. 1

Morris, J. K., Honea, R. A., Vidoni, E. D., Swerdlow, R. H., and Burns, J. M. (2014). Is Alzheimer's disease a systemic disease? *Biochim. Biophys. Acta*, 1842(9):1340–1349. 1

Moyes, C. D., Mathieu-Costello, O. A., Tsuchiya, N., Filburn, C., and Hansford, R. G. (1997). Mitochondrial biogenesis during cellular differentiation. *Am. J. Physiol.*, 272(4 Pt 1):C1345–1351. 14

Murphy, M. P., Echtay, K. S., Blaikie, F. H., Asin-Cayuela, J., Cochemé, H. M., Green, K., Buckingham, J. A., Taylor, E. R., Hurrell, F., Hughes, G., Miwa, S., Cooper, C. E., Svistunenko, D. A., Smith, R. A., and Brand, M. D. (2003).

Superoxide activates uncoupling proteins by generating carbon-centered radicals and initiating lipid peroxidation: studies using a mitochondria-targeted spin trap derived from alpha-phenyl-N-tert-butylnitrone. *J Biol Chem.*, 278(49):48534–48545. 20

Murphy, M, P. (1997). Selective targeting of bioactive compounds to mitochondria. *Trends Biotechnol.*, 15(8):326–330. 68, 80

Nedachi, T., Kadotani, A., Ariga, M., Katagiri, H., and Kanzaki, M. (2008). Ambient glucose levels qualify the potency of insulin myogenic actions by regulating SIRT1 and FoxO3a in C2C12 myocytes. *American Journal of Physiology. Endocrinology and Metabolism*, 294(4):668–678. 56

Nesher, R., Karl, I. E., and Kipnis, D. M. (1985). Dissociation of effects of insulin and contraction on glucose transport in rat epitrochlearis muscle. *American Journal of Physiology. Cell physiology*, 249(3):C226–232. 13

Newsholme, P., Gaudel, C., and Krause, M. (2012). Mitochondria and diabetes. An intriguing pathogenetic role. *Adv. Exp. Med. Biol.*, 942:235–247. 1

Nicholls, D. G. (1977). The effective proton conductance of the inner membrane of mitochondria from brown adipose tissue. Dependency on proton electrochemical potential gradient. *European Journal of Biochemistry*, 77(2):349–356. 12

Nicholls, D. G. (2012). Fluorescence measurement of mitochondrial membrane potential changes in cultured cells. *Methods Mol. Biol.*, 810:119–133. 37

Nicholls, D. G., Darley-Usmar, V. M., Wu, M., Jensen, P. B., Rogers, G. W., and Ferrick, D. A. (2010). Bioenergetic profile experiment using C2C12 myoblast cells. *J Vis Exp*, (46). 9

Nobes, C. D., Brown, G. C., Olive, P. N., and Brand, M. D. (1990). Non-ohmic proton conductance of the mitochondrial inner membrane in hepatocytes. *The Journal of Biological Chemistry*, 265(22):12903–12909. 10, 12

Ojovan, S. M., Knorre, D. A., Markova, O. V., Smirnova, E. A., Bakeeva, L. E., and Severin, F. F. (2011). Accumulation of dodecyltriphenylphosphonium in mitochondria induces their swelling and ROS-dependent growth inhibition in yeast. *J. Bioenerg. Biomembr.*, 43(2):175–180. 84, 93

O'Malley, Y., Fink, B. D., Ross, N. C., Prisinzano, T. E., and Sivitz, W. I. (2006). Reactive oxygen and targeted antioxidant administration in endothelial cell mitochondria. *J. Biol. Chem.*, 281(52):39766–39775. 20

Orsucci, D., Mancuso, M., Ienco, E. C., Simoncini, C., Siciliano, G., and Bonuccelli, U. (2013). Vascular factors and mitochondrial dysfunction: a central role in the pathogenesis of Alzheimer's disease. *Curr Neurovasc Res*, 10(1):76–80. 1

Palmfeldt, J., Vang, S., Stenbroen, V., Pedersen, C. B., Christensen, J. H., Bross, P., and Gregersen, N. (2009). Mitochondrial proteomics on human fibroblasts for identification of metabolic imbalance and cellular stress. *Proteome Science*, 7:20. 2, 15

Pan, D. A., Lillioja, S., Kriketos, A. D., Milner, M. R., Baur, L. A., Bogardus, C., Jenkins, A. B., and Storlien, L. H. (1997). Skeletal muscle triglyceride levels are inversely related to insulin action. *Diabetes*, 46(6):983–988. 64

Parthasarathy, R., Parthasarathy, L., and Vadnal, R. (1997). Brain inositol monophosphatase identified as a galactose 1-phosphatase. *Brain Res*, 778(1):99–106. 17

Patkova, J., Anděl, M., and Trnka, J. (2014). Palmitate-induced cell death and mitochondrial respiratory dysfunction in myoblasts are not prevented by mitochondria-targeted antioxidants. *Cell. Physiol. Biochem.*, 33(5):1439–1451. 21

Perseghin, G., Scifo, P., De Cobelli, F., Pagliato, E., Battezzati, A., Arcelloni, C., Vanzulli, A., Testolin, G., Pozza, G., Del Maschio, A., and Luzi, L. (1999). Intramyocellular triglyceride content is a determinant of in vivo insulin resistance in humans: a 1H-13C nuclear magnetic resonance spectroscopy assessment in offspring of type 2 diabetic parents. *Diabetes*, 48(8):1600–1606. 64

Petersen, K. F., Dufour, S., Befroy, D., Garcia, R., and Shulman, G. I. (2004). Impaired Mitochondrial Activity in the Insulin-Resistant Offspring of Patients with Type 2 Diabetes. *The New England Journal of Medicine*, 350(7):664–671. 58

Petersen, K. F., Dufour, S., Savage, D. B., Bilz, S., Solomon, G., Yonemitsu, S., Cline, G. W., Befroy, D., Zemany, L., Kahn, B. B., Papademetris, X., Rothman, D. L., and Shulman, G. I. (2007). The role of skeletal muscle insulin resistance in the pathogenesis of the metabolic syndrome. *PNAS*, 104(31):12587–12594. 12

Phielix, E. and Mensink, M. (2008). Type 2 diabetes mellitus and skeletal muscle metabolic function. *Physiol. Behav.*, 94(2):252–258. 1, 12

Plecitá-Hlavatá, L., Ježek, J., and Ježek, P. (2009). Pro-oxidant mitochondrial matrix-targeted ubiquinone MitoQ10 acts as anti-oxidant at retarded electron transport or proton pumping within Complex I. *Int. J. Biochem. Cell Biol.*, 41(8-9):1697–1707. 21, 83

Ploug, T., Galbo, H., and Richter, E. A. (1984). Increased muscle glucose uptake during contractions: no need for insulin. *American Journal of Physiology. Endocrinology and Metabolism*, 247(6):E726–731. 13

Porter, R. K. and Brand, M. D. (1995). Causes of differences in respiration rate of hepatocytes from mammals of different body mass. *American Journal of Physiology, Regulatory, Integrative and Comparative Physiology*, 269(5):R1213–1224. 10

Qi, F., Pradhan, R. K., Dash, R. K., and Beard, D. A. (2011). Detailed kinetics and regulation of mammalian 2-oxoglutarate dehydrogenase. *BMC Biochem.*, 12:53. 94

Quin, C., Trnka, J., Hay, A., Murphy, M. P., and Hartley, R. C. (2009). Synthesis of a mitochondria-targeted spin trap using a novel Parham-type cyclization. *Tetrahedron*, 65(39):8154–8160. 20

Randle, P. J., Garland, P. B., Hales, C. N., and Newsholme, E. A. (1963). The glucose fatty-acid cycle. Its role in insulin sensitivity and the metabolic disturbances of diabetes mellitus. *The Lancet*, 13(1):786–789. 63

Reichardt, J. K. (1992). Genetic basis of galactosemia. *Hum Mutat*, 1(3):190–196. 17

Reily, C., Mitchell, T., Chacko, B. K., Benavides, G., Murphy, M. P., and Darley-Usmar, V. (2013). Mitochondrially targeted compounds and their impact on cellular bioenergetics. *Redox Biol.*, 1(1):86–93. 21, 69, 81, 83, 84, 93

Resnick, O. and Hechter, O. (1957). Studies on the permeability of galactose in muscle cells of the isolated rat diaphragm. *Journal of Biological Chemistry*, 224(2):941–954. 15, 43, 56

Richter, E. A., Garetto, L. P., Goodman, M. N., and Ruderman, N. B. (1984). Enhanced muscle glucose metabolism after exercise: modulation by local factors. *American Journal of Physiology. Endocrinology and Metabolism*, 246(6):E476–82. 13

Rieusset, J. (2011). Mitochondria and endoplasmic reticulum: mitochondria-endoplasmic reticulum interplay in type 2 diabetes pathophysiology. *Int. J. Biochem. Cell Biol.*, 43(9):1257–1262. 1

Ritov, V. B., Menshikova, E. V., He, J., Ferrel, R. E., Goodpaster, B. H., and Kelley, D. E. (2005). Deficiency of Subsarcolemmal Mitochondria in Obesity and Type 2 Diabetes. *Diabetes*, 54(1):8–14. 58, 66

Robinson, K. M., Janes, M. S., Pehar, M., Monette, J. S., Ross, M. F., Hagen, T. M., Murphy, M. P., and Beckman, J. S. (2006). Selective fluorescent imaging of superoxide in vivo using ethidium-based probes. *Proc Natl Acad Sci U S A*, 103(41):15038–15043. 20

Rolfe, D. E., Newman, J. M., Buckingham, J. A., Clark, M. G., and Brand, M. D. (1999). Contribution of mitochondrial proton leak to respiration rate in working skeletal muscle and liver and to SMR. *American Journal of Physiology. Cell physiology*, 276(3):C692–699. 12

Ross, M. F., Kelso, G. F., Blaikie, F. H., James, A. M., Cochemé, H. M., Filipovska, A., Da Ros, T., Hurd, T. R., Smith, R. A., and Murphy, M. P. (2005). Lipophilic triphenylphosphonium cations as tools in mitochondrial bioenergetics and free radical biology. *Biochemistry (Mosc)*, 70(2):222–230. 19, 20, 68, 80

Ross, M. F., Prime, T. A., Abakumova, I., James, A. M., Porteous, C. M., Smith, R. A., and Murphy, M. P. P. (2008). Rapid and extensive uptake and activation of hydrophobic triphenylphosphonium cations within cells. *Biochem J.*, 411(3):633–645. 19, 20, 68, 80, 93

Rossignol, R., Gilkerson, R., Aggeler, R., Yamagata, K., Remington, S. J., and Capaldi, A. R. (2004). Energy substrate modulates mitochondrial structure and oxidative capacity in cancer cells. *Cancer Research*, 64(3):985–993. 2, 15

Sadun, A. A., La Morgia, C., and Carelli, V. (2013). Mitochondrial optic neuropathies: our travels from bench to bedside and back again. *Clin Experiment Ophthalmo.*, 41(7):702–712. 1

Salabei, J. K., Gibb, A. A., and Hill, B. G. (2014). Comprehensive measurement of respiratory activity in permeabilized cells using extracellular flux analysis. *Nat Protoc*, 9(2):421–438. 39

Salo, W. L., Nordin, J. H., Peterson, D. R., Bevill, R. D., and Kirkwood, S. (1968). The specificity of UDP-glucose 4-epimerase from the yeast Saccharomyces fragilis. *Biochimica et Biophysica Acta (BBA) - Enzymology*, 151(2):484–492. 17

Santomauro, A. T., Boden, G., Silva, M. E., Rocha, D. M., Santos, R. F., Ursich, M. J., Strassmann, P. G., and Wajchenberg, B. L. (1999). Overnight lowering of free fatty acids with Acipimox improves insulin resistance and glucose tolerance in obese diabetic and nondiabetic subjects. *Diabetes*, 48(9):1836–1841. 64

Scaduto, R. C. and Grotyohann, L. W. (1999). Measurement of mitochondrial membrane potential using fluorescent rhodamine derivatives. *Biophys. J.*, 76(1 Pt 1):469–477. 37

Scarffe, L. A., Stevens, D. A., Dawson, V. L., and Dawson, T. M. (2014). Parkin and PINK1: much more than mitophagy. *Trends Neurosci.*, 37(6):315–324. 1

Schiaffino, S., Gorza, L., Sartore, S., Saggin, L., and Carli, M. (1986). Embryonic myosin heavy chain as a differentiation marker of developing human skeletal muscle and rhabdomyosarcoma. A monoclonal antibody study. *Exp. Cell Res.*, 163(1):211–220. 46

Schmitz-Peiffer, C. (2000). Signalling aspects of insulin resistance in skeletal muscle: mechanisms induced by lipid oversupply. *Cellular Signalling*, 12(9-10):583–594. 64

Schrauwen-Hinderling, V. B., Kooi, M. E., Hesselink, M. K. C., Jeneson, J. A. L., Backes, W. H., van Echteld, C. J. A., van Engelshoven J. M. A., Mensink, M., and Schrauwen, P. (2007). Impaired in vivo mitochondrial function but similar intramyocellular lipid content in patients with type 2 diabetes mellitus and BMI-matched control subjects. *Diabetologia*, 50:113–120. 58

Schwab, M. A., Kolker, S., van den Heuvel, L. P., Sauer, S., Wolf, N. I., Rating, D., Hoffmann, G. F., Smeitink, J. A., and Okun, J. G. (2005). Optimized spectrophotometric assay for the completely activated pyruvate dehydrogenase complex in fibroblasts. *Clin. Chem.*, 51(1):151–160. 31

Semenza, G. L. (2007). Hypoxia-inducible factor 1 (HIF-1) pathway. *Sci. STKE*, 2007(407):cm8. 94

Severin, F. F., Severina, I. I., Antonenko, Y. N., Rokitskaya, T. I., Cherepanov, D. A., Mokhova, E. N., Vyssokikh, M. Y., Pustovidko, A. V., Markova, O. V., Yaguzhinsky, L. S., Korshunova, G. A., Sumbatyan, N. V., Skulachev, M. V., and Skulachev, V. P. (2010). Penetrating cation/fatty acid anion pair as a mitochondria-targeted protonophore. *Proc. Natl. Acad. Sci. U.S.A.*, 107(2):663–668. 21, 83

Sheu, K. F. and Blass, J. P. (1999). The alpha-ketoglutarate dehydrogenase complex. *Ann. N. Y. Acad. Sci.*, 893:61–78. 94

Sheu, S. S., Nauduri, D., and Anders, M. W. (2006). Targeting antioxidants to mitochondria: a new therapeutic direction. *Biochim Biophys Acta*, 1762(2):256–265. 1

Shulman, G. I., Rothman, D. L., Jue, T., Stein, P., DeFronzo, R. A., and Shulman, R. G. (1990). Quantitation of muscle glycogen synthesis in normal subjects and subjects with non-insulin-dependent diabetes by 13C nuclear magnetic resonance spectroscopy. *The New England Journal of Medicine*, 322(4):223–228. 66

Simoneau, J. A. and Kelley, D. E. (1997). Altered glycolytic and oxidative capacities of skeletal muscle contribute to insulin resistance in NIDDM. *Journal of Applied Physiology*, 83(1):166–171. 66

Sinacore, D. R. and Gulve, E. A. (1993). The role of skeletal muscle in glucose transport, glucose homeostasis, and insulin resistance: implications for physical therapy. *Physical Therapy*, 73(12):878–891. 12

Smith, R. A., Hartley, R. C., Cocheme, H. M., and Murphy, M. P. (2012). Mitochondrial pharmacology. *Trends Pharmacol. Sci.*, 33(6):341–352. 92

Smith, R. A., Porteous, C. M., Coulter, C. V., and Murphy, M. P. (1999). Selective targeting of an antioxidant to mitochondria. *Eur J Biochem.*, 263(3):709–716. 20

Sorriento, D., Pascale, A. V., Finelli, R., Carillo, A. L., Annunziata, R., Trimarco, B., and Iaccarino, G. (2014). Targeting Mitochondria as Therapeutic Strategy for Metabolic Disorders. *Scientific World Journal*, 2014. 1

Spargo, E., Pratt, O. E., and Daniel, P. M. (1979). Metabolic functions of skeletal muscles of man, mammals, birds and fishes: a review. *Journal of the Royal Society of Medicine*, 72(12):921–925. 13

Spinazzi, M., Casarin, A., Pertegato, V., Salviati, L., and Angelini, C. (2012). Assessment of mitochondrial respiratory chain enzymatic activities on tissues and cultured cells. *Nat protoc.*, 7(6):1235–1246. 27, 28, 32

Stroh, M., Swerdlow, R. H., and Zhu, H. (2014). Common defects of mitochondria and iron in neurodegeneration and diabetes (MIND): a paradigm worth exploring. *Biochem. Pharmacol.*, 88(4):573–583. 1

Summers, S. A. (2006). Ceramides in insulin resistance and lipotoxicity. *Progress in Lipid Research*, 45(1):42–72. 64

Szendroedi, J., Phielix, E., and Roden, M. (2012). The role of mitochondria in insulin resistance and type 2 diabetes mellitus. *Nat Rev Endocrinol*, 8(2):92–103. 1

Szendroedi, J., Schmid, A. I., Chmelik, M., Toth, C., Brehm, A., Krssak, M., Nowotny, P., Wolzt, M., Waldhausl, W., and Roden, M. (2007). Muscle Mitochondrial ATP Synthesis and Glucose Transport/Phosphorylation in Type 2 Diabetes. *PloS Medicine*, 4(5):e154. 58

Tapscott, S. J., Davis, R. L., Thayer, M. J., Cheng, P. F., Weintraub, H., and Lassar, A. B. (1988). MyoD1: a nuclear phosphoprotein requiring a Myc homology region to convert fibroblasts to myoblasts. *Science*, 242(4877):405–411. 48

Thoden, J. B., Timson, D. J., Reece, R. J., and Holden, H. M. (2004). Molecular structure of human galactose mutarotase. *Journal of Biological Chemistry*, 279(22):23431–23437. 17

Trendeleva, T. A., Rogov, A. G., Cherepanov, D. A., Sukhanova, E. I., Il'yasova, T. M., Severina, I. I., and Zvyagilskaya, R. A. (2012). Interaction of tetraphenylphosphonium and dodecyltriphenylphosphonium with lipid membranes and mitochondria. *Biochemistry Mosc.*, 77(9):1021–1028. 20

Trnka, J. (2008). *Mitochondria-targeted antioxidants and spin traps*. PhD thesis, University of Cambridge. 20, 26

Trnka, J., Blaikie, F. H., Logan, A., Smith, R. A., and Murphy, M. P. (2009). Antioxidant properties of MitoTEMPOL and its hydroxylamine. *Free Radic Res.*, 43(1):4–12. 20

Trnka, J., Blaikie, F. H., Smith, R. A., and Murphy, M. P. (2008). A mitochondria-targeted nitroxide is reduced to its hydroxylamine by ubiquinol in mitochondria. *Free Radic Biol Med.*, 1(44):1406–1419. 20

Trounce, I. A., Kim, Y. L., Jun, A. S., and Wallace, D. C. (1996). Assessment of mitochondrial oxidative phosphorylation in patient muscle biopsies, lymphoblasts, and transmitochondrial cell lines. *Meth. Enzymol.*, 264:484–509. 28

Wallberg-Henriksson, H., Constable, S. H., Young, D. A., and Holloszy, J. O. (1988). Glucose transport into rat skeletal muscle: interaction between exercise and insulin. *Journal of Applied Physiology*, 65(2):909–913. 13

Wallberg-Henriksson, H. and Holloszy, J. O. (1985). Activation of glucose transport in diabetic muscle: responses to contraction and insulin. *American Journal of Physiology. Cell physiology*, 249(3):C233–237. 13

Williams, R. S., Salmons, S., Newsholme, E. A., Kaufman, R. E., and Mellor, J. (1986). Regulation of nuclear and mitochondrial gene expression by contractile activity in skeletal muscle. *Journal of Biological Chemistry*, 261(1):376–380. 53

Wingrove, D. E. and Gunter, T. E. (1986). Kinetics of mitochondrial calcium transport. II. A kinetic description of the sodium-dependent calcium efflux mechanism of liver mitochondria and inhibition by ruthenium red and by tetraphenylphosphonium. *J. Biol. Chem.*, 261(32):15166–15171. 21

Winklhofer, K. F. (2014). Parkin and mitochondrial quality control: toward assembling the puzzle. *Trends Cell Biol.*, 24(6):332–341. 1

Wohlgemuth, S. E., Calvani, R., and Marzetti, E. (2014). The interplay between autophagy and mitochondrial dysfunction in oxidative stress-induced cardiac aging and pathology. *J Mol Cell Cardiol.* 1

Wright, E. M., Turk, E., Hager, K., Lescale-Matys, L., Hirayama, B., Supplisson, S., and Loo, D. D. (1992). The Na+/glucose cotransporter (SGLT1). *Acta Physiol Scand Suppl*, 607:201–207. 16

Wu, M., Neilson, A., Swift, A. L., Moran, R., Tamagnine, J., Parslow, D., Armistead, S., Lemire, K., Orrell, J., Teich, J., Chomicz, S., and Ferrick, D. A. (2007). Multiparameter metabolic analysis reveals a close link between attenuated mitochondrial bioenergetic function and enhanced glycolysis dependency in human tumor cells. *Am J Physiol Cell Physiol.*, 292(1):125–136. 39

Xu, Y. and Kalyanaraman, B. (2007). Synthesis and ESR studies of a novel cyclic nitrone spin trap attached to a phosphonium group-a suitable trap for mitochondria-generated ROS? *Free Radic Res.*, 41(1):1–7. 20

Yadava, N. and Nicholls, D. G. (2007). Spare respiratory capacity rather than oxidative stress regulates glutamate excitotoxicity after partial respiratory inhibition of mitochondrial complex I with rotenone. *The Journal of neuroscience*, 27(27):7310–7317. 12

Yang, K. C., Bonini, M. G., and Dudley Jr, S. C. (2014). Mitochondria and arrhythmias. *Free Radic Biol Med.*, 71:351–361. 1